Watershed controls on streamwater biogeochemistry in a large boreal river network

David W. French

A thesis

submitted in partial fulfillment of the

requirements for the degree of

Master of Science

University of Washington

2020

Committee:

Daniel E. Schindler

Gordon W. Holtgrieve

Program Authorized to Offer Degree:

School of Aquatic and Fishery Sciences

University of Washington

Abstract

Watershed controls on streamwater biogeochemistry in a large boreal river network

David W. French

Chair of the Supervisory Committee:

Professor Daniel E. Schindler

School of Aquatic and Fishery Sciences

Streamwater chemistry forms the base of aquatic food webs and reflects both watershed and instream controls, yet the balance of these controls has not been quantified across large river networks. Boreal river networks in particular are subject to rapid environmental change under a warming climate and growing developmental pressures from industrial activities such as mining. The impacts of these changes to nutrient and organic matter availability and contaminant loading to aquatic food webs is currently not well understood. In this thesis, I used recently developed spatial stream network models (SSNMs) that explicitly account for stream network topology, flow direction, and flow magnitude to quantify the effects of watershed versus instream transport processes on streamwater chemistry in the Kuskokwim River in western Alaska. This approach leverages a combination of instream sampling and broad scale, publicly available geospatial data. The Kuskokwim is America's largest free-flowing river network and is predominantly a pristine

watershed that supports an array of ecosystem services. The Kuskokwim is also home to numerous subsistence communities that rely on fish as a primary protein source.

In chapter 1 I examined watershed controls on streamwater biogeochemical patterning and identify the scales at which watershed controls operate. For this chapter I studied a suite of streamwater constituents ranging from labile nutrients to conservative tracers to understand the effect of instream transport processes on network-wide dissolved organic carbon (DOC) concentrations. I show that conditions such as watershed morphology and geology in small, headwater catchments are disproportionately important drivers of streamwater biogeochemical patterning across the Kuskokwim River network, and that bulk measures of DOC reflect conservative transport behavior.

In chapter 2 I extended this analysis to examine spatial patterning of mercury (Hg) contamination in tissue of slimy sculpin (*Cottus cognatus*), a small, sedentary resident fish species in the Kuskokwim. Previous work in the Kuskokwim has shown a strong, positive correlation between historic mining activity and Hg contamination of fish, which poses potential risks to subsistence communities who rely on fish for nutrition, however past research was limited in spatial scope. This chapter examined both watershed (e.g. geology) and *in situ* (e.g. [DOC]) factors shaping Hg contamination across the entire Kuskokwim network. I show that broad scale watershed morphology and geologic blocks shape spatial patterns of Hg contamination of sculpin in the Kuskokwim, and that the effects of downstream transport and instream biogeochemical factors governing Hg bioavailability ([DOC] and pH) are confounded by these broad scale watershed drivers.

Table of Contents

List of Figures

Acknowledgements

The research supporting this thesis was a collaborative effort with staff and faculty at the University of Washington School of Aquatic and Fishery Sciences (SAFS), the Alaska Department of Fish and Game, and the U.S. Fish and Wildlife Service Yukon Delta National Wildlife Refuge, and I thank those agency staff for their field efforts in the Kuskokwim. Our pilot Alex 'X-Ray' Shapiro of Alaska Land Resources was crucial in getting us safely into remote areas of the Kuskokwim. I also want to thank Jeff Baldock, Dean Freundlich, and Jackie Carter at the UW Alaska Salmon Program for their meticulous lab work and logistical support, and Diane Whited for her GIS wizardry. I would not have any data in hand without these folks.

My graduate studies were supported by fellowships from SAFS and the National Science Foundation Graduate Research Fellowship Program, and I am grateful for their support. I also thank the Arctic-Yukon-Kuskokwim Sustainable Salmon Initiative for funding this research.

My thesis committee members were invaluable resources for question-driven ideas and insightful feedback on my chapters. I thank Gordon Holtgrieve for encouraging clear, concise approaches throughout the research process. I thank Sean Brennan for being a wealth of knowledge on every aspect of my work, for his mentorship, and most of all for being a great human being and friend. My advisor Daniel Schindler challenged me to become a better scientist and was tremendously helpful in framing this work. I am grateful for Daniel's big picture ideas and for exposing me to Alaska's beautiful ecosystems. I will fondly remember tromping around in streams and bogs while picking Daniel's brain about salmon and the broader field of ecology.

The community at SAFS and my friends and family are what made the non-research hours in my day enjoyable during grad school. I thank all of you for being fun, supportive, and inspiring. I especially thank my wife Cori for her emotional labor and encouragement.

General Introduction

Despite accounting for a tiny fraction (1.5×10^{-4} %) of the earth's hydrosphere, river networks serve a major and disproportionate role in global biogeochemical cycling (Raymond *et al.*, 2013). Rivers process or store more than half of carbon (C) loadings from the terrestrial environment, exporting the remainder of watershed organic matter to coastal estuaries (Cole *et al.*, 2007). Provided that terrestrial C entering inland waters is estimated to represent 50-70 percent of terrestrial net ecosystem productivity across the globe (Butman *et al.*, 2016; Ciais *et al.*, 2008; Cole *et al.*, 2007), river networks are substantial contributors to the global C cycle. Modeled estimates for nutrient retention within streams and rivers suggest that 42 percent of terrestrial nitrogen (N) and 56 percent of terrestrial phosphorus (P) are also processed or stored within river systems, despite increased anthropogenic terrestrial loading of these constituents throughout many of the world's river basins (Beusen *et al.*, 2016). These streamwater constituents are particularly important because the uptake and metabolism of terrestrial organic matter and nutrients within rivers form the base of lotic food webs, regulating the balance between production and respiration by producers and consumers and shaping the structure of a stream's biotic community (Battin *et al.*, 2008; Meyer *et al.*, 1988; Vannote *et al.*, 1980). In turn, stream biota play an important role in determining nutrient and organic matter transport to downstream reaches, with downstream communities capitalizing on upstream losses and local inputs (Meyer *et al.*, 1988; Vannote *et al.*, 1980). Thus, contrary to acting as passive conduits between mountains and sea, river systems transport, store, and process vast amounts of terrestrial material comprising organic matter, nutrients, and minerals; forming important linkages between terrestrial and aquatic ecosystems (Cole *et al.*, 2007; Likens & Bormann, 1974).

The ecological linkages between terrestrial and aquatic habitats can be evaluated to some extent by examining dissolved streamwater constituents, which integrate both upstream watershed conditions and instream processing (Meyer *et al.,* 1988). The watershed concept (Bormann & Likens, 1967) posits that instream chemical conditions reflect broader watershed features including land-use practices, whereas the nutrient spiraling concept (Webster & Patten, 1979) describes instream processing of nutrients in terms of upstream inefficiencies fueling metabolic processes of downstream biota. The relative balance of these controls is contingent on several factors, including a constituent's lability, concentration (and by extension, runoff and flow volume), biogeochemical demand, and the stream order or position of a measurement within a river network (Lintern *et al.,* 2018). The extent of a watershed's influence on streamwater constituents is also dependent on hydrologic connectivity (eg. groundwater transport or water residence time), which can vary considerably within a catchment and over time (Meyer *et al.*, 1988). Catchment and channel characteristics are further subject to natural disturbance regimes, climate fluctuations, growing periods for vegetative cover, and land use changes and impacts that may dampen or amplify the expression of watershed conditions on streamwater constituents (Lintern *et al.,* 2018).

This diverse suite of watershed and instream processes creates a mosaic of instream habitat conditions that shape spatial and temporal distributions of aquatic biota (Vannote *et al.,* 1980). Disentangling the extent to which watershed versus instream controls shape biogeochemical conditions throughout large river networks may offer insights into spatial patterns that underlie riverine ecology. For example, measures of dissolved organic carbon (DOC) are often used to gauge ecosystem productivity and respiratory processes (Melack *et al.*, 2011). Both allochthonous and autochthonous DOC fuel microbial food webs in streams (Wetzel, 1995),

1995) and dissolved nutrient concentrations (eg. NO3 [NO_3], orthophosphate [PO_4]) regulate rates at which primary production and decomposition occur (Meyer *et al.*, 1988). Aside from their important role in aquatic food webs, these streamwater constituents influence physical conditions (e.g., light attenuation) and redox potential within the water column and stream sediments, shaping the bioavailability of contaminants such as methylmercury (MeHg), (Abbott *et al.*, 2016; Meyer *et al.*, 1988). Contaminants can also be concentrated within streamwater, despite often being dispersed at lower concentrations across a landscape (Likens & Bormann, 1974). Coupled measurements of streamwater constituents and contaminants within aquatic species may reveal broader scale landscape disturbances or baseline conditions that are difficult to detect in the terrestrial biome. Understanding the relative importance of watershed versus instream controls on streamwater composition has implications for land managers tasked with protecting both terrestrial and aquatic resources, but few studies have examined these processes at scales relevant for the management of diverse landscapes.

Network topology and the directional flow of water in rivers facilitate a suite of chemical, biological, and physical exchanges between a watershed and downstream channel reaches (Lamberti *et al.*, 2010), but the spatial configuration of dendritic river networks has only recently been accounted for in biogeochemical studies (Brennan *et al.*, 2016; McGuire *et al.*, 2014; Peterson *et al.*, 2006; Post *et al.*, 2018; Rodriguez-Castillo *et al.*, 2019; Scown *et al.*, 2017). This is partly due to logistical constraints posed by collecting data at numerous points in a watershed, and to limitations of traditional geostatistical approaches for analyzing stream data, which generally do not account for the combination of network topology, flow direction and magnitude, and catchment characteristics that govern instream conditions (Peterson *et al.*, 2013). Over the past decade, spatial stream network models (SSNMs)(Ver Hoef & Peterson, 2010) have

increasingly been used to study data from river networks. SSNMs have been successfully used to study water temperature (Ashley Steel *et al.*, 2016; Isaak *et al.*, 2014; Marsha *et al.*, 2018), examine biologic and hydrologic processes with stable isotopes (Brennan *et al.*, 2016; Segura *et al.*, 2019), evaluate impacts on water quality (Neill *et al.*, 2018; Scown *et al.*, 2017; Ver Hoef & Peterson, 2010), model ecosystem respiration (Rodriguez-Castillo *et al.*, 2019), and study fish and invertebrate ecology (Brennan *et al.*, 2019; Isaak *et al.*, 2017; Larsen *et al.*, 2019). The SSNM framework explicitly accounts for network topology and allows variance partitioning among watershed effects and instream spatial autocorrelation (Ver Hoef & Peterson, 2010). SSNMs are thus an emerging approach for inferring the relative effects of watershed versus instream controls on streamwater constituents forming the base of riverine food webs.

For this thesis work, I used SSNMs to study the behavior of streamwater constituents as water moves throughout the Kuskokwim River of western Alaska. My focal constituents have varying lability, ranging from a conservative tracer (strontium) to labile and often limiting nutrients (NO_3, PO_4). I employed these constituents as bookends to study the behavior of DOC in a large river network, which I hypothesized to behave intermediate to labile and conservative constituents. I also compared variance composition from SSNMs for these constituents across multiple spatial scales to identify the spatial scales and network locations of prevailing watershed controls on instream biogeochemical conditions. Expanding on this work, I evaluated how mercury contamination in resident fishes from this river network reflects both local scale streamwater chemical variation and broader scale geologic and geomorphic controls, and how impacts from mining activity may alter or exacerbate these controls.

References

Abbott, B. W., et al. (2016), Using multi-tracer inference to move beyond single-catchment ecohydrology, Earth-Sci Rev, 160, 19-42, doi:10.1016/j.earscirev.2016.06.014.

Ashley Steel, E., C. Sowder, and E. Peterson (2016), Spatial and Temporal Variation of Water Temperature Regimes on the Snoqualmie River Network, J Am Water Resour As, 52(3), 769-787, doi:10.1111/1752-1688.12423.

Battin, T. J., L. A. Kaplan, S. Findlay, C. S. Hopkinson, E. Marti, A. I. Packman, J. D. Newbold, and F. Sabater (2008), Biophysical controls on organic carbon fluxes in fluvial networks, Nat Geosci, 1(2), 95-100, doi:10.1038/ngeo101.

Beusen, A. H. W., A. F. Bouwman, L. P. H. Van Beek, J. M. Mogollon, and J. J. Middelburg (2016), Global riverine N and P transport to ocean increased during the 20th century despite increased retention along the aquatic continuum, Biogeosciences, 13(8), 2441-2451, doi:10.5194/bg-13-2441-2016.

Bormann, F. H., and G. E. Likens (1967), Nutrient Cycling, Science, 155(3761), 424-+, doi:DOI 10.1126/science.155.3761.424.

Brennan, S. R., D. E. Schindler, T. J. Cline, T. E. Walsworth, G. Buck, and D. P. Fernandez (2019), Shifting habitat mosaics and fish production across river basins, Science, 364(6442), 783-+, doi:10.1126/science.aav4313.

Brennan, S. R., C. E. Torgersen, J. P. Hollenbeck, D. P. Fernandez, C. K. Jensen, and D. E. Schindler (2016), Dendritic network models: Improving isoscapes and quantifying influence of landscape and in-stream processes on strontium isotopes in rivers, Geophys Res Lett, 43(10), 5043-5051, doi:10.1002/2016gl068904.

Butman, D., S. Stackpoole, E. Stets, C. P. McDonald, D. W. Clow, and R. G. Striegl (2016), Aquatic carbon cycling in the conterminous United States and implications for terrestrial carbon accounting, P Natl Acad Sci USA, 113(1), 58-63, doi:10.1073/pnas.1512651112.

Ciais, P., A. V. Borges, G. Abril, M. Meybeck, G. Folberth, D. Hauglustaine, and I. A. Janssens (2008), The impact of lateral carbon fluxes on the European carbon balance, Biogeosciences, 5(5), 1259-1271, doi:DOI 10.5194/bg-5-1259-2008.

Cole, J. J., et al. (2007), Plumbing the global carbon cycle: Integrating inland waters into the terrestrial carbon budget, Ecosystems, 10(1), 171-184, doi:10.1007/s10021-006-9013-8.

Isaak, D. J., J. M. V. Hoef, E. E. Peterson, D. L. Horan, and D. E. Nagel (2017), Scalable population estimates using spatial-stream-network (SSN) models, fish density surveys, and national geospatial database frameworks for streams, Can J Fish Aquat Sci, 74(2), 147-156, doi:10.1139/cjfas-2016-0247.

Isaak, D. J., et al. (2014), Applications of spatial statistical network models to stream data, Wires Water, 1(3), 277-294, doi:10.1002/wat2.1023.

Lamberti, G. A., D. T. Chaloner, and A. E. Hershey (2010), Linkages among aquatic ecosystems, J N Am Benthol Soc, 29(1), 245-263, doi:10.1899/08-166.1.

Larsen, S., M. C. Bruno, I. P. Vaughan, and G. Zolezzi (2019), Testing the River Continuum Concept with geostatistical stream-network models, Ecol Complex, 39, doi:UNSP 10077310.1016/j.ecocom.2019.100773.

Likens, G. E., and F. H. Bormann (1974), Linkages between Terrestrial and Aquatic Ecosystems, Bioscience, 24(8), 447-456, doi:Doi 10.2307/1296852.

Lintern, A., J. A. Webb, D. Ryu, S. Liu, U. Bende-Michl, D. Waters, P. Leahy, P. Wilson, and A. W. Western (2018), Key factors influencing differences in stream water quality across space, Wires Water, 5(1), doi:ARTN e1260 10.1002/wat2.1260.

Marsha, A., E. A. Steel, A. H. Fullerton, and C. Sowder (2018), Monitoring riverine thermal regimes on stream networks: Insights into spatial sampling designs from the Snoqualmie River, WA, Ecol Indic, 84, 11-26, doi:10.1016/j.ecolind.2017.08.028.

McGuire, K. J., C. E. Torgersen, G. E. Likens, D. C. Buso, W. H. Lowe, and S. W. Bailey (2014), Network analysis reveals multiscale controls on streamwater chemistry, P Natl Acad Sci USA, 111(19), 7030-7035, doi:10.1073/pnas.1404820111.

Melack, J. M., A. C. Finzi, D. Siegel, S. MacIntyre, C. E. Nelson, A. K. Aufdenkampe, and M. L. Pace (2011), Improving biogeochemical knowledge through technological innovation, Front Ecol Environ, 9(1), 37-43, doi:10.1890/100004.

Meyer, J. L., W. H. Mcdowell, T. L. Bott, J. W. Elwood, C. Ishizaki, J. M. Melack, B. L. Peckarsky, B. J. Peterson, and P. A. Rublee (1988), Elemental Dynamics in Streams, J N Am Benthol Soc, 7(4), 410-432, doi:Doi 10.2307/1467299.

Neill, A. J., D. Tetzlaff, N. J. C. Strachan, R. L. Hough, L. M. Avery, H. Watson, and C. Soulsby (2018), Using spatial-stream-network models and long-term data to understand and predict dynamics of faecal contamination in a mixed land-use catchment, Sci Total Environ, 612, 840-852, doi:10.1016/j.scitotenv.2017.08.151.

Peterson, E. E., A. A. Merton, D. M. Theobald, and N. S. Urquhart (2006), Patterns of spatial autocorrelation in stream water chemistry, Environ Monit Assess, 121(1-3), 571-596, doi:10.1007/s10661-005-9156-7.

Peterson, E. E., et al. (2013), Modelling dendritic ecological networks in space: an integrated network perspective, Ecol Lett, 16(5), 707-719, doi:10.1111/ele.12084.

Post, C. J., M. P. Cope, P. D. Gerard, N. M. Masto, J. R. Vine, R. Y. Stiglitz, J. O. Hallstrom, J. C. Newman, and E. A. Mikhailova (2018), Monitoring spatial and temporal variation of dissolved oxygen and water temperature in the Savannah River using a sensor network, Environ Monit Assess, 190(5), doi:ARTN 27210.1007/s10661-018-6646-y.

Raymond, P. A., et al. (2013), Global carbon dioxide emissions from inland waters, Nature, 503(7476), 355-359, doi:10.1038/nature12760.

Rodriguez-Castillo, T., E. Estevez, A. M. Gonzalez-Ferreras, and J. Barquin (2019), Estimating Ecosystem Metabolism to Entire River Networks, Ecosystems, 22(4), 892-911, doi:10.1007/s10021-018-0311-8.

Scown, M. W., M. G. McManus, J. H. Carson, and C. T. Nietch (2017), Improving Predictive Models of In-Stream Phosphorus Concentration Based on Nationally-Available Spatial Data Coverages, J Am Water Resour As, 53(4), 944-960, doi:10.1111/1752-1688.12543.

Segura, C., D. Noone, D. Warren, J. A. Jones, J. Tenny, and L. M. Ganio (2019), Climate, Landforms, and Geology Affect Baseflow Sources in a Mountain Catchment, Water Resour Res, 55(7), 5238-5254, doi:10.1029/2018WR023551.

Vannote, R. L., G. W. Minshall, K. W. Cummins, J. R. Sedell, and C. E. Cushing (1980), River Continuum Concept, Can J Fish Aquat Sci, 37(1), 130-137, doi:DOI 10.1139/f80-017.

Ver Hoef, J. M., and E. E. Peterson (2010), A Moving Average Approach for Spatial Statistical Models of Stream Networks, J Am Stat Assoc, 105(489), 6-18, doi:10.1198/jasa.2009.ap08248.

Webster, J. R., and B. C. Patten (1979), Effects of Watershed Perturbation on Stream Potassium and Calcium Dynamics, Ecol Monogr, 49(1), 51-72, doi:Doi 10.2307/1942572.

Wetzel, R. G. (1995), Death, Detritus, and Energy-Flow in Aquatic Ecosystems, Freshwater Biol, 33(1), 83-89, doi:DOI 10.1111/j.1365-2427.1995.tb00388.x.

Chapter 1. Headwater catchments govern biogeochemistry in America's largest free-flowing river network

1.1 Abstract

Riverine chemistry reflects both watershed conditions and instream processing, both of which vary across river networks, yet little is known about the scales at which watershed features regulate biogeochemical constituents. We used spatial stream network (SSN) models to quantify both watershed and instream effects on streamwater constituents in the Kuskokwim River (western Alaska), the largest free-flowing river in the US. We assessed chemical constituents spanning from labile nutrients (nitrate [NO_3], orthophosphate [PO_4]) to biologically and chemically conservative tracers (calcium [Ca], strontium [Sr], Sr isotopes [$^{87}Sr/^{86}Sr$]). We also examined the behavior of dissolved organic carbon (DOC) relative to these constituents to understand whether bulk DOC behaved conservatively in a large boreal river network, where future changes in DOC and nutrient loading are expected under a shifting climate. We derived watershed spatial covariates comprising landcover, geology, and geomorphic characteristics at 14 different spatial scales based on stream order and relative to sampling position in the river network to understand the effect of distant and proximal watershed controls on streamwater constituents. For all constituents but $^{87}Sr/^{86}Sr$, watershed features in low order headwater catchments yielded the best predictive ability for streamwater constituent concentrations across the entire network. Spatial structuring in streamwater constituents indicated that bulk DOC behaved conservatively, whereas NO_3 and PO_4 exhibited spatial patchiness indicative of more rapid instream processing. Our results have implications for understanding lentic nutrient cycling

at river basin scales, and for the management of headwater streams, which are important contributors to network-wide biogeochemical constituents supporting aquatic food webs.

1.2 Introduction

The chemical conditions in rivers reflect both watershed features (Bormann & Likens, 1967) and instream processing (Webster & Patten, 1979). Streamwater constituents including dissolved organic carbon (DOC) and inorganic nutrients (e.g., nitrate [NO_3], orthophosphate [PO_4]) are key factors controlling the productivity of riverine food webs (Meyer *et al.*, 1988). Spatial patterns in these constituents influence the distribution and productivity of aquatic biota, which in turn modify streamwater biogeochemical patterning to downstream reaches (Meyer *et al.*, 1988; Vannote *et al.*, 1980). As water and its chemical constituents flow through dendritic river networks, processes of instream uptake and tributary mixing generate spatial heterogeneity in constituents across the network. Understanding the balance of watershed versus instream controls on biogeochemical variability throughout river networks would improve our ability to manage the diverse conditions that support healthy aquatic ecosystems, yet relatively few studies (Abbott *et al.*, 2018; Creed *et al.*, 2015; Shogren *et al.*, 2019; Zimmer *et al.*, 2013) have examined how watershed controls operate across the continuum of scales that characterize river networks, or have documented the spatial patterns in chemical constituents that lie along a reactivity gradient (i.e. from labile nutrients to more conservative elements such as calcium). Streamwater constituents that have low biological demand (e.g., Sr, calcium [Ca]) or chemical reactivity generally behave as conservative indicators of watershed geophysical properties (Brennan *et al.*, 2016; Hogan & Blum, 2003). Watershed controls on streamwater chemistry

include topography, geology, hydrology, land cover, and soil properties (Lintern *et al.*, 2018), which vary across a range of spatial scales within watersheds. These watershed controls can be grouped broadly into three main effects: source variation (e.g. bedrock geology), mobilization constraints (e.g. weathering, solubility), and delivery to the river network (e.g. hydrologic connectivity), (Granger *et al.*, 2010). Of these effects, source variation can be quantified using publicly available geospatial datasets, from which physical features that affect delivery processes (e.g. slope, connectivity) can also be inferred. For example, 70.5% of variation in Sr isotope ratios ($^{87}Sr/^{86}Sr$) in a large Alaskan river network was explained using a spatial stream network model(Peterson & Hoef, 2010; Ver Hoef & Peterson, 2010) with geologic cover, watershed relief, and historic glacial extents, and much of the additional variation (22.9%) was accounted for by spatial autocovariance associated with downstream transport and mixing of source waters (Brennan *et al.*, 2016).

Instream processing of labile constituents may result in spatially patchy constituent concentrations that are difficult to quantify using watershed features alone (Gooseff *et al.*, 2008; McGuire *et al.*, 2014; Peterson *et al.*, 2001). Nutrients like NO_3 and PO_4 whose availability often limits biological activity in rivers have a wide range of spiraling lengths (0.08 – 4.92 km and 0.02 – 61 km, respectively), which generally increase with stream order (Ensign & Doyle, 2006). Streams with rapid nutrient uptake tend to exhibit stronger spatial autocorrelation in concentrations at fine spatial scales and random or patchy autocorrelation at broader scales (Dent & Grimm, 1999; McGuire *et al.*, 2014; Peterson *et al.*, 2001). This fine scale heterogeneity is governed by numerous factors, including constituent concentration (Casas-Ruiz *et al.*, 2017; Teodoru *et al.*, 2009), leaching or decomposition (Kaplan & Bott, 1982; Meyer, 1990), diel changes in algal production or microbial transformations (Jankowski & Schindler, 2019; Kaplan

& Bott, 1982), photolysis (Blaen *et al.*, 2016), and groundwater and riparian inputs (Dick *et al.*, 2015). Because these processes are challenging to quantify at the network scale, leveraging spatial autocorrelation to analyze patterns in labile constituents may offer improvements over models employing only aggregate watershed features (Peterson *et al.*, 2006).

The spatial scale at which watershed features are quantified, and instream sampling distance and frequency also influence interpretations of ecological or biogeochemical processes shaping streamwater constituents (Loreau *et al.*, 2013; McGuire *et al.*, 2014; Wiens, 1989). Watershed landscape *composition* provides information on the relative or absolute amounts of watershed features, while watershed landscape *configuration* provides information on where those features are relative to one another or relative to a point of interest such as a sampling location in the river channel. Dendritic river networks have a nested hierarchical spatial arrangement, and linkages between watershed composition, configuration, and instream conditions are scale-dependent (Hunsaker & Levine, 1995). Understanding how landscape features across a watershed influence instream biogeochemistry throughout river networks thus necessitates quantifying watershed conditions at a range of scales.

Most studies examining instream processing are conducted within a channel reach, or via comparison of multiple reaches (Gooseff *et al.*, 2008; Lintern *et al.*, 2018) and watershed effects are often coarsely quantified at the aggregate watershed scale in terms of watershed composition. Few studies have evaluated the watershed position or configuration of these controls at the network scale (Abbott *et al.*, 2018; Shogren *et al.*, 2019). Gergel *et al.* (1999) showed the importance of total watershed wetlands versus riparian buffer wetland cover in determining instream DOC, and more recent work found that headwater bedrock outcrops may be substantial sources of calcium, magnesium, and silica minerals (Ingri *et al.*, 2005) to downstream sites.

Much of the existing research examining nutrient delivery to stream networks has focused on the extent of agricultural, industrial, or urban land uses and their proximity to streams, with limited work in pristine river systems (see Lintern et al., 2018).

Low gradient riparian zones adjacent to stream channels often have elevated terrestrial organic matter accumulation and higher potential for biogeochemical transformations. Some work has shown that riparian zones thus have disproportionate effects on stream chemistry relative to the broader watershed or upland conditions (e.g. Dick et al., 2015), whereas other work has shown that carbon and nutrient concentrations are best explained using whole watershed characteristics (Andersson & Nyberg, 2008; Varanka & Hjort, 2016). In boreal stream networks the majority (90%) of hydrologic connectivity between low gradient riparian zones and stream channels occurs in low order headwaters (Ledesma *et al.*, 2018) that are often characterized by rich organic soils, however to our knowledge no study has examined the effects of headwater versus higher order catchment features on stream biogeochemistry across an entire boreal river network. Recently developed spatial stream network (SSN) models (Peterson & Hoef, 2010; Ver Hoef & Peterson, 2010) leverage spatial correlation among observations and partition instream variance among watershed controls and downstream mixing and transport. This modeling approach provides a framework for studying the balance of watershed versus instream controls on streamwater constituents. Here we use SSNs to examine spatial controls on constituents ranging from what we expect to be highly labile (NO_3, PO_4) to highly conservative (Sr, Ca), and hypothesize that DOC is controlled by watershed features at scales intermediate to these constituents. We quantify watershed effects on streamwater constituent concentrations across multiple spatial scales according to stream order, while simultaneously accounting for spatial correlation in observations. In doing so, we identify the network spatial scales at which

watershed features control streamwater constituents, and quantify the relative importance of watershed and instream controls.

1.3 Study Area

1.3.1 *Watershed overview*

We conducted this study in the Kuskokwim River, a large (124,000 km^2) free-flowing, boreal river basin in western Alaska. The study region includes 54,000 km of channel length (2^{nd} order and larger, Figure 1.1), with sample sites spanning 2nd – 8th order streams. The Kuskokwim River is the largest free-flowing river in the US and spans from headwaters in the Kuskokwim Mountains and glacially influenced tributaries of the Alaska Range (3550 m) to its outlet in Kuskokwim Bay on the Bering Sea (0 m), with a mean discharge of 1897 m^3 sec^{-1} (U.S. Geological Survey, 2018).

1.3.2 *Watershed morphology*

The Kuskokwim has a complex watershed with a heterogeneous geomorphologic template overlain by a mosaic of land cover types, including high elevation barren mountain ranges and broad boreal lowlands, rolling hills, and wetlands (Fig 1a). Basin geology reflects the progressive western growth of Alaska along the ancestral North American continental margin from the Precambrian to the early Cenozoic (Colpron *et al.,* 2007)(Colpron et al., 2007). The geologic evolution of the watershed results in a strong east-west gradient in Sr isotopic signatures and Ca and Sr weathering patterns across the Kuskokwim basin (Brennan *et al.,* 2014). Several major

tributaries draining the Alaska Range carry high silt loads from glacial headwaters to the mainstem. Low-lying regions are predominantly overlain by Quaternary surficial deposits of glacial, alluvial, colluvial, and eolian origin and thick layers of organic material associated with peatlands and permafrost (Fernald, 1960). Braided alluvial channels span much of the piedmont, with meandering river floodplains in the lowlands.

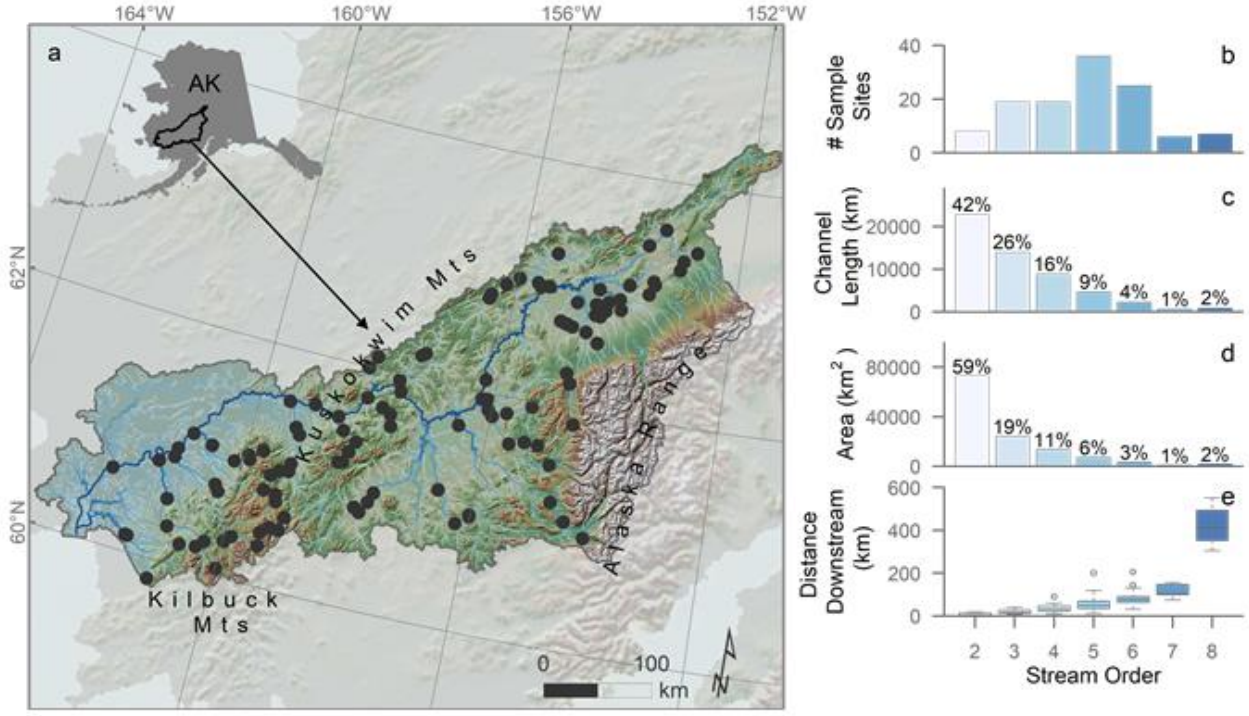

Figure 1.1. Map of the Kuskokwim River watershed study area and sampling locations (a), and sample counts by stream order (b). Total channel length (c) and watershed area (d) within each stream order, and average downstream distance traveled from headwaters to each sample site based on each sample site's stream order (e).

1.3.3 *Watershed land cover*

Land cover within the Kuskokwim maps closely to the geomorphic template, comprising barren rock, snow, and glaciers in mountainous regions, mixed shrub and dwarf shrub in subalpine

areas, wet and dry-type tundra, and mixed deciduous-evergreen forest in riparian corridors and lowlands below 600 m elevation (Fernald, 1960; U.S. Geological Survey, 2016). Wetlands dominate the low-lying western portion of the watershed at the Yukon – Kuskokwim delta and the low-relief interior between the Kuskokwim Mountains and Alaska Range to the north and east (U.S. Geological Survey, 2016). Modern peat soils are widespread in these bogs and adjacent lowlands, underlying muskeg vegetation, and variable soil types are mapped in higher relief areas (Fernald, 1960; Rieger *et al.*, 1979). Discontinuous, sporadic, and isolated permafrost occur throughout the watershed beginning at shallow depths of 0.5 – 2 m, with patches of continuous permafrost in upper reaches of the Tonzona River and Swift Fork (Fernald, 1960) (Jorgenson *et al.*, 2008).

1.3.4 *Watershed climate*

Climate generally varies with elevation and latitude in the Kuskokwim. Modeled mean annual precipitation ranges from 36 cm in the lowlands to 296 cm in the Alaska Range and Kilbuck Mountains (Scenarios Network for Alaska and Arctic Planning (SNAP), 2017a). High altitude areas receive greater precipitation in the form of snow during the winter months, and summer rainfall from late July through August spans much of the watershed. As such, the hydrograph in the lower Kuskokwim peaks with snowmelt in late spring, followed by a smaller secondary peak in August (U.S. Geological Survey, 2018). Mean summer temperatures in the watershed are lowest in the mountains (-1.9 °C) and generally increase with latitude in the lowlands, with the highest mean summer temperatures (15.9 °C) in the North Fork Kuskokwim (Scenarios Network for Alaska and Arctic Planning (SNAP), 2017b).

1.4 Methods

Water samples were collected throughout the Kuskokwim watershed at sites spanning a range of stream orders (2^{nd} – 8^{th}) and major geomorphic and landcover types. We measured concentrations of a suite of streamwater constituents and evaluated spatial structuring in these constituents in terms of distance traveled from headwaters, by stream order, and using empirical semivariograms. We constructed SSN models for each constituent across a range of spatial scales. We then compared the performance of models across spatial scales to assess where watershed controls best explained instream biogeochemical conditions. We also compared the relative effects of watershed versus instream controls using SSN model variance composition for each constituent to evaluate differences between labile and conservative solutes.

1.4.1 *Sample collection*

Water samples were collected in July and August of 2017 at 120 sites distributed across the Kuskokwim watershed to maximize coverage of major landcovers and stream orders (Fig. 1.1b). At each sample site water was collected from the channel thalweg or at the maximum wadable depth, facing upstream of the collector after allowing channel bed disturbance to settle-out or mobilize downstream. Samples for DOC and nutrients (NO_3, NO_2, PO_4) were syringe filtered through a 0.45 μm surfactant-free cellulose acetate (SFCA) filter after rinsing the syringe 3 times with sample water. DOC samples were filtered into 40 mL carbon-clean glass vials, and nutrient samples were filtered into acid-cleaned high density polyethylene (HDPE) bottles. Water samples for trace elements (Ca, Sr) and Sr isotope analysis were collected into acid-cleaned, low density polyethylene (LDPE) bottles after three rinses with sample water and filtered through a polyethylene Luer-lock syringe filter (0.45 μm polypropylene membrane) into acid-washed 125

ml LDPE narrow-mouth bottles within 48 hours of collection (Brennan *et al.*, 2014). All samples were stored in dark and cold conditions until analysis. To evaluate consistency in field collection methods, field triplicates were collected at 5 of the sample sites. Field-related contamination was evaluated through collection of 5 blank samples using the same methods described above for samples, but with NANOpure de-ionized water (type I, 18.0 MΩ).

1.4.2 *Sample analyses*

1.4.2.1 *DOC analyses*

Water samples for DOC were prepared and analyzed in a clean environment at the University of Washington Marine Chemistry Laboratory (UWMCL) following EPA standard method 5310 B-00 (www.standardmethods.org) and protocols detailed in UNESCO (1994). [DOC] was analyzed on a Shimadzu TOC-Vcsh carbon analyzer (Shimadzu Scientific Instruments, Kyoto, Japan), using the high temperature catalytic oxidation method and measured on a non-dispersive infrared detector. Water samples were acidified with 6N HCl to remove interference by carbonates and bicarbonates and sparged to remove volatile organics prior to analysis. Potassium hydrogen phthalate was used as the C standard. The limit of detection (LoD) for these analyses was estimated at 20.0 μg L^{-1}. Blank sample measurements were all below the LoD and analytical precision (2SE [standard error]) between triplicate samples was ± 30.0 μg L^{-1}.

1.4.2.2 *Nutrient analyses*

Nutrient samples were analyzed at the UWMCL following the methods detailed in UNESCO (1994) and EPA standard methods 353.4-2-199 (NO_3), 353.4-2-1997 (NO_2), and 365.5-1.4-1997 (PO_4, www.epa.gov/nerl). All nutrients were analyzed using segmented continuous flow

colorimetry on a SEAL AA3 (SEAL Analytical, Norderstedt, Germany). Standards of known nutrient concentrations and blanks were analyzed at the start and end of all sample batches. LoDs were 4.0, 2.0, and 0.4 μg L^{-1} for NO_3, NO_2, and PO_4, respectively. All blank measurements (n = 8) were below LoDs, and analytical precision between triplicate samples was ± 0.25, 0.02 and 0.09 μg L^{-1} for NO_3, NO_2, and PO_4, respectively.

1.4.2.3 *$^{87}Sr/^{86}Sr$ analyses*

Water samples for $^{87}Sr/^{86}Sr$ analysis were acidified using 2 ml ultra pure concentrated HNO_3 (BDH Aristar Ultra) in a clean laboratory environment at the University of Utah Department of Geology and Geophysics inductively coupled plasma mass spectrometry (ICPMS) laboratory within two weeks of sample collection. $^{87}Sr/^{86}Sr$ ratios of sample water were determined using multi-collector (MC) ICPMS (Thermo Scientific, High Resolution NEPTUNE, Bremen, Germany). During these analyses, the $^{87}Sr/^{86}Sr$ ratio of the standard reference material SRM987 (NIST; www.nist.gov) was determined to be 0.71028 ± 0.00001 (2σSE). The $^{87}Sr/^{86}Sr$ ratios were corrected for mass bias using an exponential law, normalizing to $^{86}Sr/^{88}Sr = 0.11940$ (Steiger & Jager, 1977). Isobaric interferences (e.g., ^{87}Rb and ^{86}Kr on ^{87}Sr and ^{86}Kr, respectively) were corrected by simultaneous monitoring of ^{85}Rb and ^{83}Kr using the corresponding assumed invariant ratios $^{87}Rb/^{85}Rb = 0.38571$ and $^{86}Kr/^{83}Kr = 1.50252$ (Steiger & Jager, 1977). Analytical precision (2SE) of field triplicates was determined to be ± 0.00002, and analytical precision of all water samples ranged from ± 0.000004 – 0.00002.

1.4.2.4 *Elemental analyses*

Water samples for Ca and Sr analysis were acidified using 2 ml ultra pure concentrated HNO_3 (BDH Aristar Ultra) in a clean environment at the University of Utah ICPMS laboratory within

two weeks of sample collection. Major and trace element concentration analyses were conducted using an Agilent 7500ce ICPMS (Agilent Technologies, Santa Clara, CA, USA). Samples were diluted 4:1 with 2.4% ultra pure HNO_3 (BDH Aristar Ultra) and Indium (In) at a concentration of 25 ng mL^{-1} was added as an internal standard. [Sr] and [Ca] were determined using a six-point calibration curve. The standard reference material SRM 1343e (NIST) was analyzed after every 30 samples (n = 4) as an external consistency standard. During our analyses, we determined the [Sr] and [Ca] in SRM1343e to be within 3.2% and 3.6% of their respective mean reported reference values. Precision of field triplicates was ± 0.88 μg Sr L^{-1} and ± 170 μg Ca L^{-1}. Measures of [Sr] and [Ca] in field blanks were both below LoDs (maximum LoDs of all runs were 0.60 μg Sr L^{-1} and 1030 μg Ca L^{-1}, respectively).

1.4.3 *Statistical analysis*

We used a statistical modeling approach that includes spatial covariates for watershed features and accounts for spatial autocorrelation among sampling sites throughout the Kuskokwim River based on flow connectivity, flow magnitude, and flow direction (Ver Hoef & Peterson, 2010) to understand how biogeochemical constituents were transported throughout the river network. This approach allowed us to partition variance in streamwater constituents among watershed and instream controls.

We first used empirical semivariograms to identify spatial relationships among sample sites and evaluate the range at which spatial covariates might be important (McGuire *et al.*, 2014). We then fit spatial models for each streamwater constituent throughout the network using spatial watershed covariates derived at 14 different spatial scales based on stream order (Fig. 1.2). Model performance for each constituent was assessed across a range of spatial scales to identify

the network position or extent of watershed controls on streamwater constituents. The relative importance of instream versus watershed controls was then compared across streamwater constituents ranging from labile (e.g., PO_4) to biogeochemically conservative (e.g., Sr).

1.4.3.1 *Empirical semivariograms*

Empirical semivariograms show the strength of spatial correlation between sites across a range of distances (Olea, 1994), and observed patterns can yield insights into the spatial structure of ecological or biogeochemical processes governing streamwater constituents (McGuire *et al.*, 2014). Distance in a semivariogram is traditionally measured as the Euclidean, or straight line, distance between two sample points (Matheron, 1963). For data on stream networks, and especially for streamwater constituents where downstream transport and processing are important (Closs *et al.*, 2004), hydrologic distance between sites sharing flow (flow connected) is often a more meaningful spatial dimension for assessing spatial structure (Cressie *et al.*, 2006; Ganio *et al.*, 2005; Peterson *et al.*, 2006). We compared semivariance in both Euclidian and hydrologic spatial dimensions to examine watershed and instream controls on spatial structuring in streamwater constituents using:

$$\gamma(h) = \frac{1}{2|N(h)|} \sum_{N(h)} \left(z_i - z_j\right)^2 \qquad (1)$$

Where γ is semivariance, N(h) is the set of all pairwise distances i – j = h, |N(h)| is the number of distinct pairs in N(h), and z_i and z_j are data values at spatial locations i and j, respectively (Matheron, 1963). We used a maximum separation distance of 1200 km, 40 lag bins, and a minimum of 15 point pairs per lag bin in semivariance computations. Semivariograms for stream constituents were compared in terms of general trends in both Euclidian and hydrologic spatial dimensions, range (distance of asymptote or peak in semivariance), nugget (variance at finest

spatial scale), and nested spatial structures as denoted by inflection points in the data (McGuire *et al.*, 2014; Rossi *et al.*, 1992).

1.4.3.2 *Spatial stream network models*

We used SSNs to analyze streamwater constituent concentrations that differ in their expected biological lability (DOC, NO_3+ NO_2, PO_4, Ca, and Sr) and $^{87}Sr/^{86}Sr$ ratios for all sites sampled (n = 120). These models are described in detail elsewhere (Peterson & Hoef, 2010; Ver Hoef *et al.*, 2006; Ver Hoef & Peterson, 2010). In brief, SSNs explicitly account for complex relationships within a stream network, including flow direction, longitudinal connectivity, and flow magnitude. SSNs provide flexible covariance structures for stream data and leverage spatial autocorrelation among sample sites to improve model performance (Peterson *et al.*, 2006; Peterson *et al.*, 2007). Covariance is determined via both hydrologic and Euclidean distance. Spatial relationships among sites are incorporated into covariance matrices via moving average spatial autocorrelation functions (Ver Hoef & Peterson, 2010).

We used a mixed-effects modeling framework in which the observed variance in a constituent across the river network (e.g. [DOC]) is explained by a set of watershed spatial covariates modeled as fixed effects (e.g., % bog cover and basin slope), and the spatial covariance matrices as random effects. The general form of the spatial linear mixed model is:

$$y = X\beta + z_H + z_E + \epsilon, \qquad (2)$$

Where y is the vector of a response variable (e.g. [DOC]), X is a matrix of covariates (e.g. % bog cover), β is a vector of parameters for each covariate in X, and z_H, and z_E are vectors of random variables with hydrologic (flow connected) and Euclidean correlation structures, respectively; ϵ is a vector of independent random errors.

Autocovariance functions for flow-connected relationships within the SSNs require a spatial weight or segment proportional influence (SPI) to inform how the moving average function behaves at stream confluences (Ver Hoef *et al.*, 2006). We derived SPI based on watershed area and precipitation amount as a proxy for stream flow. To estimate stream flow proportional to watershed area, we used gridded decadal mean annual precipitation (Table S1.1) throughout the entire Kuskokwim basin and accumulated all grid cells upstream of each stream segment using the Spatial Toolbox for the Analysis of River Systems (STARS) toolbox in ArcGIS (Peterson & Hoef, 2014). Flow accumulation and a synthetic channel network for input to the SSNs were derived from a digital elevation model (DEM) extracted from the USGS National Elevation Dataset.

1.4.3.3 *Spatial covariates*

Potential spatial watershed covariates for each streamwater constituent were compiled using the STARS toolbox and publicly available geospatial datasets (Table S1.1) (Peterson & Hoef, 2014). To compare covariate effect sizes in final models, all covariates were standardized to a mean of 0 and standard deviation of 1. A set of *a priori* candidate models was developed for each streamwater constituent with spatial covariates selected based on predictors for other study systems and factors which we hypothesized to affect streamwater constituents. A complete list of spatial covariates used in candidate model development is in Table S1.1 of the supplementary materials.

For all constituents, modeled mean annual precipitation, watershed slope, and watershed relief were included in candidate models as these watershed features are expected to affect the movement of water and solutes from uplands to the stream channel (Lintern *et al.*, 2018; Smits *et*

al., 2017). We expected positive correlations between DOC and features related to the accumulation of soil organic matter, such as low basin relief, peat bogs, and wetland areas (e.g. (Agren *et al.*, 2014; Gergel *et al.*, 1999; Laudon *et al.*, 2011; Mulholland, 1997; Varanka *et al.*, 2015). Because no complete wetland inventory is available for the entire Kuskokwim watershed, we used separate geospatial datasets for peat bogs, open water wetlands, marshes, and spruce forest swamps (Table S1.1).

NO_3 and NO_2 (hereafter referred to as 'NO_3') were pooled for each site and modeled together. Candidate models for NO_3 included alder (*Alnus* spp.) plant cover, which has been shown to influence NO_3 concentrations in Alaskan streams (Callahan *et al.*, 2017; Hiatt *et al.*, 2017; Shaftel *et al.*, 2012). NO_3 is also negatively correlated with DOC in some Alaskan watersheds (Harms *et al.*, 2016), with steeper basins having higher NO_3 and lower DOC (Rodriguez-Cardona *et al.*, 2016; Walker *et al.*, 2012). This is likely related to both shorter residence times limiting nitrogen transformations in steeper basins and organic matter accumulation and soil saturation fueling microbial denitrification and N-limitation in lower relief basins. DOC measurements were included in candidate models for NO_3 and PO_4 to evaluate this relationship in the Kuskokwim.

Ca, Sr, and PO_4 are generally influenced by rock weathering in high relief areas where bedrock exposures correspond with mechanical weathering and higher precipitation, and $^{87}Sr/^{86}Sr$ are strongly correlated with surface geology and precipitation in much of western Alaska (Bataille *et al.*, 2014; Brennan *et al.*, 2019; Brennan *et al.*, 2015). Surface geology was simplified into 12 major groups based on lithology type and age from the Global Lithological Map database (Hartmann & Moosdorf, 2012). *A priori* candidate models for PO_4 included apatite-bearing

geology types and candidate models for Ca and Sr included mafic and calcareous lithologies, predominantly within mixed sedimentary classes.

1.4.3.4 *Spatial Scaling*

Watershed covariates upstream of each sample site were quantified at 14 different nested spatial scales (Fig. 1.2). We derived watershed covariates in a reverse nested spatial scaling by including only watershed characteristics for the local catchment area draining to the sample site between stream confluences, and then iterating upstream to include contributing areas based on the sample site's stream order, the site's stream order and drainages for stream order -1, stream order – 2, and so forth until the entire upstream drainage was accounted for (Fig. 1.2, A -E). We also derived watershed attributes in a downstream direction by including only 2^{nd} order stream basins, 2^{nd}-3^{rd} order basins, 2^{nd} – 4^{th} order, 2^{nd} – 5^{th} order, 2^{nd} – 6^{th} order, 2^{nd} – 7^{th} order, 2^{nd} – 8^{th} order, and all stream orders (Fig. 1.2, F – J). In doing so, we evaluate the effect of small, low order stream catchments on downstream biogeochemical conditions. By evaluating the effect of watershed covariates across both upstream and downstream spatial scales, we quantified the effect of local and distant watershed features on streamwater constituents at each sample point in the Kuskokwim network.

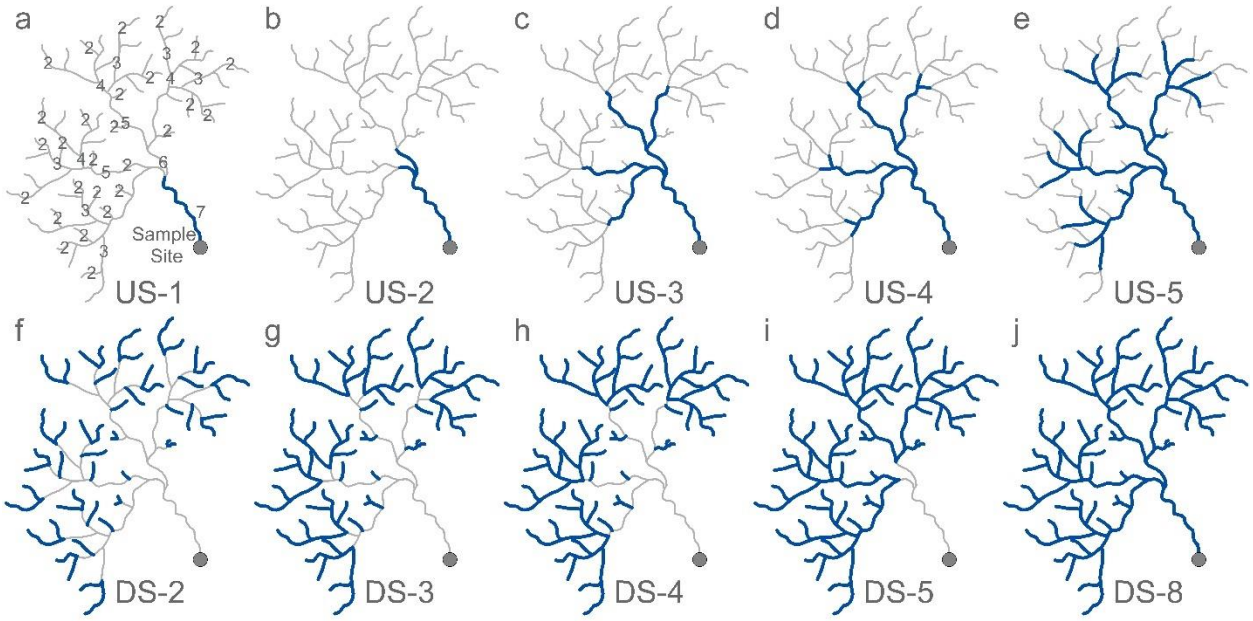

Figure 1.2. Diagrams of spatial scaling approach for deriving watershed attributes by stream order moving upstream (a-e) and downstream (f-j). Upstream (US-) scaling begins with local watershed attributes at a sample site, and iterates upstream by one stream order for each scale. Downstream (DS-) scaling begins with 2nd order streams and iterates downstream by one stream order for each scale.

1.4.3.5 *Model selection*

SSN model formulations were initially fit to univariate models using the SSN package in R (Ver Hoef & Peterson, 2010), with parameters for hypothesized predictor variables estimated using maximum-likelihood. For these model fits, all runs used the same random effect structure with exponential tail-up (flow-connected) and Euclidean spatial autocovariance components (Ver Hoef *et al.*, 2014). Univariate models for each stream constituent were compared using root mean square prediction error (RMSPE) derived from leave-one-out cross validation (LOOCV) predictions, and a spatial corrected Akaike information criterion (AIC_c) (Hoeting *et al.*, 2006).

This metric is similar to standard AIC, but penalizes models based on the number of parameters used to estimate the spatial autocovariance structure:

$$AIC_c = -2\backslash\ell_{profile} + 2\mathrm{n}\,\frac{p+k+1}{n-p-k-2} \qquad (3)$$

Where ℓ_{profile} is the profile log-likelihood function (Cressie, 1993), n is the sample size, $p - 1$ is the number of covariates, and k is the number of autocorrelation parameters.

Additional candidate predictor variables were then combined iteratively with the best performing univariate models in a stepwise fashion, and again selected using RMSPE and AIC_c. The best combination of predictor variables for each streamwater constituent was then used to parameterize the spatial autocovariance structures using restricted maximum likelihood estimation. We expected the spatial predictor variables (e.g., % bog) to capture the Euclidean spatial structure in our data and for instream processing and transport to comprise the flow-connected dimension. As such, we first fit models for each constituent using only the fixed effects and a flow-connected spatial dimension for the random error structure. We then computed empirical semivariance for the residual error to evaluate any remaining spatial structure in the Euclidean and flow-unconnected dimensions. For constituents with spatial structure in the residuals, we then tested different combinations of spatial autocorrelation functions in the flow-connected and Euclidean dimensions (e.g. exponential, Gaussian, linear with sill), (Ver Hoef & Peterson, 2010) and again used AIC_c to select the spatial autocovariance structure for each streamwater constituent. Residual semivariance was then computed to check for remaining spatial autocorrelation in the data. For comparison, we also parameterized models with only the predictor variables using non-spatial multiple linear regression.

1.4.3.6 *Streamwater constituent comparison*

The flexible covariance structures in SSN models are well-suited for evaluating the relative effects of instream processing and transport (flow-connected) and watershed factors mediating delivery of constituents from watershed to stream network by examining variance composition (Ver Hoef *et al.*, 2014; Ver Hoef & Peterson, 2010). Variance composition for SSN models is partitioned among the various autocovariance structures (e.g. Euclidian, flow-connected) and spatial covariates (e.g. bog area or watershed slope). Variance composition was determined for each constituent at each spatial scale, with the relative proportion of variance explained by autocovariance and spatial covariates compared across constituents and across spatial scales. In doing so, we compared the behavior of the constituents (e.g. conservative Sr vs. biologically reactive NO_3) and identified the spatial scales at which watershed features controlled each streamwater constituent.

1.5 Results

1.5.1 *Spatial structuring in streamwater constituents*

All streamwater constituents exhibited distinct spatial patterns across the Kuskokwim watershed, but the scales of these patterns varied by constituent and by spatial distance metric (e.g., stream order, Euclidian vs. hydrologic, Fig. 1.3). [PO_4], [NO_3], and [DOC] generally trended toward higher concentrations with distance downstream, whereas [Ca], [Sr], and $^{87}Sr/^{86}Sr$ generally trended toward watershed average values with distance downstream (Fig. 1.3a – f). Mean [PO_4] and [DOC] were lowest in 2nd order streams, and generally increased with stream order. [Sr] and [Ca] decreased from 2nd to 6th order streams, followed by increases in 7th and 8th order streams

(Fig 3g-1). Mean values for [NO_3] and $^{87}Sr/^{86}Sr$ showed no significant differences among stream orders, however mean $^{87}Sr/^{86}Sr$ was highest in 2nd order streams (Fig. 1.3l). Variation in constituent concentrations was generally greatest within the first 100-150 km of the stream network (Fig. 1.3a – f), corresponding with 2nd – 5th order channels (Fig. 1.1e, Fig. 1.3g – l). Constituent concentrations within 2nd order streams were less variable than all other stream orders, except for [NO_3] and $^{87}Sr/^{86}Sr$, which were least variable in 8th order sample sites. Semivariograms revealed distinct contrasts in the spatial structuring of different chemical constituents across the watershed (Fig 3m-r). Semivariance in [PO_4] had a large nugget (semivariance at shortest lag distance), indicating high variance among samples at the finest sampling distance, and exhibited nearly random spatial distribution (no clear trend in semivariance) in the flow-connected dimension (Fig. 1.3m). Within the Euclidian dimension, however, [PO_4] showed spatial autocorrelation (as exhibited by increasing semivariance with distance) with [PO_4] subject to multi-scale controls (exhibited by inflection points in Euclidian semivariance at approximately 200, 300, and 400 km lag distances).

[NO_3] exhibited flow-connected autocorrelation at distances up to 200 km and multi-scale Euclidian controls on [NO_3] were also evident via inflection points in semivariance at 100, 200, and 350 km (Fig. 1.3n). [DOC] were spatially autocorrelated in both Euclidian and flow-connected dimensions at short to medium lag distances; however, flow-connected semivariance generally exceeded that of Euclidian at mid-range lag distances (Fig. 1.3o), which was a pattern unique to the DOC semivariogram.

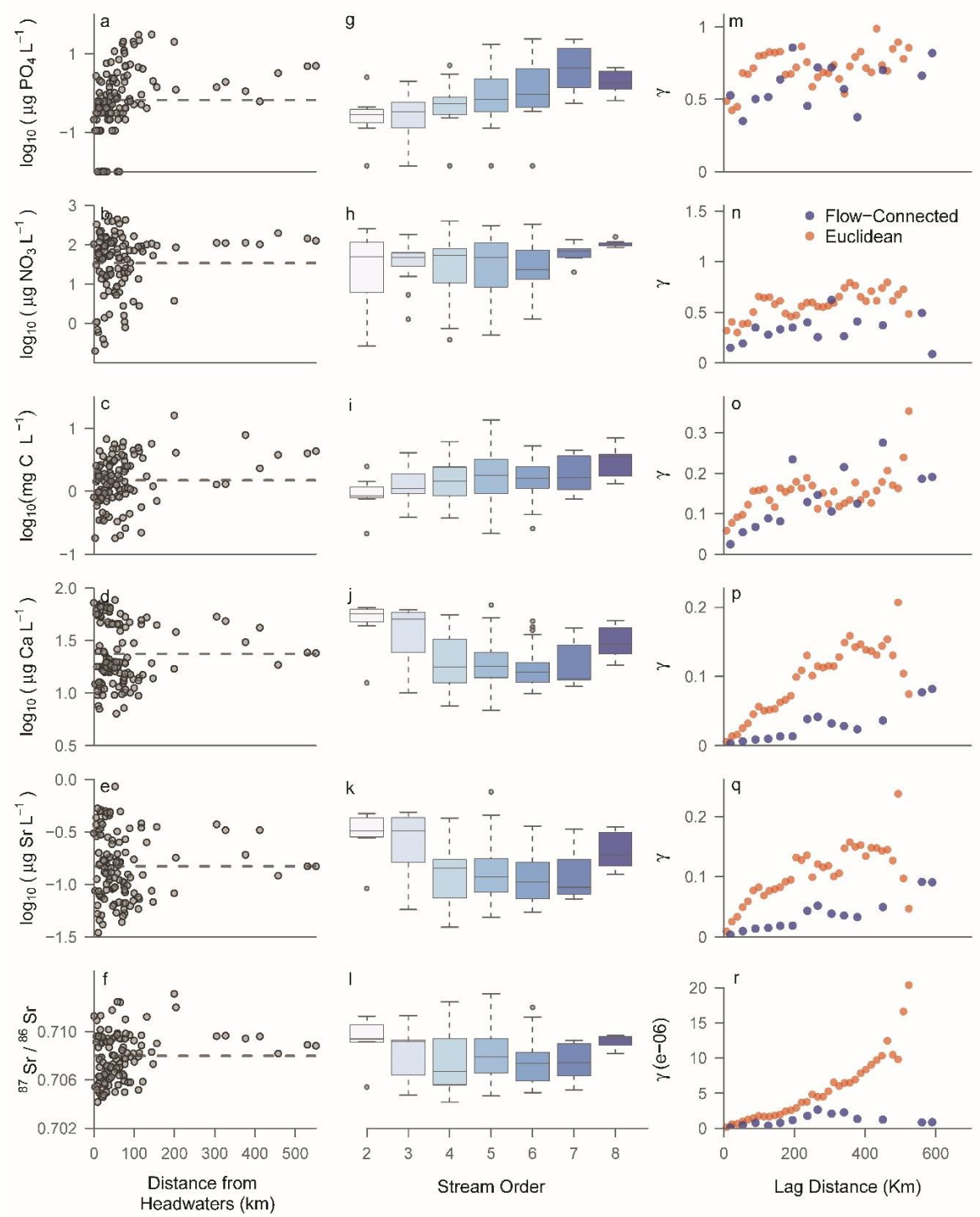

Figure 1.3. Changes in streamwater constituent concentrations with average distance from headwaters for each sample site (a-f), and constituent variation by stream order (g-l). Boxes in g-l include the interquartile range (IQR) and whiskers extend to 1.5 times the IQR from 1st and 3rd quartiles. Empirical semivariograms (m-r) are plotted based on flow-connected (blue) and Euclidian distance (orange).

Conservative constituents showed strong spatial autocorrelation, with broad-scale Euclidian and instream controls (Fig. 1.3p-r). Flow-connected semivariance for [Sr], [Ca], and $^{87}Sr/^{86}Sr$ increased up to 300 km, with declining semivariance for $^{87}Sr/^{86}Sr$ at distances beyond 300 km. Inflection points in flow-connected semivariance for both [Ca] and [Sr] occurred at 250 and 500 km. Euclidian semivariance increased to a range of approximately 350 km for [Ca] and 400 km for [Sr]. Euclidian semivariance for $^{87}Sr/^{86}Sr$ increased beyond the range of our sample sites.

1.5.2 *Watershed covariates governing streamwater constituents*

The best SSN models for streamwater constituents in the Kuskokwim River included covariates reflecting both broad- and fine scale watershed attributes (Fig. 1.4, Fig. S1.1, Table S1.2). For all constituents in our study, watershed controls could be grouped into three primary drivers: 1) watershed relief, 2) landcover shaped by watershed morphology, and 3) the Farewell Terrane geologic unit. Sample site constituent measures and significant spatial covariates are mapped in Figure S1.1.

The best model for $[PO_4]$ included covariates for the watershed portion overlain by the Farewell Terrane (β = -0.39), sample site [DOC] (β = 0.39), and the portion of the watershed overlain by mixed sedimentary rock (β = -0.18, Fig. S1.1a). PO_4 was the only constituent without watershed relief or mean watershed elevation in the best model; however, $[PO_4]$ was generally lower in the mountainous portions of the watershed (Fig. 1.4a).

NO_3 spatial patterns were patchier across the watershed, with highest concentrations in streams draining the lower slopes of the Alaska Range and in the central Kuskokwim. $[NO_3]$ was positively correlated with watershed relief but negatively correlated with mean watershed elevation (Fig. 1.4b). $[NO_3]$ was also strongly positively correlated with alder (*Alnus* spp.) plant

cover, and [NO_3] was best modeled using covariates for watershed alder (*Alnus* spp.) plant cover ($\beta = 0.29$), sample site [DOC] ($\beta = -0.14$), watershed latitude ($\beta = 0.05$), and mean watershed elevation ($\beta = -0.01$).

[DOC] was highest in low-gradient portions of the Kuskokwim, with streams draining the Alaska Range and Kuskokwim/Kilbuck Mountains generally having lower DOC (Fig. 1.4c). [DOC] was positively correlated with bogs, peat, and marshes; however, the best model for [DOC] included only mean watershed relief ($\beta = -0.19$) and watershed latitude ($\beta = 0.11$).

[Ca] and [Sr] in the Kuskokwim generally followed similar spatial patterns: high concentrations in portions of the Alaska Range coinciding with the Farewell Terrane and lower concentrations in the western watershed (Fig. 1.4d,e). [Sr] were also elevated in some portions of the Kilbuck mountains (Fig. 1.4e). The best model for [Ca] included watershed coverage by the Farewell Terrane ($\beta = 0.07$), acidic volcanic and plutonic rocks ($\beta = -0.04$), intermediate volcanic and plutonic rocks ($\beta = -0.04$), and mean watershed elevation ($\beta = 0.02$). [Sr] was best modeled by the Farewell Terrane ($\beta = 0.10$), intermediate volcanic and plutonic rocks ($\beta = -0.06$), acidic volcanic and plutonic rocks ($\beta = -0.06$), and mean watershed elevation ($\beta = 0.05$).

$^{87}Sr/^{86}Sr$ was highest in the northeastern portion of the Kuskokwim, with high values spanning the Farewell Terrane, and $^{87}Sr/^{86}Sr$ generally decreasing toward the western watershed (Fig. 1.4f). The best model for $^{87}Sr/^{86}Sr$ included the Farewell Terrane ($\beta = 0.0008$), watershed relief ($\beta = 0.0004$), watershed extent covered by the last glacial maximum ($\beta = -0.0003$), intermediate volcanic and plutonic rocks ($\beta = -0.0003$), and siliciclastic sedimentary rock units in the Kilbuck and Kuskokwim mountains ($\beta = -0.0003$, Fig. S1.1f).

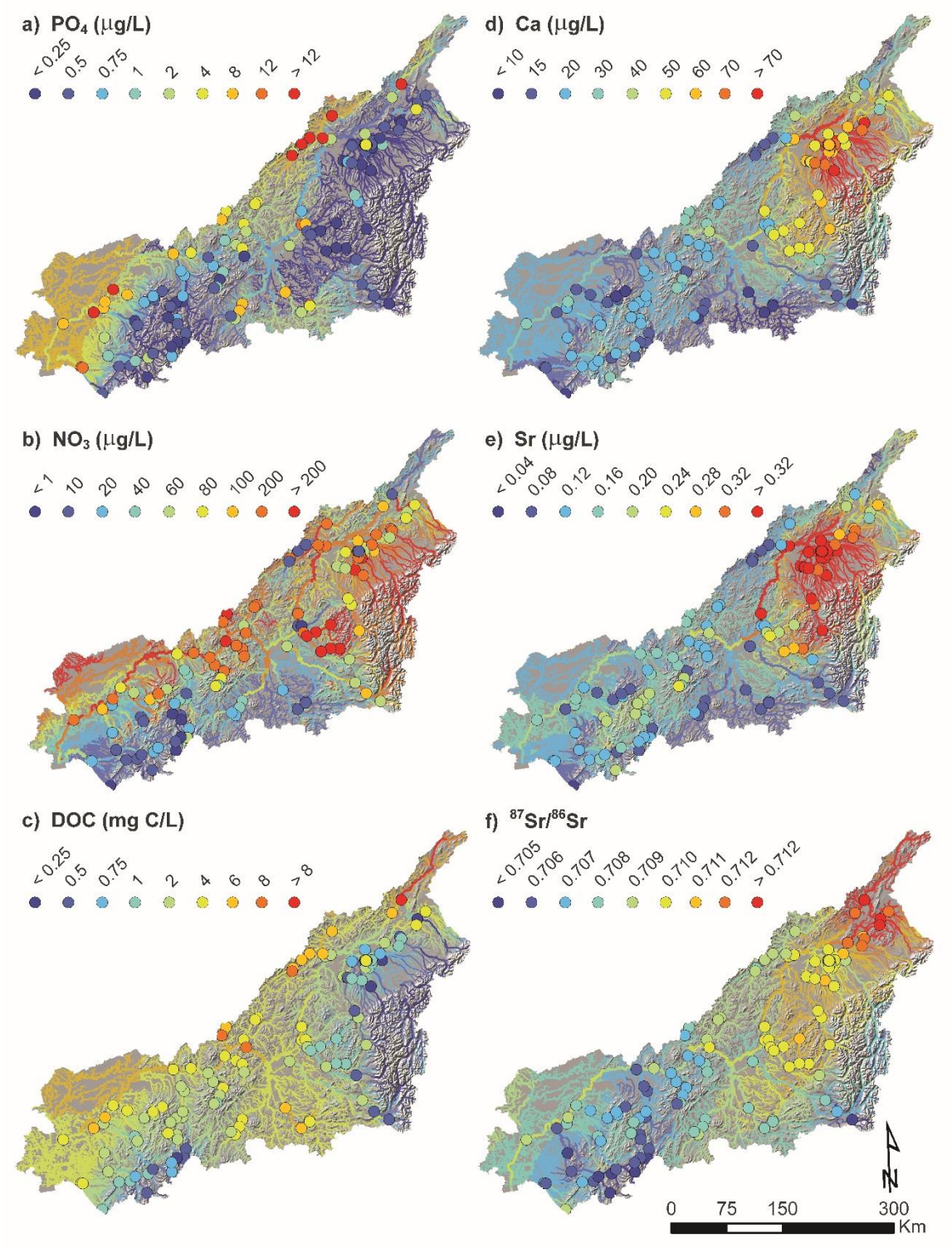

Figure 1.4. Watershed maps of streamwater constituent values at each sample point and spatial stream network model predictions for streamwater constituents for all 2nd-8th order channels in the Kuskokwim River.

1.5.3 *Variance decomposition across constituents and spatial scales*

For most of the constituents in our study, covariates derived at spatial scales emphasizing low order headwater stream catchments performed the best, with watershed covariates and instream spatial autocorrelation accounting for more of the overall variance for conservative versus labile constituents (Fig. 1.5). In general, watershed covariates for most constituents performed better as spatial scales moved in the upstream direction to include more of the headwaters and low order streams (Fig. 1.5a-f). Moving in the downstream direction, models accounting for 2^{nd} – 3^{rd} order streams generally performed best (Fig. 1.5g-l).

Models for [PO_4] had the lowest predictive power (mean LOOCV R^2 of 0.44) and the largest nugget effect among the constituents in our study (Fig. 1.5a,g). The nugget effect decreased with upstream scaling for PO_4. The best model for PO_4 was at scale DS-3 (Fig 1XX), and with the exception of DS-2, downstream scaled models for PO_4 had variance composition split roughly equally among nugget, Euclidian spatial autocorrelation, and watershed covariates.

NO_3 had better model performance than for PO4 (mean LOOCV R^2 of 0.71), with over 80% of explained variance in [NO_3] attributed to Euclidian spatial autocorrelation and minor fractions explained by flow-connected spatial autocorrelation, and watershed covariates (Fig. 1.5b,h). The best model for NO_3 used watershed covariates derived at spatial scale DS-2, accounting for 2^{nd} order streams only; however, models for NO_3 performed similarly across most spatial scales.

DOC models performed better when headwater areas were included, and the best model for DOC included only 2^{nd} and 3^{rd} order streams (DS-3, Fig. 1.5c,i). Mean model performance across all scales for DOC was comparable to NO_3, with a mean LOOCV R^2 of 0.70. Downstream scaling models for DOC had comparable predictive performance (mean LOOCV R^2 of 0.73). Watershed covariates and Euclidian spatial autocorrelation accounted for roughly one third and one half of

explained variance in [DOC], respectively, with flow-connected autocorrelation accounting for 12-22% of explained variance in [DOC].

Models for both Ca and Sr performed better when low order streams were included moving in the upstream direction, and the best model for both constituents was at DS-3, including just 2nd and 3rd order watershed conditions. Mean LOOCV R^2 was 0.88 for Ca and 0.84 for Sr. Euclidian spatial autocorrelation accounted for the majority of explained variance in both [Ca] and [Sr], with tail-up spatial autocorrelation accounting for an average of 10 and 14% of explained variance in [Ca] and [Sr], respectively. Fixed watershed effects accounted for roughly 22% of explained variance in both [Ca] and [Sr].

Models for $^{87}Sr/^{86}Sr$ had the highest explanatory power of the constituents in our study (mean LOOCV R^2 of 0.93, Fig. 1.5f,i). For $^{87}Sr/^{86}Sr$, the best model was at the US-4 spatial scale, however the top six models for $^{87}Sr/^{86}Sr$ had only minor differences in AIC_c and prediction error (Table S1.3). Euclidian spatial autocorrelation accounted for an average of 61% of explained $^{87}Sr/^{86}Sr$ variance across all spatial scales, tail-up autocorrelation accounted for 7.6%, and fixed effects accounted for 32% of explained variance.

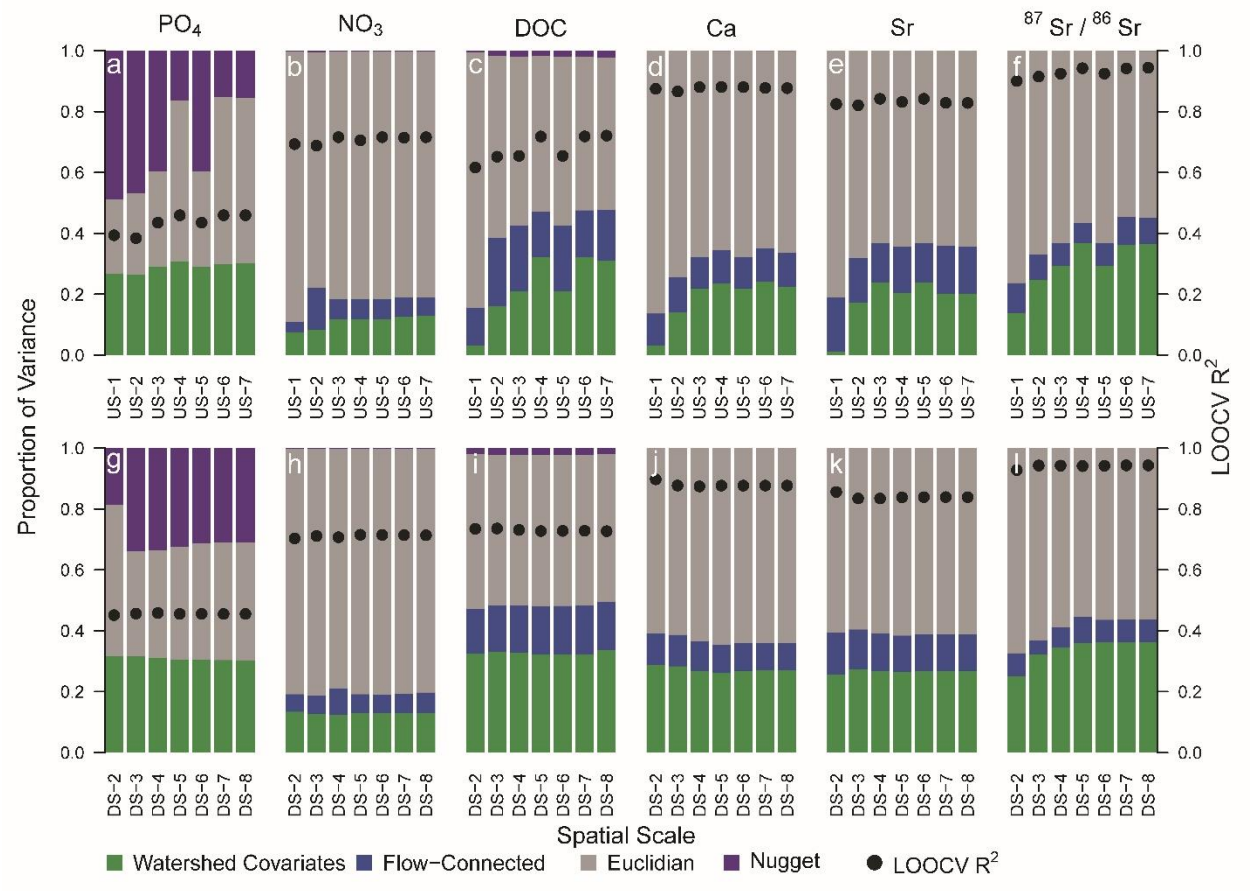

Figure 1.5. Variance composition and leave-one-out-cross-validation R^2 statistics (black dots) from spatial stream network models for all constituents across upstream (a-f) and downstream (g-l) spatial scales. Variance composition includes the proportion of overall variance explained by watershed effects (green bars), flow-connected spatial autocorrelation (blue bars), Euclidian spatial autocorrelation (grey bars), and the nugget or random error (purple bars).

1.6 Discussion

1.6.1 *Spatial structuring in streamwater chemistry throughout the river network*

Spatial structuring in streamwater chemical conditions across the Kuskokwim watershed revealed several differences in both watershed controls and instream behavior between the labile

(PO_4, NO_3, and DOC) and conservative (Ca, Sr, $^{87}Sr/^{86}Sr$) constituents in our study. These differences can be viewed in terms of variation with distance downstream (Fig. 1.3a-f), changes in mean concentration and variance across stream orders (Fig. 1.3g-l), and in empirical semivariograms derived using both Euclidian and hydrologic distance (Fig. 1.3m-r).

For all constituents we measured in the Kuskokwim, high chemical variation in the upper 100-150 km of stream channels highlights the importance of headwater and low order catchment conditions in governing biogeochemical heterogeneity across the river network. However, despite spatial heterogeneity at relatively fine scales, all constituent concentrations in the Kuskokwim trended toward the watershed average with distance downstream, with higher than average [PO_4], [NO_3], and [DOC] in the lower mainstem Kuskokwim sample sites. These trends toward watershed average values reflect flow-weighted contributions from a mixture of more variable, low order streams.

These results are consistent with previous work in other river systems showing greater biogeochemical variation among smaller catchments and decreasing variation at broader scales (Abbott *et al.*, 2018; Shogren *et al.*, 2019; Temnerud *et al.*, 2010; Temnerud *et al.*, 2007). In temperate rivers, Alexander *et al.* (2007) showed that NO_3 retention is highest in headwaters, governing downstream nutrient availability. Abbott *et al.* (2018) assessed variation in [DOC], [NO_3,] and [PO_4] in a range of nested catchment sizes, and showed significant reductions in biogeochemical variation at catchment areas of 18-68 km^2, with larger scale catchment patches (113-216 km^2) regulating more conservative constituents like chloride and fluoride. Similar work in northern Alaskan streams found smaller scale patch controls on instream DOC and NO_3 (3-21 km^2), but broader or non-significant patch sizes for PO_4, which was hypothesized to be driven by rapid instream uptake masking source signals (Shogren *et al.*, 2019).

For labile nutrients like PO_4 and NO_3, this pattern of variance collapse has been attributed to reduced nutrient uptake with increasing discharge, driven mainly by lower biological reactivity opportunity due to shorter residence times in larger channels (Marcé *et al.*, 2018; Mulholland *et al.*, 2009). This is contrary to previous work showing more rapid uptake and shorter spiraling lengths for NO_3 in larger channels (Ensign & Doyle, 2006). For DOC, variance collapse with increasing catchment area has been attributed to net gains of instream organic matter, due primarily to accumulation of allochthonous inputs along the network (Shogren *et al.*, 2019). Recent work in boreal headwaters suggests that terrestrial DOC inputs are passively transported in 1st to 4th order channels (Kothawala *et al.*, 2015), while other work shows that nearly half of labile terrestrial DOC from permafrost is metabolized instream within several weeks (Textor *et al.*, 2019). Increasing [DOC] along the Kuskokwim network may suggest that most DOC is simply transported through the river network with little instream processing. However, without measures of DOC composition, any instream processing of labile fractions is unknown. For the conservative tracers in our study, variance collapse and a trend toward watershed average values appears to reflect accumulation, transport, and mixing of heterogeneous landscape signals along the network. The spatial behavior of bulk DOC is largely consistent with these patterns. Patterns in constituent means and variance according to stream order also provide some evidence for rapid nutrient uptake in lower order streams, reduced uptake rates and longer spiraling lengths in larger streams, and the passive transport and mixing of the more conservative tracers (Fig. 1.3g-l). Increases in [PO_4] with stream order may be indicative of longer spiraling lengths in larger streams. This pattern was also shown in a meta-analysis of nutrient data across 1st -5th order streams (Ensign & Doyle, 2006). Their study also showed increased uptake and shortened spiraling lengths for NO_3 with increasing stream order. Rapid uptake may explain the lack of

significant differences in [NO_3] across stream orders in the Kuskokwim (Fig. 1.3h). [DOC] slightly increased across stream orders, providing additional support for relatively passive transport and accumulation of bulk DOC across the network.

Changes in [Ca], [Sr], and $^{87}Sr/^{86}Sr$ across stream orders were less pronounced, but likely reflected mixing of various tributaries draining broad scale geologic blocks and morphologic features across the network. Concentrations and $^{87}Sr/^{86}Sr$ values were generally highest in the low order streams, consistent with higher mechanical weathering and precipitation in the mountainous headwaters of the Kuskokwim (Brennan *et al.*, 2014). In the mid-size and large rivers, however, concentrations were more dilute and $^{87}Sr/^{86}Sr$ values were lower with increasing discharge (Fig. 1.3j,k). Average concentrations in the mainstem (8^{th} order) channel reflected a mixture of both concentrated headwater signals from the eastern watershed, the integration of signals from the central basin, and slightly elevated concentrations and enriched $^{87}Sr/^{86}Sr$ values from the Kilbuck mountains in the western Kuskokwim (Fig. 1.4d,e).

Semivariograms revealed multi-scale watershed and instream controls on the spatial structuring of chemical constituents across the Kuskokwim (Fig 3m-r). Contrasting Euclidian and flow-connected patterns in semivariance for each constituent can provide insights into watershed versus instream controls on instream biogeochemical constituents (McGuire *et al.*, 2014). Similarly, comparing semivariance patterns of labile versus conservative constituents can yield information on the behavior of one constituent relative to more- and less-reactive constituents. The lack of instream (flow-connected) spatial autocorrelation and a large nugget in semivariance for [PO_4] is consistent with instream cycling of PO_4 at substantially finer spatial scales than our sampling efforts(McGuire *et al.*, 2014). Inflection points at lag distances of roughly 200 and 400 km were also consistent with the broad-scale geologic features included in the best model for

PO_4 (Fig. S1.1a). Taken together with the broad-scale spatial patterns in [DOC] that were also included in the best model for PO_4, there appeared to be multi-scale watershed controls on [PO_4] in the Kuskokwim, whereas instream spatial structure was nearly random (zero slope in semivariance) across all lag distances. [NO_3] had stronger spatial autocorrelation in the flow-connected dimension up to a distance of roughly 200 km, which may indicate longer spiraling lengths for NO_3 in the Kuskokwim compared with PO_4, or the transport of various watershed signals and groundwater inflows (McGuire *et al.*, 2014).

[DOC] exhibited instream spatial autocorrelation at coarse scales up to 600 km, providing some additional support for the conservative transport of bulk DOC through the Kuskokwim network. Multi-scale structuring in Euclidian spatial autocorrelation for [DOC] was consistent with the scale of the geomorphic gradients that shape [DOC] in the Kuskokwim, such as transitions from high relief mountains to low-gradient peat and bog environments in the Kuskokwim lowlands. Finer scale spatial autocorrelation may reflect more local features such as wetlands or acidic peat soils that result in smaller patches of high [DOC] (McGuire *et al.*, 2014). Broad scale spatial dependence in [DOC] may be driven by the latitudinal trend we observed in the Kuskokwim (Fig. 1.4c).

[Ca], [Sr], and $^{87}Sr/^{86}Sr$ all exhibited strong spatial autocorrelation in both flow-connected and Euclidian spatial dimensions (Fig. 1.3p-r). Euclidian spatial dependence for [Ca] and [Sr] extended to a range of 300 km, which roughly coincides in scale with the alkaline Farewell Terrane and the neighboring Kuskokwim Group. $^{87}Sr/^{86}Sr$ Euclidian spatial dependence extended beyond the range of our sampling, despite strong correlation with the Farewell Terrane and other broad-scale geologic blocks in the Kuskokwim (Fig. S1.1f). Flow-connected or instream spatial dependence for the conservative constituents showed spatial autocorrelation at multiple scales

(250 and 500 km), which may reflect the inflows of major tributaries draining distinct geologic regions in the southern portion of the Kuskokwim basin (Fig. 1.1a, Fig. 1.4f). Several of these inflows in the central Kuskokwim have considerably lower concentrations and $^{87}Sr/^{86}Sr$ values than the Farewell Terrane and the Kilbuck mountains. These broad scale geologic differences likely also shaped the decline in $^{87}Sr/^{86}Sr$ semivariance beyond a range of 300 km, wherein $^{87}Sr/^{86}Sr$ variation increased from northeast to the west, then decreased again at the confluence of tributaries draining the Kilbuck mountains.

1.6.2 *Watershed features governing streamwater constituents*

Streamwater constituents in the Kuskokwim reflected both broad- and fine-scale watershed controls such as landcover and watershed geology in addition to covarying with DOC. With the exception of PO_4, watershed relief or elevation were either directly included in the best SSN models for all constituents, or indirectly included via landcover covariates or instream constituents (e.g. DOC) reflecting watershed geomorphology. The importance of watershed relief in regulating the movement of water, constituents and material between terrestrial and aquatic systems has been shown for many streamwater constituents across most ecoregions (Lintern *et al.*, 2018).

Watershed relief shaped the more labile constituents in the Kuskokwim, presumably by regulating catchment hydrology, the accumulation of organic matter, and nutrient transformations. High relief basins draining the Alaska Range and Kuskokwim/Kilbuck Mountains generally had lower [PO_4] and [DOC] and higher [NO_3]. [DOC] is typically positively correlated with wetlands and peat bogs in boreal river systems (Agren *et al.*, 2008; Laudon *et al.*, 2011; Mulholland, 1997) and peat bogs in the Kuskokwim were strongly

negatively correlated with watershed relief (Pearson correlation coefficient = -0.64, $p < 0.01$). However, the most parsimonious model for DOC included covariates for watershed relief and watershed latitude, but no landcover covariates. This is likely due in part to collinearity between relief and these wetland landcover types or to a mismatch between field conditions and wetlands mapped from geospatial data from combined sources. Additionally, previous work has found watershed slope to be a better predictor of DOC flux than wetlands within both the entire watershed and riparian zones (Andersson & Nyberg, 2008). Furthermore, because our data only provide a snapshot of Kuskokwim biogeochemistry, seasonal hydrology may mask landcover effects on instream DOC to some extent (Laudon *et al.*, 2011)(Laudon et al., 2011). For example, Buffam *et al.* (2007) showed reduced sub-catchment variation in DOC during spring runoff, wherein DOC from wetland dominated catchments was diluted and DOC inputs from upper soil horizons in forested catchments increased.

The positive effect of latitude on both [DOC] and [NO_3] may be driven by watershed air temperature. Modeled mean summer air temperatures in the Kuskokwim generally increase with latitude and longitude to the east, with the exception of high relief mountainous areas (Scenarios Network for Alaska and Arctic Planning (SNAP), 2017b). Some recent work in boreal regions shows a positive relationship between temperature and [DOC] due to higher terrestrial ecosystem productivity and deeper active layer soils (Hawkes *et al.*, 2018; Winterdahl *et al.*, 2016). [NO_3] was positively correlated with watershed relief but negatively correlated with mean watershed elevation (Fig. 1.4b). This pattern has been observed elsewhere in Alaska and is likely due to an upper elevation limit for alder (*Alnus* spp.) growth (Devotta et al., 2020). [DOC] was a significant covariate in SSN models for both NO_3 ($p = 0.01$) and PO_4 ($p < 0.01$), which were negatively and positively correlated with instream [DOC], respectively. DOC probably precluded

watershed relief as a covariate in candidate models for PO_4, given the strong influence of relief on [DOC] in the Kuskokwim (Fig. 1.4c). The negative relationship between [DOC] and [NO_3] in the Kuskokwim is likely linked to higher denitrification rates and nitrogen retention in drainages to DOC-rich streams. Low gradient watersheds have increased potential for saturated soils lending to both anaerobic conditions enhancing denitrification and longer residence times promoting nitrogen transformations (Lintern *et al.*, 2018), and boreal streams draining peat/bog catchments generally have higher C:N (Aitkenhead & McDowell, 2000). These low gradient catchments and associated wetlands and peat bogs can also yield higher total phosphorus in boreal streams due to phosphorus complexation with DOC in saturated soils and wetland environments (Dillon & Molot, 1997). Elevated groundwater tables and anoxic soil conditions can mobilize phosphorus to streamwater (Dupas *et al.*, 2015), and these conditions are prevalent in the low relief catchments where [DOC] was highest in the Kuskokwim. Water saturated soils also prevent the establishment of N-fixing alder, one of the dominant sources of NO_3 in western Alaska.

[Ca], [Sr], and $^{87}Sr/^{86}Sr$ were generally much higher in the mountainous portions of the Kuskokwim (Fig. 1.4 a-f). The positive relationship between relief and base cations and $^{87}Sr/^{86}Sr$ has been shown for many rivers in western Alaska and is attributed to higher rates of physical erosion and exposed, reactive calcite in exposed rock material in steep basins (Brennan *et al.*, 2014; Brennan *et al.*, 2016). Portions of the high relief Alaska Range in the eastern Kuskokwim also coincide with a broad, alkaline geologic unit called the Farewell Terrane (Fig. 1.4d-f, Fig S1). Together with physical weathering processes associated with the steep terrain, high precipitation, and freeze-thaw cycles in these mountains, the meta-sedimentary rocks and

Paleozoic limestone in the Farewell Terrane yielded high concentrations of Ca and Sr in the eastern Kuskokwim basin (Fig. S1.1)(Brennan *et al.*, 2014).

Watershed morphology also shapes landcover types, which can modify or amplify watershed effects on instream biogeochemical patterning. In the Kuskokwim and in other Alaskan watersheds (Callahan *et al.*, 2017; Shaftel *et al.*, 2012), $[NO_3]$ was strongly positively correlated with alder (*Alnus* spp.) plant cover due to alder's N-fixing capacity. Alder in the Kuskokwim grows in thickets on well-drained low- to mid-elevation hillslopes below 1000 m on south-facing slopes and below 740 m elevations at other aspects. Previous work in southwest Alaska showed stronger relationships between alder and stream $[NO_3]$ when alder cover exceeded 30 percent (Devotta et al., 2020). The upper range of alder cover in the Kuskokwim (at spatial scale DS-8) was 30.2 percent, with a median of 4.75 percent, considerably lower than alder cover (6-75 percent) in the study area of Devotta *et al.* (2020). Their study, and work by Shaftel *et al.* (2012) evaluated alder effects in smaller Alaskan streams at the individual catchment scale, with $[NO_3]$ in both studies roughly three times higher than the mean for the Kuskokwim (85.2 ± 9.28 [1 SE] $\mu g\ L^{-1}$). Despite lower overall $[NO_3]$, lower alder coverage, longer residence times and thus increased potential for denitrification in our study region, the strong relationship between alder and $[NO_3]$ in the Kuskokwim highlights the importance of terrestrial plant communities in regulating stream nutrient availability in pristine boreal watersheds. The northward expansion of shrubs including alder is predicted to increase rapidly in boreal and subarctic regions under a warming climate (Pearson *et al.*, 2013) and this expansion will likely alter nitrogen loading and nutrient stoichiometry in the Kuskokwim.

1.6.3 *Headwater watershed controls on network-wide conditions*

Low order headwater streams can account for up to 90% of channel length in boreal river networks (Ledesma *et al.*, 2018) and shorter water residence times in headwater channels reduce potential for biogeochemical modification of terrestrial signatures in streamwater solutes (Kothawala *et al.*, 2015). However, previous work on dendritic river networks also shows that low order streams can play a key role in terrestrial DOC processing (Bertuzzo *et al.*, 2017), that headwaters regulate water and nutrient fluxes to larger rivers downstream (Alexander *et al.*, 2007), and that biogeochemical heterogeneity is governed by conditions in small stream catchments (Abbott *et al.*, 2018; Shogren *et al.*, 2019; Zimmer *et al.*, 2013). Our results in the Kuskokwim demonstrate that low order stream catchments play an important role in regulating streamwater conditions across the river network.

Streamwater constituents in the Kuskokwim network largely reflected watershed conditions in 2nd and 3rd order catchments (Fig. 1.5). These low order headwaters composed 78 percent of the total Kuskokwim watershed area and 68 percent of total channel length (Fig. 1.1c,d), and also accounted for much of the biogeochemical heterogeneity in the watershed (Fig. 1.3a-f). With the exception of $^{87}Sr/^{86}Sr$, spatial covariates derived using just 2nd (DS-2) or 2nd and 3rd order (DS-3) catchment conditions performed as well or better than watershed-wide covariates in SSN models (Fig. 1.5). The predictive ability of SSN models using downstream scaling from headwaters highlights the importance low order stream catchments in determining network-scale biogeochemical conditions in the Kuskokwim.

For most constituents in our study, models performed similarly ($\Delta AIC < 2$) for spatial scales that included headwater catchment areas (Table S1.3). The majority (90%) of our sample sites were on 6th order or smaller streams (Fig. 1.1b). Given this distribution of sampling sites, the bulk of Kuskokwim headwaters are included in spatial covariates derived at spatial scales larger than (to

the right of- in Fig. 1.2) US-4 in the upstream direction and DS-2 in the downstream direction. These patterns can also be seen in the increasing proportion of variance explained by fixed effects in Figure 1.5 when moving upstream, with only minor or no changes when moving downstream. The inclusion of a broader range of stream orders in the best models for $^{87}Sr/^{86}Sr$ is indicative of the importance of flow routing and mixing of variable watershed signals in determining network-wide $^{87}Sr/^{86}Sr$, which is strongly influenced by both [Sr] and the $^{87}Sr/^{86}Sr$ of source waters (Brennan *et al.*, 2014; Brennan *et al.*, 2016).

What was surprising for the conservative constituents was the relatively small effect of instream spatial autocorrelation, which accounted for only 4-18 percent of explained variance in [Ca], [Sr], and $^{87}Sr/^{86}Sr$. Given the passive transport of these solutes through the river network, we expected the flow-connected or instream autocorrelation to account for a higher proportion of variance. The flexible nature of SSNs has interesting effects on the variance composition, however, and when Euclidian autocorrelation was removed from SSN models, flow-connected covariance increased to account for up to 60 percent of explained variance, with only minor changes in model prediction error for the conservative constituents. This suggests that constituents in the Kuskokwim which were highly spatially autocorrelated within the stream channel were generally also highly correlated in Euclidian space due to the arrangement and/or scale of watershed features influencing constituent concentrations. There was, however, remaining spatial autocorrelation in residuals from flow-connected only models, indicating that both Euclidian and flow-connected functions were needed to account for the spatial structure in our streamwater data.

Instream or flow-connected spatial autocorrelation accounted for up to 22% of explained variance in [DOC], the highest of the constituents we measured. These results suggest that for

the streamwater constituents in the Kuskokwim, bulk DOC behaved more similarly to conservative solutes (Ca, Sr, and $^{87}Sr/^{86}Sr$) than with labile nutrients PO_4 and NO_2, and that [DOC] reflected both watershed controls and instream transport and mixing. Because we did not quantify DOC composition throughout the river network, it is difficult to interpret the degree of instream DOC processing for the Kuskokwim. Previous studies provide ample evidence of instream processing of DOC during transit along the river corridor (see reviews by Mineau et al., 2016 and Wohl et al., 2017), and labile portions of DOC in boreal streams are subject to uptake and transformation during transit to river mouths (Weyhenmeyer & Conley, 2017; Weyhenmeyer *et al.*, 2012). Meta-analysis of previous work examining DOC turnover in studies using DOC additions shows that labile fractions of DOC have uptake velocities similar to PO_4, but uptake velocities for ambient DOC (mixture of leachates and biolabile DOC) are roughly 10 times slower (Mineau *et al.*, 2016). For Alaskan streams draining permafrost soils, labile material released from recently thawed soils is subject to more rapid uptake and decomposition than organic matter from seasonally-thawed active soil layers (Textor *et al.*, 2019; Wickland *et al.*, 2018). Additionally, NO_3 retention decreases as permafrost thaw depths increase, thereby increasing terrestrial NO_3 inputs to streams (Harms & Jones, 2012). Under a warming climate, increases in labile DOC and NO_3 inputs from permafrost regions to high latitude rivers will likely modify the biogeochemical basis of aquatic food webs in boreal river networks.

1.7 Conclusions

Isolating instream processing of carbon and nutrients from broader watershed controls on streamwater chemistry necessitates an accounting of the nested, hierarchical, spatial configuration of dendritic river networks and the downstream movement of water. SSNs provide

a flexible, quantitative framework for studying stream biogeochemistry across entire river networks using a combination of field sampling and publicly available geospatial data. Low order headwater streams generally account for the majority of watershed channel length and watershed area in dendritic river networks, and our study indicates that watershed features in these small catchments are the key watershed attributes that affect stream biogeochemistry across a boreal river network. Understanding how watershed features shape spatial patterning for chemical drivers of aquatic food web productivity may aid the management of aquatic resources as watershed conditions change under a warming climate and growing developmental pressures.

1.8 References

Abbott, B. W., et al. (2018), Unexpected spatial stability of water chemistry in headwater stream networks, Ecol Lett, 21(2), 296-308, doi:10.1111/ele.12897.

Agren, A., I. Buffam, M. Berggren, K. Bishop, M. Jansson, and H. Laudon (2008), Dissolved organic carbon characteristics in boreal streams in a forest-wetland gradient during the transition between winter and summer, J Geophys Res-Biogeo, 113(G3), doi:ArtnG0303110.1029/2007jg000674.

Agren, A. M., I. Buffam, D. M. Cooper, T. Tiwari, C. D. Evans, and H. Laudon (2014), Can the heterogeneity in stream dissolved organic carbon be explained by contributing landscape elements?, Biogeosciences, 11(4), 1199-1213, doi:10.5194/bg-11-1199-2014.

Aitkenhead, J. A., and W. H. McDowell (2000), Soil C:N ratio as a predictor of annual riverine DOC flux at local and global scales, Global Biogeochem Cy, 14(1), 127-138, doi:10.1029/1999GB900083.

Alexander, R. B., E. W. Boyer, R. A. Smith, G. E. Schwarz, and R. B. Moore (2007), The Role of Headwater Streams in Downstream Water Quality1, JAWRA Journal of the American Water Resources Association, 43(1), 41-59, doi:10.1111/j.1752-1688.2007.00005.x.

Andersson, J.-O., and L. Nyberg (2008), Spatial variation of wetlands and flux of dissolved organic carbon in boreal headwater streams, Hydrol Process, 22(12), 1965-1975, doi:doi:10.1002/hyp.6779.

Bataille, C. P., S. R. Brennan, J. Hartmann, N. Moosdorf, M. J. Wooller, and G. J. Bowen (2014), A geostatistical framework for predicting variations in strontium concentrations and isotope ratios in Alaskan rivers, Chem Geol, 389, 1-15, doi:10.1016/j.chemgeo.2014.08.030.

Bertuzzo, E., A. M. Helton, R. O. Hall, and T. J. Battin (2017), Scaling of dissolved organic carbon removal in river networks, Advances in Water Resources, 110, 136-146, doi:https://doi.org/10.1016/j.advwatres.2017.10.009.

Blaen, P. J., K. Khamis, C. E. M. Lloyd, C. Bradley, D. Hannah, and S. Krause (2016), Real-time monitoring of nutrients and dissolved organic matter in rivers: Capturing event dynamics, technological opportunities and future directions, Sci Total Environ, 569, 647-660, doi:10.1016/j.scitotenv.2016.06.116.

Bormann, F. H., and G. E. Likens (1967), Nutrient Cycling, Science, 155(3761), 424-+, doi:DOI 10.1126/science.155.3761.424.

Brennan, S. R., D. P. Fernandez, G. Mackey, T. E. Cerling, C. P. Bataille, G. J. Bowen, and M. J. Wooller (2014), Strontium isotope variation and carbonate versus silicate weathering in rivers from across Alaska: Implications for provenance studies, Chem Geol, 389, 167-181, doi:10.1016/j.chemgeo.2014.08.018.

Brennan, S. R., D. E. Schindler, T. J. Cline, T. E. Walsworth, G. Buck, and D. P. Fernandez (2019), Shifting habitat mosaics and fish production across river basins, Science, 364(6442), 783-+, doi:10.1126/science.aav4313.

Brennan, S. R., C. E. Torgersen, J. P. Hollenbeck, D. P. Fernandez, C. K. Jensen, and D. E. Schindler (2016), Dendritic network models: Improving isoscapes and quantifying influence of landscape and in-stream processes on strontium isotopes in rivers, Geophys Res Lett, 43(10), 5043-5051, doi:10.1002/2016gl068904.

Brennan, S. R., C. E. Zimmerman, D. P. Fernandez, T. E. Cerling, M. V. McPhee, and M. J. Wooller (2015), Strontium isotopes delineate fine-scale natal origins and migration histories of Pacific salmon, Sci Adv, 1(4), doi:ARTN e140012410.1126/sciadv.1400124.

Buffam, I., H. Laudon, J. Temnerud, C. M. Morth, and K. Bishop (2007), Landscape-scale variability of acidity and dissolved organic carbon during spring flood in a boreal stream network, J Geophys Res-Biogeo, 112(G1), doi:Artn G0102210.1029/2006jg000218.

Callahan, M. K., D. F. Whigham, M. C. Rains, K. C. Rains, R. S. King, C. M. Walker, J. R. Maurer, and S. J. Baird (2017), Nitrogen Subsidies from Hillslope Alder Stands to Streamside Wetlands and Headwater Streams, Kenai Peninsula, Alaska, J Am Water Resour As, 53(2), 478-492, doi:10.1111/1752-1688.12508.

Casas-Ruiz, J. P., N. Catalan, L. Gomez-Gener, D. von Schiller, B. Obrador, D. N. Kothawala, P. Lopez, S. Sabater, and R. Marce (2017), A tale of pipes and reactors: Controls on the in-stream dynamics of dissolved organic matter in rivers, Limnol Oceanogr, 62, S85-S94, doi:10.1002/lno.10471.

Closs, G., B. J. Downes, and A. J. Boulton (2004), Freshwater ecology : a scientific introduction, Malden, MA. : Blackwell Pub. Co., Malden, MA.

Colpron, M., J. L. Nelson, and D. C. Murphy (2007), Northern Cordilleran terranes and their interactions through time, GSA Today, 17(4), 4-10, doi:10.1130/GSAT01704-5A.1.

Creed, I. F., et al. (2015), The river as a chemostat: fresh perspectives on dissolved organic matter flowing down the river continuum, Can J Fish Aquat Sci, 72(8), 1272-1285, doi:10.1139/cjfas-2014-0400.

Cressie, N., J. Frey, B. Harch, and M. Smith (2006), Spatial prediction on a river network, J Agr Biol Envir St, 11(2), 127-150, doi:10.1198/108571106x110649.

Cressie, N. A. C. (1993), Statistics for spatial data, Rev. ed. ed., New York : Wiley, New York.

Dent, C. L., and N. B. Grimm (1999), Spatial heterogeneity of stream water nutrient concentrations over successional time, Ecology, 80(7), 2283-2298.

Dick, J. J., D. Tetzlaff, C. Birkel, and C. Soulsby (2015), Modelling landscape controls on dissolved organic carbon sources and fluxes to streams, Biogeochemistry, 122(2-3), 361-374, doi:10.1007/s10533-014-0046-3.

Dillon, P. J., and L. A. Molot (1997), Effect of landscape form on export of dissolved organic carbon, iron, and phosphorus from forested stream catchments, Water Resour Res, 33(11), 2591-2600, doi:Doi 10.1029/97wr01921.

Dupas, R., G. Gruau, S. Gu, G. Humbert, A. Jaffrézic, and C. Gascuel-Odoux (2015), Groundwater control of biogeochemical processes causing phosphorus release from riparian wetlands, Water Research, 84, 307-314, doi:https://doi.org/10.1016/j.watres.2015.07.048.

Ensign, S. H., and M. W. Doyle (2006), Nutrient spiraling in streams and river networks, J Geophys Res-Biogeo, 111(G4), doi:Artn G0400910.1029/2005jg000114.

Fernald, A. T. (1960), Geomorphology of the upper Kuskokwim region, Alaska, Washington, D.C. : United States Department of the Interior, Geological Survey, Washington, D.C.

Ganio, L. M., C. E. Torgersen, and R. E. Gresswell (2005), A geostatistical approach for describing spatial pattern in stream networks, Front Ecol Environ, 3(3), 138-144, doi:Doi 10.2307/3868541.

Gergel, S. E., M. G. Turner, and T. K. Kratz (1999), Dissolved organic carbon as an indicator of the scale of watershed influence on lakes and rivers, Ecol Appl, 9(4), 1377-1390, doi:Doi 10.1890/1051-0761(1999)009[1377:Docaai]2.0.Co;2.

Gooseff, M. N., K. E. Bencala, and S. M. Wondzell (2008), Solute Transport Along Stream and River Networks, 395-417 pp., doi:10.1002/9780470760383.ch18.

Granger, S. J., R. Bol, S. Anthony, P. N. Owens, S. M. White, and P. M. Haygarth (2010), Towards a holistic classification of diffuse agricultural water pollution from intensively managed grasslands on heavy soils, 83-115 pp., doi:10.1016/S0065-2113(10)05003-0.

Harms, T. K., J. W. Edmonds, H. Genet, I. F. Creed, D. Aldred, A. Balser, and J. B. Jones (2016), Catchment influence on nitrate and dissolved organic matter in Alaskan streams across a latitudinal gradient, Journal of Geophysical Research: Biogeosciences, 121(2), 350-369, doi:10.1002/2015JG003201.

Harms, T. K., and J. B. Jones (2012), Thaw depth determines reaction and transport of inorganic nitrogen in valley bottom permafrost soils, Global Change Biol, 18(9), 2958-2968, doi:10.1111/j.1365-2486.2012.02731.x.

Hartmann, J., and N. Moosdorf (2012), The new global lithological map database GLiM: A representation of rock properties at the Earth surface, Geochem Geophy Geosy, 13, doi:Artn Q1200410.1029/2012gc004370.

Hawkes, J. A., N. Radoman, J. Bergquist, M. B. Wallin, L. J. Tranvik, and S. Löfgren (2018), Regional diversity of complex dissolved organic matter across forested hemiboreal headwater streams, Sci Rep-Uk, 8(1), 16060, doi:10.1038/s41598-018-34272-3.

Hiatt, D. L., C. J. Robbins, J. A. Back, P. K. Kostka, R. D. Doyle, C. M. Walker, M. C. Rains, D. F. Whigham, and R. S. King (2017), Catchment-scale alder cover controls nitrogen fixation in boreal headwater streams, Freshwater Science, 36(3), 523-532, doi:10.1086/692944.

Hoeting, J. A., R. A. Davis, A. A. Merton, and S. E. Thompson (2006), Model selection for geostatistical models, Ecol Appl, 16(1), 87-98, doi:Doi 10.1890/04-0576.

Hogan, J. F., and J. D. Blum (2003), Tracing hydrologic flow paths in a small forested watershed using variations in (87)Sr(/8)6Sr, [Ca]/[Sr], [Ba]/[Sr] and delta O-18, Water Resour Res, 39(10), doi:Artn 128210.1029/2002wr001856.

Hunsaker, C. T., and D. A. Levine (1995), Hierarchical Approaches to the Study of Water Quality in Rivers: Spatial scale and terrestrial processes are important in developing models to translate research results to management practices, Bioscience, 45(3), 193-203, doi:10.2307/1312558.

Ingri, J., A. Widerlund, and M. Land (2005), Geochemistry of major elements in a pristine boreal river system; Hydrological compartments and flow paths, Aquat Geochem, 11(1), 57-88, doi:DOI 10.1007/s10498-004-2248-0.

Jankowski, K. J., and D. E. Schindler (2019), Watershed geomorphology modifies the sensitivity of aquatic ecosystem metabolism to temperature, Sci Rep-Uk, 9(1), 17619, doi:10.1038/s41598-019-53703-3.

Jorgenson, T., K. Yoshikawa, M. Kanevskiy, Y. Shur, V. Romanovsky, S. Marchenko, G. Grosse, J. Brown, and B. Jones (2008), Permafrost characteristics of Alaska, Fairbanks, AK, United States: University of Alaska Fairbanks, Institute of Northern Engineering, Fairbanks, AK.

Kaplan, L. A., and T. L. Bott (1982), Diel Fluctuations of Doc Generated by Algae in a Piedmont Stream, Limnol Oceanogr, 27(6), 1091-1100, doi:DOI 10.4319/lo.1982.27.6.1091.

Kothawala, D. N., X. Ji, H. Laudon, A. M. Ågren, M. N. Futter, S. J. Köhler, and L. J. Tranvik (2015), The relative influence of land cover, hydrology, and in-stream processing on the composition of dissolved organic matter in boreal streams, Journal of Geophysical Research: Biogeosciences, 120(8), 1491-1505, doi:10.1002/2015JG002946.

Laudon, H., M. Berggren, A. Agren, I. Buffam, K. Bishop, T. Grabs, M. Jansson, and S. Kohler (2011), Patterns and Dynamics of Dissolved Organic Carbon (DOC) in Boreal Streams: The Role of Processes, Connectivity, and Scaling, Ecosystems, 14(6), 880-893, doi:10.1007/s10021-011-9452-8.

Ledesma, J. L. J., M. N. Futter, M. Blackburn, F. Lidman, T. Grabs, R. A. Sponseller, H. Laudon, K. H. Bishop, and S. J. Köhler (2018), Towards an Improved Conceptualization of Riparian Zones in Boreal Forest Headwaters, Ecosystems, 21(2), 297-315, doi:10.1007/s10021-017-0149-5.

Lintern, A., J. A. Webb, D. Ryu, S. Liu, U. Bende-Michl, D. Waters, P. Leahy, P. Wilson, and A. W. Western (2018), Key factors influencing differences in stream water quality across space, Wires Water, 5(1), doi:ARTN e126010.1002/wat2.1260.

Loreau, M., T. Daufresne, A. Gonzalez, D. Gravel, F. Guichard, S. J. Leroux, N. Loeuille, F. Massol, and N. Mouquet (2013), Unifying sources and sinks in ecology and Earth sciences, Biol Rev, 88(2), 365-379, doi:10.1111/brv.12003.

Manley, W. F. K., D.S. (2002), Alaska PaleoGlacier Atlas, edited by U. o. C. Institute of Arctic and Alpine Research (INSTAAR).

Marcé, R., D. von Schiller, R. Aguilera, E. Martí, and S. Bernal (2018), Contribution of Hydrologic Opportunity and Biogeochemical Reactivity to the Variability of Nutrient Retention in River Networks, Global Biogeochem Cy, 32(3), 376-388, doi:10.1002/2017GB005677.

Matheron, G. (1963), Principles of geostatistics, Economic Geology and the Bulletin of the Society of Economic Geologists, 58(8), 1246-1266, doi:10.2113/gsecongeo.58.8.1246.

McGuire, K. J., C. E. Torgersen, G. E. Likens, D. C. Buso, W. H. Lowe, and S. W. Bailey (2014), Network analysis reveals multiscale controls on streamwater chemistry, P Natl Acad Sci USA, 111(19), 7030-7035, doi:10.1073/pnas.1404820111.

Meyer, J. L. (1990), A Blackwater Perspective on Riverine Ecosystems, Bioscience, 40(9), 643-651, doi:Doi 10.2307/1311431.

Meyer, J. L., W. H. Mcdowell, T. L. Bott, J. W. Elwood, C. Ishizaki, J. M. Melack, B. L. Peckarsky, B. J. Peterson, and P. A. Rublee (1988), Elemental Dynamics in Streams, J N Am Benthol Soc, 7(4), 410-432, doi:Doi 10.2307/1467299.

Mineau, M. M., W. M. Wollheim, I. Buffam, S. E. G. Findlay, R. O. Hall Jr, E. R. Hotchkiss, L. E. Koenig, W. H. McDowell, and T. B. Parr (2016), Dissolved organic carbon uptake in streams: A review and assessment of reach-scale measurements, Journal of Geophysical Research: Biogeosciences, 121(8), 2019-2029, doi:10.1002/2015JG003204.

Mulholland, P. J. (1997), Dissolved organic matter concentration and flux in streams, J N Am Benthol Soc, 16(1), 131-141, doi:Doi 10.2307/1468246.

Mulholland, P. J., et al. (2009), Nitrate removal in stream ecosystems measured by 15N addition experiments: Denitrification, Limnol Oceanogr, 54(3), 666-680, doi:10.4319/lo.2009.54.3.0666.

Olea, R. A. (1994), Fundamentals of semivariogram estimation, modeling, and usage, in AAPG Computer Applications in Geology, edited by J. M. Yarus and R. L. Chambers, pp. 27-35, Tulsa, OK.

Pearson, R. G., S. J. Phillips, M. M. Loranty, P. S. A. Beck, T. Damoulas, S. J. Knight, and S. J. Goetz (2013), Shifts in Arctic vegetation and associated feedbacks under climate change, Nature Climate Change, 3(7), 673-677, doi:10.1038/nclimate1858.

Peterson, B. J., et al. (2001), Control of Nitrogen Export from Watersheds by Headwater Streams, Science, 292(5514), 86, doi:10.1126/science.1056874.

Peterson, E. E., and J. M. V. Hoef (2010), A mixed-model moving-average approach to geostatistical modeling in stream networks, Ecology, 91(3), 644-651, doi:Doi 10.1890/08-1668.1.

Peterson, E. E., and J. M. V. Hoef (2014), STARS: An ArcGIS Toolset Used to Calculate the Spatial Information Needed to Fit Spatial Statistical Models to Stream Network Data, J Stat Softw, 56(2), 1-17.

Peterson, E. E., A. A. Merton, D. M. Theobald, and N. S. Urquhart (2006), Patterns of spatial autocorrelation in stream water chemistry, Environ Monit Assess, 121(1-3), 571-596, doi:10.1007/s10661-005-9156-7.

Peterson, E. E., D. M. Theobald, and J. M. V. Hoef (2007), Geostatistical modelling on stream networks: developing valid covariance matrices based on hydrologic distance and stream flow, Freshwater Biol, 52(2), 267-279, doi:10.1111/j.1365-2427.2006.01686.x.

Rieger, S., D. B. Schoephorster, and C. E. Furbush (1979), Exploratory soil survey of Alaska, Washington: U.S. Dept. of Agriculture, Soil Conservation Service.

Rodriguez-Cardona, B., A. S. Wymore, and W. H. McDowell (2016), DOC:NO3- ratios and NO3- uptake in forested headwater streams, J Geophys Res-Biogeo, 121(1), 205-217, doi:10.1002/2015jg003146.

Rossi, R. E., D. J. Mulla, A. G. Journel, and E. H. Franz (1992), Geostatistical Tools for Modeling and Interpreting Ecological Spatial Dependence, Ecol Monogr, 62(2), 277-314, doi:Doi 10.2307/2937096.

Scenarios Network for Alaska and Arctic Planning (SNAP) (2017), Historical Monthly and Derived Precipitation Products Downscaled from CRU TS data via the delta method - 2 km, edited, University of Alaska.

Scenarios Network for Alaska and Arctic Planning (SNAP) (2017), Historical Monthly and Derived Temperature Products Downscaled from CRU TS data via the delta method - 2 km, edited, University of Alaska.

Shaftel, R. S., R. S. King, and J. A. Back (2012), Alder cover drives nitrogen availability in Kenai lowland headwater streams, Alaska, Biogeochemistry, 107(1-3), 135-148, doi:10.1007/s10533-010-9541-3.

Shogren, A. J., J. P. Zarnetske, B. W. Abbott, F. Iannucci, R. J. Frei, N. A. Griffin, and W. B. Bowden (2019), Revealing biogeochemical signatures of Arctic landscapes with river chemistry, Sci Rep-Uk, 9, doi:ARTN 1289410.1038/s41598-019-49296-6.

Smits, A. P., D. E. Schindler, G. W. Holtgrieve, K. J. Jankowski, and D. W. French (2017), Watershed geomorphology interacts with precipitation to influence the magnitude and source of CO2 emissions from Alaskan streams, J Geophys Res-Biogeo, 122(8), 1903-1921, doi:10.1002/2017jg003792.

Soil Survey Staff, Natural Resources Conservation Service, and United States Department of Agriculture (2016), USDA-NRCS Soil Survey Geographic (SSURGO), edited by USDA/NRCS National Geospatial Center of Excellence, Forth Worth, TX.

Steiger, R. H., and E. Jager (1977), Subcommission on Geochronology - Convention on Use of Decay Constants in Geochronology and Cosmochronology, Earth Planet Sc Lett, 36(3), 359-362, doi:Doi 10.1016/0012-821x(77)90060-7.

Temnerud, J., J. Fölster, I. Buffam, H. Laudon, M. Erlandsson, and K. Bishop (2010), Can the distribution of headwater stream chemistry be predicted from downstream observations?, Hydrol Process, 24(16), 2269-2276, doi:10.1002/hyp.7615.

Temnerud, J., J. Seibert, M. Jansson, and K. Bishop (2007), Spatial variation in discharge and concentrations of organic carbon in a catchment network of boreal streams in northern Sweden, J Hydrol, 342(1), 72-87, doi:https://doi.org/10.1016/j.jhydrol.2007.05.015.

Teodoru, C. R., P. A. Del Giorgio, Y. T. Prairie, and M. Camire (2009), Patterns in pCO(2) in boreal streams and rivers of northern Quebec, Canada, Global Biogeochem Cy, 23, doi:Artn Gb201210.1029/2008gb003404.

Textor, S. R., K. P. Wickland, D. C. Podgorski, S. E. Johnston, and R. G. M. Spencer (2019), Dissolved Organic Carbon Turnover in Permafrost-Influenced Watersheds of Interior Alaska: Molecular Insights and the Priming Effect, Frontiers in Earth Science, 7(275), doi:10.3389/feart.2019.00275.

U.S. Geological Survey (2016), LANDFIRE Existing Vegetation Type, edited by E. R. O. a. S. C. Wildland Fire Science, U.S. Geological Survey, Sioux Falls, SD.

U.S. Geological Survey (2017), Alaska 2 Arc-second Digital Elevation Models (DEMs) - USGS National Map 3DEP Downloadable Data Collection, edited by U.S. Geological Survey.

U.S. Geological Survey (2018), National Water Information System data available on the World Wide Web (USGS Water Data for the Nation), edited.

Vannote, R. L., G. W. Minshall, K. W. Cummins, J. R. Sedell, and C. E. Cushing (1980), River Continuum Concept, Can J Fish Aquat Sci, 37(1), 130-137, doi:DOI 10.1139/f80-017.

Varanka, S., and J. Hjort (2016), Spatio-temporal aspects of the environmental factors affecting water quality in boreal rivers, Environmental Earth Sciences, 76(1), 21, doi:10.1007/s12665-016-6338-2.

Varanka, S., J. Hjort, and M. Luoto (2015), Geomorphological factors predict water quality in boreal rivers, Earth Surface Processes and Landforms, 40(15), 1989-1999, doi:10.1002/esp.3601.

Ver Hoef, J., E. Peterson, D. Clifford, and R. Shah (2014), SSN: An R Package for Spatial Statistical Modeling on Stream Networks, Journal of Statistical Software; Vol 1, Issue 3 (2014).

Ver Hoef, J. M., E. Peterson, and D. Theobald (2006), Spatial statistical models that use flow and stream distance, Environ Ecol Stat, 13(4), 449-464, doi:10.1007/s10651-006-0022-8.

Ver Hoef, J. M., and E. E. Peterson (2010), A Moving Average Approach for Spatial Statistical Models of Stream Networks, J Am Stat Assoc, 105(489), 6-18, doi:10.1198/jasa.2009.ap08248.

Walker, C. M., R. S. King, D. F. Whigham, and S. J. Baird (2012), Landscape and Wetland Influences on Headwater Stream Chemistry in the Kenai Lowlands, Alaska, Wetlands, 32(2), 301-310, doi:10.1007/s13157-011-0260-x.

Webster, J. R., and B. C. Patten (1979), Effects of Watershed Perturbation on Stream Potassium and Calcium Dynamics, Ecol Monogr, 49(1), 51-72, doi:Doi 10.2307/1942572.

Weyhenmeyer, G. A., and D. J. Conley (2017), Large differences between carbon and nutrient loss rates along the land to ocean aquatic continuum—implications for energy:nutrient ratios at downstream sites, Limnol Oceanogr, 62(S1), S183-S193, doi:10.1002/lno.10589.

Weyhenmeyer, G. A., M. Froberg, E. Karltun, M. Khalili, D. Kothawala, J. Temnerud, and L. J. Tranvik (2012), Selective decay of terrestrial organic carbon during transport from land to sea, Global Change Biol, 18(1), 349-355, doi:10.1111/j.1365-2486.2011.02544.x.

Wickland, K. P., M. P. Waldrop, G. R. Aiken, J. C. Koch, M. T. Jorgenson, and R. G. Striegl (2018), Dissolved organic carbon and nitrogen release from boreal Holocene permafrost and seasonally frozen soils of Alaska, Environmental Research Letters, 13(6), 1-11, doi:10.1088/1748-9326/aac4ad.

Wiens, J. A. (1989), Spatial Scaling in Ecology, Funct Ecol, 3(4), 385-397, doi:Doi 10.2307/2389612.

Winterdahl, M., H. Laudon, S. W. Lyon, C. Pers, and K. Bishop (2016), Sensitivity of stream dissolved organic carbon to temperature and discharge: Implications of future climates, Journal of Geophysical Research: Biogeosciences, 121(1), 126-144, doi:10.1002/2015JG002922.

Wohl, E., R. O. Hall Jr, K. B. Lininger, N. A. Sutfin, and D. M. Walters (2017), Carbon dynamics of river corridors and the effects of human alterations, Ecol Monogr, 87(3), 379-409, doi:10.1002/ecm.1261.

Zimmer, M. A., S. W. Bailey, K. J. McGuire, and T. D. Bullen (2013), Fine scale variations of surface water chemistry in an ephemeral to perennial drainage network, Hydrol Process, 27(24), 3438-3451, doi:10.1002/hyp.9449.

Chapter 2. Watershed features shape spatial patterns of fish tissue mercury in a boreal river network

2.1 Abstract

Freshwater mercury (Hg) contamination is a widespread environmental concern, but how proximate sources and downstream transport shape Hg spatial patterns in riverine food webs is poorly understood. We measured total Hg in slimy sculpin (*Cottus cognatus*) across the Kuskokwim River, a large boreal river network in Alaska and home to subsistence fishing communities who rely on fish for nutrition. We used spatial stream network models (SSNMs) to identify both watershed and instream conditions influencing sculpin Hg. Spatial covariates for watershed geology and slope accounted for 55% of sculpin Hg variation. Empirical semivariograms indicate these spatial covariates also accounted for most spatial autocorrelation in observed Hg. Watershed geology and slope explained up to 70% of sculpin Hg variation when SSNMs accounted for instream spatial dependence. Hg is often correlated with instream biogeochemical conditions such as pH (negative correlation) and dissolved organic carbon (positive correlation); however, the effect of these instream conditions in the Kuskokwim was confounded by broad scale watershed features (e.g. geology, slope). Our results provide network-wide predictions for fish tissue Hg based largely on publicly available geospatial data and open-source software for SSNMs. This approach may be useful for aquatic resource managers to understand future changes in Hg contamination.

2.2 Introduction

Mercury (Hg) contamination of aquatic food webs and its potential negative impacts on fish consumers is a widely recognized, global environmental concern (Krabbenhoft & Rickert, 1995; Selin *et al.*, 2018), but factors governing Hg distributions in river networks are still not well understood. Hg occurs naturally in nearly all ecosystems, but substantial increases in global environmental Hg concentrations since the mid-19th century are attributed to anthropogenic activity such as fossil fuel combustion, mining, and other industrial processes (Sundseth *et al.*, 2017). Monomethylmercury (MeHg) is the most common toxic form of environmental Hg that bioaccumulates in aquatic ecosystems(Bloom, 1992), and is then biomagnified in food webs that support large, piscivorous fish(Wiener & Spry, 1996), even in remote waterways with no point sources of Hg (Baker *et al.*, 2009; Southworth *et al.*, 2004). Upwards of 90% of Hg in fish is from dietary uptake (Wiener *et al.*, 2003), and elevated levels of fish tissue MeHg can also reduce reproductive success, damage cells and tissue, and compromise embryonic development in some fish species (Sandheinrich & Wiener, 2011; Wiener & Spry, 1996).

Human exposure to MeHg is primarily via fish and seafood consumption (Rice *et al.*, 2014; Wiener *et al.*, 2003), and subsistence fishing communities are often prone to higher rates of MeHg exposure (Chan & Receveur, 2000; Chan *et al.*, 2003; Oliveira *et al.*, 2010; Trasande *et al.*, 2010) because of their high dependency on local freshwater food webs for nutrition. Environmental Hg has both local (e.g. watershed geology) and distant (e.g. atmospheric deposition) natural and anthropogenic sources (Sundseth *et al.*, 2017) and MeHg bioavailability exhibits spatial variation relative to ambient Hg at broad scales (Driscoll *et al.*, 2013; Eagles-Smith *et al.*, 2016). Quantifying how Hg is distributed throughout river networks would provide

insight into the processes contributing to spatial variation in Hg, and management options for controlling exposure to fishery-dependent communities.

Spatial variation in the bioavailability of Hg within aquatic systems is mediated by both watershed and *in situ* environmental conditions (Driscoll *et al.*, 2013). Broad scale patterning in Hg is shaped by atmospheric deposition of elemental Hg from anthropogenic emissions and lithospheric reservoirs (e.g., volcanoes) (Fitzgerald *et al.*, 1998); however terrestrial Hg loads to inland waters generally exceed atmospheric inputs (Hsu-Kim *et al.*, 2018). Watershed geology and weathering properties can create sub-watershed scale spatial heterogeneity in Hg, with hydrologic connectivity and landscape characteristics (e.g. flow paths, soil properties) mediating delivery to streams and lakes (Driscoll *et al.*, 2013; Hsu-Kim *et al.*, 2018). At the catchment scale, positive relationships have been shown between Hg and watershed landcover such as coniferous forest (Drenner *et al.*, 2013) and wetland percentage (Burns *et al.*, 2012; Chasar *et al.*, 2009; Shanley *et al.*, 2012; Wiener *et al.*, 2003), and mining or industrial pollution within a catchment can increase freshwater Hg concentrations by 1-2 orders of magnitude (Wiener *et al.*, 2003). Broad scale climatic forcing and watershed features thus shape Hg availability to freshwater systems, but uptake into aquatic food webs throughout river networks exhibits variation at multiple spatial scales (Walters *et al.*, 2010).

Fine scale spatial patterning in the bioavailability of Hg is largely linked with physical and biogeochemical conditions that promote Hg (Driscoll *et al.*, 2013; Wiener *et al.*, 2003). MeHg formation is positively associated with redox gradients favoring sulfate reducing bacteria in sediments or the water column and high concentrations of organic matter (OM), which fuels microbial metabolism and limits photochemical demethylation of MeHg via light attenuation (Klapstein & O'Driscoll, 2018; Wiener *et al.*, 2003). Channel and valley morphology also play a

role in Hg bioavailability. For example, photochemical demethylation of MeHg is positively associated with stream channel size due to increased light availability (Tsui *et al.*, 2013). Previous work has shown positive correlations between fish tissue Hg and concentrations of sulfate and dissolved organic carbon (DOC), and negative correlations with pH, acid neutralizing capacity, and phosphorus concentration (Wiener *et al.*, 2003). Many of these biogeochemical conditions are common attributes of DOC-rich aquatic environments such as wetlands, peat bogs, and lakes, however several studies have found weak or inconsistent relationships between Hg and DOC in rivers (Barbosa *et al.*, 2003; Peterson *et al.*, 2007b). Chasar *et al.* (2009) however, found a strong positive correlation between fish Hg, DOC, and catchment wetlands in 8 different stream types across the U.S. Combined measures of DOC, Hg, and other biogeochemical parameters in tandem with landscape metrics may yield insights into biotic and abiotic factors contributing to elevated Hg in riverine food webs (Hsu-Kim *et al.*, 2018) at the riverscape scale.

The Kuskokwim River (Kuskokwim) is a large, free-flowing boreal river in western Alaska that supports numerous subsistence fishing communities and encompasses diverse geologic conditions and land cover types. Large swaths of the Kuskokwim watershed coincide with a well-documented metal-bearing mineral deposit that has been actively mined since the early 20th century for Hg, gold, and other metals (Mertie, 1936). Previous work showed elevated levels of tissue-bound Hg in fish from heavily mined tributaries in the Kuskokwim (Matz *et al.*, 2017), but this effort was limited in spatial scope to the middle portion of the basin. Additional large-scale mining activity is proposed in remote tributary valleys of the Kuskokwim, including areas where Hg conditions have not been studied. Quantifying Hg spatial patterning throughout the

Kuskokwim river network will aide managers in identifying existing and potential risks to subsistence food resources.

We sampled a small-bodied fish with a narrow home range (slimy sculpin [*Cottus cognatus]*, Gray et al., 2018), throughout the watershed and used recently developed spatial stream network models (SSNMs) (Peterson & Hoef, 2010; Ver Hoef & Peterson, 2010) to identify both watershed scale and *in situ* biogeochemical factors contributing to Hg in resident fish in the Kuskokwim, and to make network-wide predictions of tissue Hg. We expected broad scale spatial patterns in Hg sources driven by surface geology and watershed morphology and finer scale spatial patterning in Hg associated with factors such as wetlands or bogs that shape *in situ* biogeochemical conditions such as DOC concentration and pH.

2.3 Methods

2.3.1 *Study area*

The Kuskokwim River (Kuskokwim), a large (124,000 km^2) boreal river basin in western Alaska, spans from glacially influenced tributaries in the Alaska range at its eastern margin to the low-lying Yukon-Kuskokwim Delta on the Bering Sea (Fig. S2.1). The Kuskokwim extends over a complex geomorphologic template overlain by a diversity of land cover types, including barren mountain ranges, forested rolling hills, and broad boreal lowlands and wetland complexes. The eastern and central portions of the Kuskokwim largely coincide with two broad-scale geologic features: the alkaline Farewell terrane comprising complex metamorphosed lithologies of continental origin; and vast Cretaceous flysch deposits of the mineral-bearing Kuskokwim Group

(Beikman, 1980; Wilson, 2015). The entire Kuskokwim watershed composes a portion of the Tintina Gold Province (TGP), a broad metal-bearing region north of the Denali Fault that spans much of Alaska and the Yukon province in western Canada. Previous work in the central Kuskokwim basin found elevated tissue Hg in several fish species harvested by subsistence communities (Matz *et al.*, 2017), and historic and active mining activity throughout the TGP has raised broad scale concerns around potential impacts to freshwater resources and fisheries.

2.3.2 *Sample collection*

Slimy sculpins (*Cottus cognatus*) were collected using a 2 x 6m stick seine with 7mm mesh net along river banks at 68 sample sites spanning 2^{nd} – 8^{th} order streams. Slimy sculpins are commonly sampled as indicators of environmental conditions due to their small home range and ubiquity in many North American streams (Gray *et al.*, 2018). Sample sites were chosen to maximize network coverage and to ensure a mixture of sites that share flow (e.g. upstream from one another) and those that do not (e.g. adjacent drainages). A total of 120 sites were sampled for water chemistry (French et al., 2020, *in review*), with sculpin collection attempted at 88 sites. A total of 272 sculpin were collected across all sites, with a mean of 5 fish per site, and 58 sites having 2 or more fish collected for duplicate tissue measurements. Sculpins were euthanized immediately following removal from the stream (IACUC protocol #3142-01), placed in Whirl-Pak bags, and frozen. All samples were stored frozen in the dark until lab processing. At sites with active mining nearby, fish were collected upstream and downstream of observed mining activity, and in the middle of the actively mined reach where accessible

2.3.3 *Mercury analyses*

Whole sculpins were weighed, freeze-dried, and then re-weighed in a clean environment at the University of Washington School of Aquatic and Fishery Sciences to measure wet and dry mass. Freeze-dried samples were analyzed for total Hg (THg) at the Biotron Analytical Laboratory at Western University in London, Ontario. Samples were analyzed on a Milestone DMA-80 (Milestone Scientific, Inc., Shelton, Connecticut) by thermal decomposition atomic adsorption direct mercury analyzer (DMA) following a modified EPA standard method 7473, lab method TM.0813 (www.standardmethods.org), with a LoD of 0.08 ng and a method reporting limit of 0.24 ng. Mean relative percentage difference in sample duplicates was 2.0%, with a calibration curve coefficient of determination equal to 0.995. Analysis of a certified reference material (DORM-4) indicated recovery of 97 – 102%, with a relative percentage difference of 1% between duplicate samples.

Because a large fraction of THg in fish tissue is MeHg and inorganic Hg is rapidly eliminated from fish tissue, THg is a commonly used surrogate for measuring MeHg concentrations in fish (Driscoll *et al.*, 2013; Wiener *et al.*, 2003). We measured total Hg from our samples and infer based on previous work in the Kuskokwim by Matz *et al.* (2017) that approximately 60% of this THg is MeHg. THg measures from freeze-dried fish were converted to wet mass concentrations using the wet:dry mass ratio for each individual fish. All THg measures provided in this paper are expressed relative to wet fish mass in units of mg kg^{-1}.

2.3.4 *Statistical analysis*

We used a statistical modeling approach that includes spatial covariates for watershed features and leverages spatial autocorrelation among sampling sites throughout the Kuskokwim river network based on flow connectivity, flow magnitude, and flow direction (Ver Hoef & Peterson,

2010). We evaluated correlations between THg and *a priori* candidate covariates and used empirical semivariograms to identify spatial relationships among sample sites. We then fit spatial models for Hg using spatial covariates derived for each study site throughout the Kuskokwim network. Model performance was assessed to identify both watershed and *in situ* biogeochemical controls on tissue Hg, and variance composition was used to compare the effect size of these controls. Each of these components is detailed below.

2.3.4.1 *Mass-corrections for tissue Hg*

Positive relationships between fish body size and tissue Hg concentrations are well documented for many fish species (Peterson *et al.*, 2007b; Scudder Eikenberry *et al.*, 2015; Walters *et al.*, 2010; Wiener *et al.*, 2003) and a clear positive correlation between Hg and fish mass was present in our dataset. As such, we examined mass-corrected fish Hg concentrations to understand broader scale watershed and biogeochemical controls on tissue Hg versus patterns associated with individual growth. To obtain mass-corrected values, we fit a linear model for tissue Hg as a function of $\log_{10}$-transformed fish mass and then used the product of the covariate estimate from that model and each fish's mass to obtain a mass-corrected Hg concentration for each sample site. This approach is similar to length-based corrections used in other studies of fish Hg (Eagles-Smith & Ackerman, 2014; Eagles-Smith *et al.*, 2016). These mass-corrected Hg values were then assessed for spatial autocorrelation using empirical semivariance (see below) and mapped to identify spatial patterns in fish Hg. Due to some spatial autocorrelation in fish mass, and to reduce bias in parameter estimation in SSNMs, fish Hg values were used as the response variable, with log-transformed fish mass included as a covariate in all candidate spatial models.

2.3.4.2 *Empirical semivariograms*

Empirical semivariograms show the strength of spatial dependence between sites at given distances (Olea, 1994), and observed patterns can reveal spatial structure of ecological or biogeochemical processes underlying sample data (McGuire *et al.*, 2014). Semivariogram distances are generally measured as the Euclidean or straight line distance between two sample points (Matheron, 1963); however hydrologic distance is often a more meaningful spatial dimension for assessing spatial structure in data from stream networks (Cressie *et al.*, 2006; Ganio *et al.*, 2005; Peterson *et al.*, 2006). Hydrologic distance can be further subdivided into flow-connected and flow-unconnected dimensions (Ver Hoef & Peterson, 2010). Flow-connected sites share flow (e.g. a site downstream of another), whereas flow-unconnected sites may share a common downstream junction, but flow does not pass from one site to the other (e.g. adjacent drainages). Fish movement downstream and then upstream is an example of where flow-unconnected spatial relationships may be important (Isaak *et al.*, 2010). Comparing semivariance in both Euclidian and hydrologic spatial dimensions can yield insights into both watershed and instream factors influencing observations (McGuire *et al.*, 2014). We calculated semivariance of sample THg values according to Euclidean and hydrologic distances using:

$$\gamma(h) = \frac{1}{2|N(h)|} \sum_{N(h)} \left(z_i - z_j\right)^2 \qquad (1)$$

Where γ is semivariance, N(h) is the set of all pairwise distances i – j = h, |N(h)| is the number of distinct pairs in N(h), and z_i and z_j are data values at spatial locations i and j, respectively (Matheron, 1963). We used a maximum separation distance of 1200 km, 20 lag bins, and a minimum of 15 point pairs per lag bin in semivariance computations. We assessed general trends in spatial dependence, range (distance of asymptote or peak in semivariance), nugget (variance at

finest spatial scale), and nested spatial structures as denoted by inflection points in the data (McGuire *et al.*, 2014; Rossi *et al.*, 1992). This approach aids in interpreting spatial scales underlying observed Hg patterns and in covariate and model selection.

2.3.4.3 *Spatial stream network models*

We used SSNMs to analyze THg for all sites sampled (n = 68). These models are described in detail elsewhere (Peterson & Hoef, 2010; Ver Hoef *et al.*, 2006; Ver Hoef & Peterson, 2010) and additional detail is in the supporting information (SI). In brief, these models explicitly account for spatial relationships within a stream network, including flow magnitude, direction, and connectivity. SSNMs provide flexible covariance structures and improved model performance for spatially autocorrelated data (Peterson *et al.*, 2006; Peterson *et al.*, 2007a). Covariance is determined via both hydrologic (tail-up or flow-connected) and Euclidean distance. We used a mixed-effects modeling framework in which the observed variance in THg across the river network is explained by a set of covariates modeled as fixed effects (e.g. wetland cover %), and these spatial covariance matrices as random effects. All SSNMs were fit within R using the SSN package (R Core Team, 2020; Ver Hoef *et al.*, 2014).

2.3.4.4 *Spatial covariates*

Potential covariates were compiled using the STARS toolbox in ArcGIS and publicly available geospatial datasets (Table S2.1) (Peterson & Hoef, 2014). Watershed covariates for each sample site were accumulated based on upstream drainage areas, and were derived as percent cover for categorical datatypes (e.g. wetland cover percent) and as watershed mean values for continuous data (e.g. watershed slope). All covariates were centered to a mean of 0 and standard deviation of

1 to compare the effect size of covariates. A set of *a priori* candidate models was developed and spatial covariates were selected based on factors which we hypothesized to affect instream Hg.

Sample site DOC measures were included in candidate models because DOC and mercury are strongly positively correlated in many freshwater systems (Lavoie *et al.*, 2019). Mean annual precipitation, watershed slope, and watershed relief were included in candidate models as these factors are expected to affect the movement of water and materials from uplands to the stream channel (Lintern *et al.*, 2018; Smits *et al.*, 2017) and can also influence groundwater transport through bog and peat environments contributing to elevated instream Hg (Krabbenhoft & Babiarz, 1992; Krabbenhoft *et al.*, 1995). Watershed wetland cover was also included in candidate models due to positive effects on Hg in some river systems (Hurley *et al.*, 1995). Hg-bearing quartz vein systems of the Kuskokwim Mineral Belt within the Tintina Gold Province span much of the Kuskokwim river watershed, with Hg occurrences noted throughout the central portion of the watershed between the Takotna and Aniak rivers (Gough & Day, 2010; Miller *et al.*, 2007). *A priori* model covariates for Hg include a subset of surficial geology types associated with these features. Surface geology was simplified into 12 major groups based on lithology type and age from the Global Lithological Map database (Hartmann & Moosdorf, 2012). A complete list of spatial covariates and data sources is in Table S2.1.

2.3.4.5 *Variance composition*

The flexible covariance structures in SSNMs are well-suited for evaluating the relative effects of watershed controls (e.g. wetlands) and instream processing and transport by examining variance composition (Ver Hoef *et al.*, 2014; Ver Hoef & Peterson, 2010). Variance composition for SSNMs is partitioned among the various autocovariance structures (e.g. Euclidian, flow-

connected [tail-up]) and the fixed effects or covariates (e.g. wetland %, DOC). Variance composition was determined to compare the relative proportion of variance explained by the random and fixed effects to evaluate broad scale watershed controls, *in situ* biogeochemical conditions, and downstream transport processes that mediate tissue Hg in the Kuskokwim.

2.3.4.6 *Model selection*

SSNM formulations were initially fit to univariate models, with parameters for hypothesized predictor variables estimated using maximum-likelihood. For these model fits, all runs used the same random effect structure with exponential tail-up (flow-connected, see SI) and Euclidean spatial autocovariance components (Ver Hoef *et al.*, 2014). Univariate models were compared using root mean square prediction error (RMSPE) derived from leave-one-out cross-validation (LOOCV) predictions, and a spatial corrected Akaike information criterion (AIC) (Hoeting *et al.*, 2006). This metric is similar to standard AIC but penalizes SSNMs based on the number of parameters used in the spatial autocovariance structure:

$$AIC = -2\backslash\ell_{profile} + 2\mathrm{n}\,\frac{p+k+1}{n-p-k-2} \qquad (3)$$

Where ℓ_{profile} is the profile log-likelihood function (Cressie, 1993), n is the sample size, $p - 1$ is the number of covariates, and k is the number of autocorrelation parameters.

Additional candidate predictor variables were then combined with the best covariates in a stepwise fashion, and again selected using RMSPE and AIC. We then compared various spatial autocovariance structures on models fit using restricted maximum likelihood estimation. We expected spatial covariates (e.g. wetland %) to capture the Euclidean spatial structure in our data and for instream conditions (e.g. DOC) and downstream transport to influence the flow-

connected (tail-up) dimension. As such, we first fit models for THg using only the fixed effects and a flow-connected spatial dimension for the random error structure. We then computed empirical semivariance for the residual error to evaluate any remaining spatial structure in the data. For comparison, we also fit non-spatial linear models.

2.3.4.7 *Network-wide Hg predictions*

The best SSNM was used to develop river-wide predictions for tissue THg (Fig. 2.1). Mean observed sculpin mass (1.9 ± 0.13 g [1 SE]) was used for model predictions. Spatial covariates for model predictions were derived for all 2^{nd} – 8^{th} order stream segments in the Kuskokwim using the STARS toolbox in ArcGIS (Peterson & Hoef, 2014).

2.4 Results

Sculpin tissue THg in the Kuskokwim displayed both broad, watershed scale and finer scale instream spatial patterning, generally with lower THg values in the eastern portion of the basin and higher values to the west (Fig. 2.1), though there were some exceptions to this general trend. THg in our samples ranged from 0.02 – 0.50 mg kg^{-1} (wet mass), with a mean of 0.13 ± 0.01 mg kg^{-1} (1 SE).

Tissue THg was positively correlated with fish mass and DOC (Fig. 2.2a,b). THg was also weakly positively correlated with the Kuskokwim Group geologic formation and sporadic permafrost coverage, derived as watershed percentage upstream of each sample site. THg was negatively correlated with the proportion of the watershed overlain by the Farewell Terrane, with glaciers and barren rock, and with mean watershed slope (Fig. 2.2 c,d,e). For sites downstream of

historic or actively mined areas (n = 90), THg was negatively correlated with distance from mined sites (Fig. 2.2f).

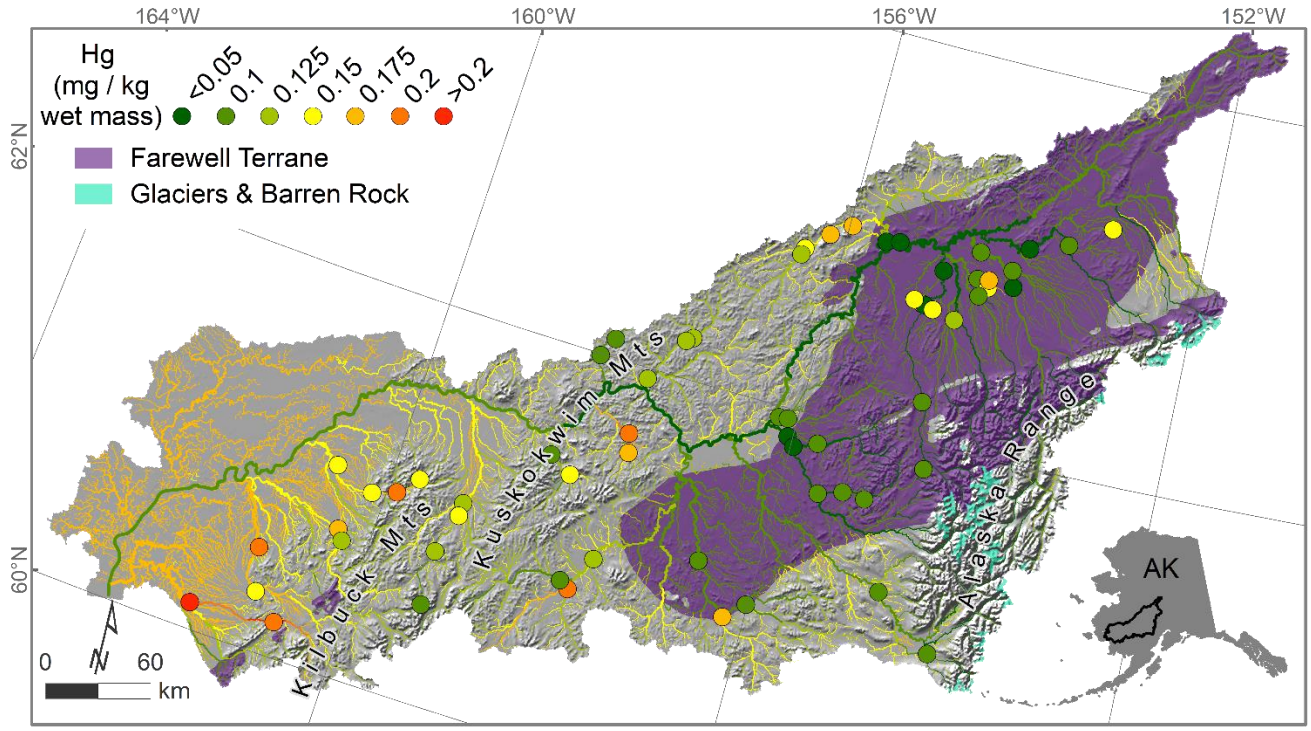

Figure 2.1. *Map of mass-corrected THg sample measures (colored points), network-wide predictions for sculpin tissue THg (colored stream lines), and geologic units used as SSNM spatial covariates for THg.*

Semivariograms for THg revealed distinct spatial structuring in both Euclidian and flow-unconnected spatial dimensions, with weak or random spatial structure in the flow-connected spatial dimension (Fig. 2.3a). Euclidian spatial dependence increased to a range of approximately 600 km, while flow-unconnected spatial dependence had multi-scale controls, exhibited by inflection points in the semivariograms at ranges of 600 and 1100 km.

The best SSNM for THg included covariates for fish mass (log_{10}) (β = 0.10), watershed % covered by the Farewell Terrane (β = -0.13), watershed % glaciers and barren rock (β = -0.08), and mean watershed slope (β = -0.07). Of the candidate models for THg, those within 2 AIC points of the best model also included covariates for DOC, the Kuskokwim Group geologic formation, and mean watershed relief (Table S2.2).

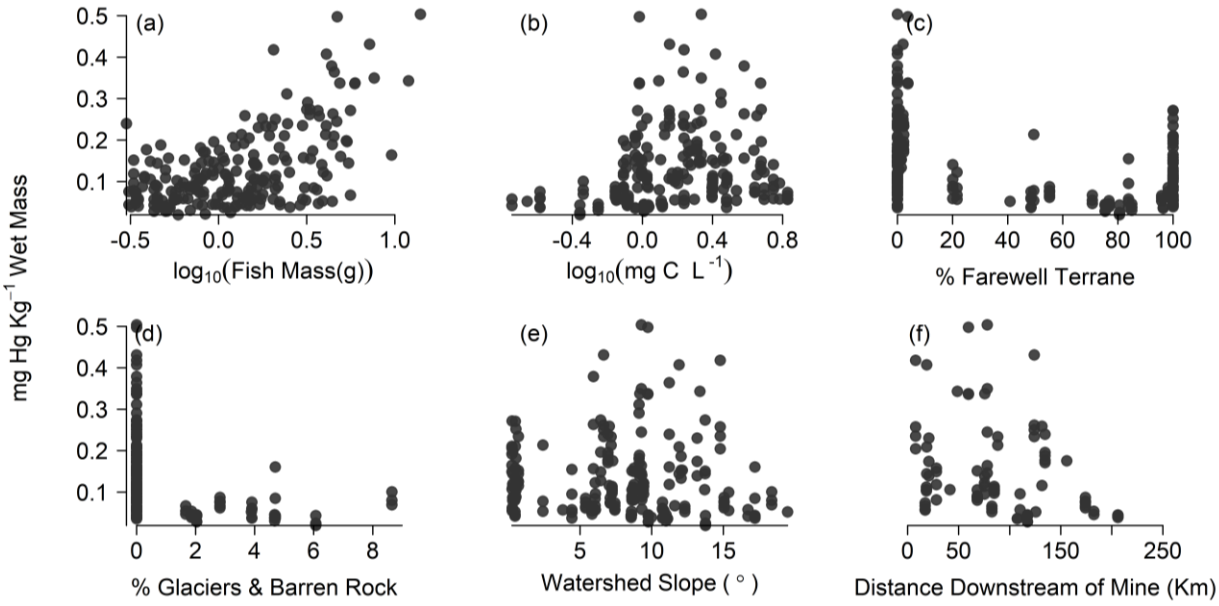

Figure 2.2. *Scatterplots of sculpin tissue THg versus fish mass (a), dissolved organic carbon concentration (b), watershed cover by the Farewell Terrane geologic unit (c), watershed cover by glaciers and barren rock (d), mean watershed slope (e), and distance downstream of mine sites (f).*

The best model for sculpin THg was a full spatial model that included tail-up (flow-connected) autocovariance (Table S2.3), however, semivariograms of residuals from the non-spatial model (using only fish mass, Farewell Terrane, glaciers, and slope) indicated that most of the spatial

structure in THg was captured by fixed effects alone (Fig. 2.3b,d). Residual variance, RMSPE and AIC were considerably lower for the full spatial model (Fig. 2.3c), and leave-one-out-cross-validation (LOOCV) r^2 was also higher for the full spatial model (Fig. S2.2). Fixed effects, tail-up, and nugget variance components accounted for 36, 41, and 23% of the total explained variance in the spatial model (Fig. 2.3e).

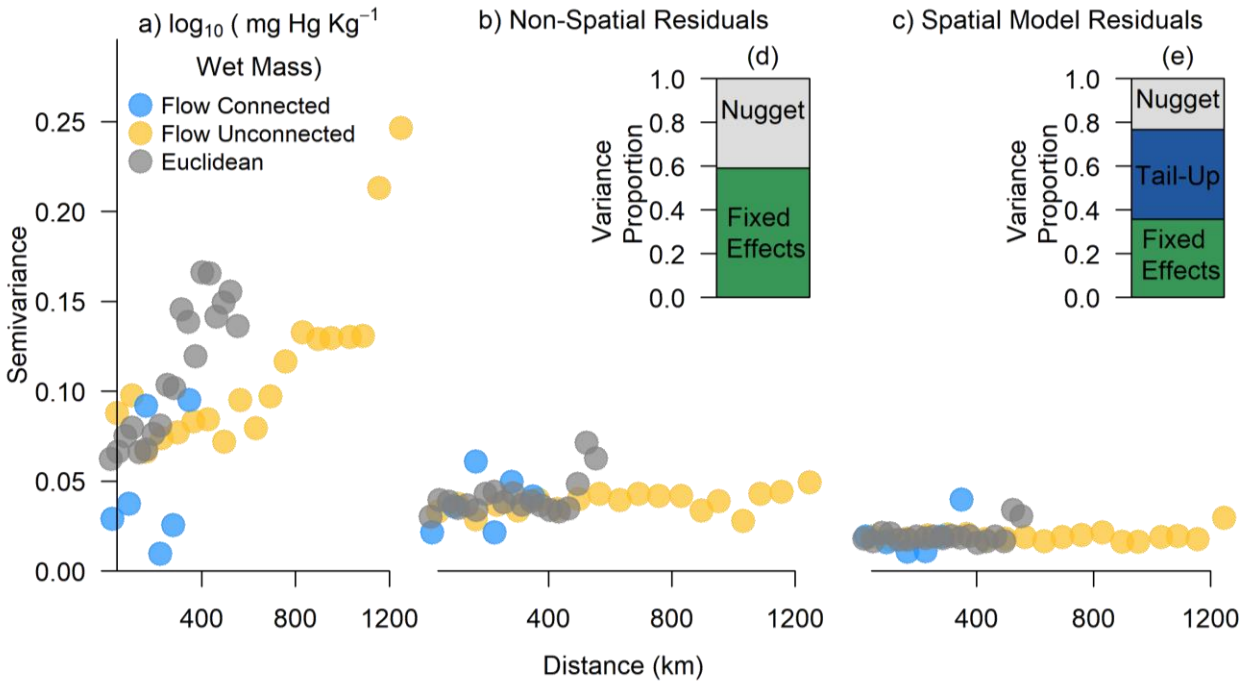

Figure 2.3. *Empirical semivariograms computed in flow-connected, flow-unconnected, and Euclidian distances for sculpin tissue Hg measurements (a), residuals from a non-spatial model for tissue THg (b), and residuals from a full SSNM model for tissue THg (c). Variance composition for the non-spatial (d) and full SSNM (e) are separated into fixed effects, tail-up (flow-connected) effects, and nugget (random error).*

2.5 Discussion

Spatial structure in riverine fish Hg yields insights into the processes underlying Hg bioavailability to aquatic organisms and their consumers. Spatial patterns for sculpin tissue THg in the Kuskokwim River largely reflected broad scale watershed controls, however these watershed controls likely also governed instream biogeochemical conditions mediating Hg bioavailability (French et al., 2020, *in review)*.

The distinct east-west spatial patterning for THg was strongly correlated with broad-scale geologic blocks comprising the alkaline Farewell Terrane and mixed-sedimentary rocks of the Kuskokwim Group (Fig. 2.1). The Kuskokwim Group in particular includes known metal-bearing quartz veins and has been mined for Hg and other metals for over a century (Goldfarb *et al.*, 2007). These lithologies are also important drivers of instream conditions like alkalinity and pH (Fig. S2.3, French et al., 2020, *in review*). Previous work in temperate stream systems has shown higher levels of instream THg in lower pH streams, despite uniform atmospheric Hg deposition between study streams (Mason *et al.*, 2000). Low pH promotes complexation of Hg with organic ligands (Watras *et al.*, 1995), including humic acids (Gu *et al.*, 2011), and combined measures of DOC and pH can account for 85-90% of Hg variation in lakes (Watras *et al.*, 1995). In the Kuskokwim, streams draining catchments overlying the Farewell Terrane generally had high pH, high alkalinity, low DOC, and also low THg, whereas those streams draining the Kuskokwim Group and low-lying areas to the west had lower pH, lower alkalinity, higher DOC, and higher THg (Fig. 2.1, Fig. S2.3). These broad scale watershed features thus shape biogeochemical conditions affecting Hg bioavailability to sculpins throughout the Kuskokwim watershed.

The effect of DOC on sculpin THg in the Kuskokwim was likely controlled by broad scale geomorphic factors shaping instream biogeochemistry. We expected SSNMs for Hg to include features associated with OM-rich environments such as wetlands, bogs, and peat soils. For example, a positive correlation between fish THg and watershed wetland cover was expected due to environmental conditions in wetlands that promote Hg methylation, including an abundance of labile DOC, anaerobic sediments, microbial activity, and seasonal wetting and drying that enhances redox cycles (St. Louis *et al.*, 1994; Wiener *et al.*, 2003). For our dataset, however, broad-scale features like watershed slope and geology were better predictors of sculpin THg than finer scale landscape features such as wetlands and bogs (Table S2.2). In boreal river systems, low gradient basins generally have lower pH and more colored water (proxy for DOC) (Agren *et al.*, 2014; Varanka *et al.*, 2015). Because both pH and DOC followed similar east-west spatial patterning to Hg in the Kuskokwim, the underlying geomorphic mechanisms for this east-west trend (relief, geology) had better predictive power for THg than site-specific DOC.

The effect of these broad-scale controls is further supported by semivariograms and in variance composition from SSNM models for THg (Fig. 2.3b-e). Semivariograms of raw data (Fig. 2.3a) showed strong spatial dependence in both Euclidian and flow-unconnected space up to broad-scale ranges of 600-1100 km. This spatial range is consistent with the spatial scales of geologic blocks used as spatial covariates. An SSNM with no spatial autocovariance components (Fig. 2.3b) had little spatial structure remaining in residual semivariance, suggesting that the spatial covariates themselves (Farewell Terrane, watershed slope) accounted for spatial patterning in THg, and that spatial patterning in THg was not predominated by downstream transport along the network. The full spatial model with a tail-up (flow-connected) spatial autocovariance

function did reduce overall residual semivariance (Fig. 2.3c) and improve predictive power (Fig. S2.2), however the spatial dependence of residuals was similar to the non-spatial model.

Slimy sculpins are at a low trophic level relative to the piscivorous fish consumed by subsistence communities in the Kuskokwim basin. Previous work has shown higher levels of Hg in larger fish (e.g. burbot, Northern pike) in Kuskokwim streams draining heavily mined areas in the watershed (Matz *et al.*, 2017). Although our samples included sites adjacent to recently or actively mined areas, we did not sample sites specifically mined for Hg, or 1st order channels sampled by Matz *et al.* (2017) where THg is elevated. For sites downstream of historically mined areas, sculpin THg did show a positive relationship with proximity to mines (Fig. 2.2f), however this relationship should be explored further with more accurate and complete current and historic mining data than what is currently publicly available (U.S. Geological Survey, 2008). The pattern observed in our data may simply reflect spatial controls on Hg in streams that happen to coincide with the locations of metal mines in the Kuskokwim watershed.

Our results indicate that Kuskokwim sculpin tissue THg reflected both broad scale watershed controls and instream factors. However, the effect of instream conditions on THg in the Kuskokwim were largely controlled by geomorphic conditions that also shape biogeochemistry, such as the effect of watershed slope on DOC in streams. Strong Euclidian and flow-unconnected spatial dependence among sample sites also supports the strong effect of broad-scale watershed features on Hg when compared to transport processes along the Kuskokwim network. The use of broad-scale, publicly available geospatial data and SSNMs to predict instream THg in boreal river networks provides an easily accessible approach for resource managers to identify current spatial patterns in Hg contamination and to understand how

changing watershed conditions may impact the Hg contamination of subsistence resources in the future under altered climate regimes or changes in land use.

2.6 References

Agren, A. M., I. Buffam, D. M. Cooper, T. Tiwari, C. D. Evans, and H. Laudon (2014), Can the heterogeneity in stream dissolved organic carbon be explained by contributing landscape elements?, Biogeosciences, 11(4), 1199-1213, doi:10.5194/bg-11-1199-2014.

Baker, M. R., D. E. Schindler, G. W. Holtgrieve, and V. L. St. Louis (2009), Bioaccumulation and Transport of Contaminants: Migrating Sockeye Salmon As Vectors of Mercury, Environ Sci Technol, 43(23), 8840-8846, doi:10.1021/es901798f.

Barbosa, A. C., J. de Souza, J. G. Dorea, W. F. Jardim, and P. S. Fadini (2003), Mercury biomagnification in a tropical black water, Rio Negro, Brazil, Arch Environ Con Tox, 45(2), 235-246, doi:10.1007/s00244-003-0207-1.

Beikman, H. M. (1980), Geologic map of Alaska, U.S. Geological Survey.

Bloom, N. S. (1992), On the Chemical Form of Mercury in Edible Fish and Marine Invertebrate Tissue, Can J Fish Aquat Sci, 49(5), 1010-1017, doi:DOI 10.1139/f92-113.

Burns, D. A., K. Riva-Murray, P. M. Bradley, G. R. Aiken, and M. E. Brigham (2012), Landscape controls on total and methyl Hg in the upper Hudson River basin, New York, USA, J Geophys Res-Biogeo, 117, doi:Artn G0103410.1029/2011jg001812.

Chan, H. M., and O. Receveur (2000), Mercury in the traditional diet of indigenous peoples in Canada, Environ Pollut, 110(1), 1-2, doi:Doi 10.1016/S0269-7491(00)00061-0.

Chan, H. M., A. M. Scheuhammer, A. Ferran, C. Loupelle, J. Holloway, and S. Weech (2003), Impacts of mercury on freshwater fish-eating wildlife and humans, Hum Ecol Risk Assess, 9(4), 867-883, doi:Doi 10.1080/713610013.

Chasar, L. C., B. C. Scudder, A. R. Stewart, A. H. Bell, and G. R. Aiken (2009), Mercury Cycling in Stream Ecosystems. 3. Trophic Dynamics and Methylmercury Bioaccumulation, Environ Sci Technol, 43(8), 2733-2739, doi:10.1021/es8027567.

Cressie, N., J. Frey, B. Harch, and M. Smith (2006), Spatial prediction on a river network, J Agr Biol Envir St, 11(2), 127-150, doi:10.1198/108571106x110649.

Cressie, N. A. C. (1993), Statistics for spatial data, Rev. ed. ed., New York : Wiley, New York.

Drenner, R. W., M. M. Chumchal, C. M. Jones, C. M. B. Lehmann, D. A. Gay, and D. I. Donato (2013), Effects of Mercury Deposition and Coniferous Forests on the Mercury Contamination of Fish in the South Central United States, Environ Sci Technol, 47(3), 1274-1279, doi:10.1021/es303734n.

Driscoll, C. T., R. P. Mason, H. M. Chan, D. J. Jacob, and N. Pirrone (2013), Mercury as a Global Pollutant: Sources, Pathways, and Effects, Environ Sci Technol, 47(10), 4967-4983, doi:10.1021/es305071v.

Eagles-Smith, C. A., and J. T. Ackerman (2014), Mercury bioaccumulation in estuarine wetland fishes: Evaluating habitats and risk to coastal wildlife, Environ Pollut, 193, 147-155, doi:10.1016/j.envpol.2014.06.015.

Eagles-Smith, C. A., et al. (2016), Spatial and temporal patterns of mercury concentrations in freshwater fish across the Western United States and Canada, Sci Total Environ, 568, 1171-1184, doi:10.1016/j.scitotenv.2016.03.229.

Fitzgerald, W. F., D. R. Engstrom, R. P. Mason, and E. A. Nater (1998), The case for atmospheric mercury contamination in remote areas, Environ Sci Technol, 32(1), 1-7, doi:DOI 10.1021/es970284w.

Ganio, L. M., C. E. Torgersen, and R. E. Gresswell (2005), A geostatistical approach for describing spatial pattern in stream networks, Front Ecol Environ, 3(3), 138-144, doi:Doi 10.2307/3868541.

Goldfarb, R. J., E. E. Marsh, C. J. R. Hart, J. L. Mair, M. L. Miller, and C. Johnson (2007), Geology and origin of epigenetic lode gold deposits, Tintina Gold Province, Alaska and Yukon: Chapter A in Recent U.S. Geological Survey studies in the Tintina Gold Province, Alaska, United States, and Yukon, Canada--results of a 5-year project, Report Rep. 2007-5289A, 22 pp, Reston, VA.

Gough, L. P., and W. C. Day (2010), Recent U.S. Geological Survey studies in the Tintina Gold Province, Alaska, United States, and Yukon, Canada : results of a 5-year project, Reston, Va. : U.S. Geological Survey, Reston, Va.

Gray, M. A., R. A. Curry, T. J. Arciszewski, K. R. Munkittrick, and S. M. Brasfield (2018), The biology and ecology of slimy sculpin: A recipe for effective environmental monitoring, Facets, 3, 103-127, doi:10.1139/facets-2017-0069.

Gu, B., Y. Bian, C. L. Miller, W. Dong, X. Jiang, and L. Liang (2011), Mercury reduction and complexation by natural organic matter in anoxic environments, Proceedings of the National Academy of Sciences, 108(4), 1479, doi:10.1073/pnas.1008747108.

Hartmann, J., and N. Moosdorf (2012), The new global lithological map database GLiM: A representation of rock properties at the Earth surface, Geochem Geophy Geosy, 13, doi:Artn Q12004 10.1029/2012gc004370.

Hoeting, J. A., R. A. Davis, A. A. Merton, and S. E. Thompson (2006), Model selection for geostatistical models, Ecol Appl, 16(1), 87-98, doi:Doi 10.1890/04-0576.

Hsu-Kim, H., C. S. Eckley, D. Acha, X. B. Feng, C. C. Gilmour, S. Jonsson, and C. P. J. Mitchell (2018), Challenges and opportunities for managing aquatic mercury pollution in altered landscapes, Ambio, 47(2), 141-169, doi:10.1007/s13280-017-1006-7.

Hurley, J. P., J. M. Benoit, C. L. Babiarz, M. M. Shafer, A. W. Andren, J. R. Sullivan, R. Hammond, and D. A. Webb (1995), Influences of Watershed Characteristics on Mercury Levels in Wisconsin Rivers, Environ Sci Technol, 29(7), 1867-1875, doi:10.1021/es00007a026.

Isaak, D. J., C. H. Luce, B. E. Rieman, D. E. Nagel, E. E. Peterson, D. L. Horan, S. Parkes, and G. L. Chandler (2010), Effects of climate change and wildfire on stream temperatures and salmonid thermal habitat in a mountain river network, Ecol Appl, 20(5), 1350-1371, doi:10.1890/09-0822.1.

Klapstein, S. J., and N. J. O'Driscoll (2018), Methylmercury Biogeochemistry in Freshwater Ecosystems: A Review Focusing on DOM and Photodemethylation, B Environ Contam Tox, 100(1), 14-25, doi:10.1007/s00128-017-2236-x.

Krabbenhoft, D. P., and C. L. Babiarz (1992), The role of groundwater transport in aquatic mercury cycling, Water Resour Res, 28(12), 3119-3128, doi:10.1029/92wr01766.

Krabbenhoft, D. P., J. M. Benoit, C. L. Babiarz, J. P. Hurley, and A. W. Andren (1995), Mercury cycling in the Allequash Creek watershed, northern Wisconsin, Water, Air, and Soil Pollution, 80(1), 425-433, doi:10.1007/BF01189692.

Krabbenhoft, D. P., and D. A. Rickert (1995), Mercury contamination of aquatic ecosystems, Report Rep. 216-95, 4 pp.

Lavoie, R. A., M. Amyot, and J. F. Lapierre (2019), Global Meta-Analysis on the Relationship Between Mercury and Dissolved Organic Carbon in Freshwater Environments, J Geophys Res-Biogeo, 124(6), 1508-1523, doi:10.1029/2018jg004896.

Lintern, A., J. A. Webb, D. Ryu, S. Liu, U. Bende-Michl, D. Waters, P. Leahy, P. Wilson, and A. W. Western (2018), Key factors influencing differences in stream water quality across space, Wires Water, 5(1), doi:ARTN e1260 10.1002/wat2.1260.

Mason, R. P., J. M. Laporte, and S. Andres (2000), Factors Controlling the Bioaccumulation of Mercury, Methylmercury, Arsenic, Selenium, and Cadmium by Freshwater Invertebrates and Fish, Arch Environ Con Tox, 38(3), 283-297, doi:10.1007/s002449910038.

Matheron, G. (1963), Principles of geostatistics, Economic Geology and the Bulletin of the Society of Economic Geologists, 58(8), 1246-1266, doi:10.2113/gsecongeo.58.8.1246.

Matz, A., M. Varner, M. Albert, and K. Wuttig (2017), Mercury, arsenic, and antimony in aquatic biota from the Middle Kuskokwim River region, Alaska, 2010-2014Rep. Technical Report #61, Bureau of Land Management.

McGuire, K. J., C. E. Torgersen, G. E. Likens, D. C. Buso, W. H. Lowe, and S. W. Bailey (2014), Network analysis reveals multiscale controls on streamwater chemistry, P Natl Acad Sci USA, 111(19), 7030-7035, doi:10.1073/pnas.1404820111.

Mertie, J. B. (1936), Mineral deposits of the Ruby-Kuskokwim region Alaska, Washington D.C. : United States Department of the Interior, Geological Survey : United States Government Printing Office, Washington [D.C.].

Miller, M. L., D. C. Bradley, R. J. Goldfarb, and T. K. Bundtzen (2007), Tectonic setting of Late Cretaceous gold and mercury metallogenesis, Kuskokwim mineral belt, southwestern

Alaska, USA, edited by C. J. Andrew, et al., pp. 683-686, [varies], International: [varies], [varies].

Olea, R. A. (1994), Fundamentals of semivariogram estimation, modeling, and usage, in AAPG Computer Applications in Geology, edited by J. M. Yarus and R. L. Chambers, pp. 27-35, Tulsa, OK.

Oliveira, R. C., J. G. Dorea, J. V. E. Bernardi, W. R. Bastos, R. Almeida, and A. G. Manzatto (2010), Fish consumption by traditional subsistence villagers of the Rio Madeira (Amazon): Impact on hair mercury, Ann Hum Biol, 37(5), 629-642, doi:10.3109/03014460903525177.

Peterson, E. E., and J. M. V. Hoef (2010), A mixed-model moving-average approach to geostatistical modeling in stream networks, Ecology, 91(3), 644-651, doi:Doi 10.1890/08-1668.1.

Peterson, E. E., and J. M. V. Hoef (2014), STARS: An ArcGIS Toolset Used to Calculate the Spatial Information Needed to Fit Spatial Statistical Models to Stream Network Data, J Stat Softw, 56(2), 1-17.

Peterson, E. E., A. A. Merton, D. M. Theobald, and N. S. Urquhart (2006), Patterns of spatial autocorrelation in stream water chemistry, Environ Monit Assess, 121(1-3), 571-596, doi:10.1007/s10661-005-9156-7.

Peterson, E. E., D. M. Theobald, and J. M. V. Hoef (2007), Geostatistical modelling on stream networks: developing valid covariance matrices based on hydrologic distance and stream flow, Freshwater Biol, 52(2), 267-279, doi:10.1111/j.1365-2427.2006.01686.x.

Peterson, S. A., J. Van Sickle, A. T. Herlihy, and R. M. Hughes (2007), Mercury Concentration in Fish from Streams and Rivers Throughout the Western United States, Environ Sci Technol, 41(1), 58-65, doi:10.1021/es061070u.

R Core Team (2020), R: A language and environmental for statistical computing, edited, R Foundation for Statistical Computing, Vienna, Austria.

Rice, K. M., E. M. Walker, Jr., M. Wu, C. Gillette, and E. R. Blough (2014), Environmental mercury and its toxic effects, J Prev Med Public Health, 47(2), 74-83, doi:10.3961/jpmph.2014.47.2.74.

Rossi, R. E., D. J. Mulla, A. G. Journel, and E. H. Franz (1992), Geostatistical Tools for Modeling and Interpreting Ecological Spatial Dependence, Ecol Monogr, 62(2), 277-314, doi:Doi 10.2307/2937096.

Sandheinrich, M., and J. Wiener (2011), Methylmercury in freshwater fish: Recent advances in assessing toxicity of environmentally relevant exposures, in Environmental Contaminants in Biota: Interpreting Tissue Concentrations, edited by W. Beyer and J. Meador, pp. 169-190, CRC Press, Boca Raton, FL, USA.

Scudder Eikenberry, B. C., K. Riva-Murray, C. D. Knightes, C. A. Journey, L. C. Chasar, M. E. Brigham, and P. M. Bradley (2015), Optimizing fish sampling for fish–mercury bioaccumulation factors, Chemosphere, 135, 467-473, doi:https://doi.org/10.1016/j.chemosphere.2014.12.068.

Selin, H., S. E. Keane, S. X. Wang, N. E. Selin, K. Davis, and D. Bally (2018), Linking science and policy to support the implementation of the Minamata Convention on Mercury, Ambio, 47(2), 198-215, doi:10.1007/s13280-017-1003-x.

Shanley, J. B., et al. (2012), MERGANSER: An Empirical Model To Predict Fish and Loon Mercury in New England Lakes, Environ Sci Technol, 46(8), 4641-4648, doi:10.1021/es300581p.

Smits, A. P., D. E. Schindler, G. W. Holtgrieve, K. J. Jankowski, and D. W. French (2017), Watershed geomorphology interacts with precipitation to influence the magnitude and source of CO2 emissions from Alaskan streams, J Geophys Res-Biogeo, 122(8), 1903-1921, doi:10.1002/2017jg003792.

Southworth, G. R., M. J. Peterson, and M. A. Bogle (2004), Bioaccumulation Factors for Mercury in Stream Fish, Environmental Practice, 6(2), 135-143, doi:10.1017/S1466046604000249.

St. Louis, V. L., J. W. M. Rudd, C. A. Kelly, K. G. Beaty, N. S. Bloom, and R. J. Flett (1994), Importance of Wetlands as Sources of Methyl Mercury to Boreal Forest Ecosystems, Can J Fish Aquat Sci, 51(5), 1065-1076, doi:10.1139/f94-106.

Sundseth, K., J. M. Pacyna, E. G. Pacyna, N. Pirrone, and R. J. Thorne (2017), Global Sources and Pathways of Mercury in the Context of Human Health, Int J Env Res Pub He, 14(1), doi:ARTN 105 10.3390/ijerph14010105.

Trasande, L., J. E. Cortes, P. J. Landrigan, M. I. Abercrombie, R. F. Bopp, and E. Cifuentes (2010), Methylmercury exposure in a subsistence fishing community in Lake Chapala, Mexico: an ecological approach, Environ Health-Glob, 9, doi:Artn 110.1186/1476-069x-9-1.

Tsui, M. T. K., J. D. Blum, J. C. Finlay, S. J. Balogh, S. Y. Kwon, and Y. H. Nollet (2013), Photodegradation of methylmercury in stream ecosystems, Limnol Oceanogr, 58(1), 13-22, doi:10.4319/lo.2013.58.1.0013.

U.S. Geological Survey (2008), Alaska Resource Data File (ARDF), in U.S. Geological Survey Open-File Report, edited by U.S. Geological Survey.

Varanka, S., J. Hjort, and M. Luoto (2015), Geomorphological factors predict water quality in boreal rivers, Earth Surface Processes and Landforms, 40(15), 1989-1999, doi:10.1002/esp.3601.

Ver Hoef, J., E. Peterson, D. Clifford, and R. Shah (2014), SSN: An R Package for Spatial Statistical Modeling on Stream Networks, Journal of Statistical Software; Vol 1, Issue 3 (2014).

Ver Hoef, J. M., E. Peterson, and D. Theobald (2006), Spatial statistical models that use flow and stream distance, Environ Ecol Stat, 13(4), 449-464, doi:10.1007/s10651-006-0022-8.

Ver Hoef, J. M., and E. E. Peterson (2010), A Moving Average Approach for Spatial Statistical Models of Stream Networks, J Am Stat Assoc, 105(489), 6-18, doi:10.1198/jasa.2009.ap08248.

Walters, D. M., K. A. Blocksom, J. M. Lazorchak, T. Jicha, T. R. Angradi, and D. W. Bolgrien (2010), Mercury Contamination in Fish in Midcontinent Great Rivers of the United States: Importance of Species Traits and Environmental Factors, Environ Sci Technol, 44(8), 2947-2953, doi:10.1021/es903754d.

Watras, C. J., K. A. Morrison, J. S. Host, and N. S. Bloom (1995), Concentration of mercury species in relationship to other site-specific factors in the surface waters of northern Wisconsin lakes, Limnol Oceanogr, 40(3), 556-565, doi:10.4319/lo.1995.40.3.0556.

Wiener, J. G., D. P. Krabbenhoft, G. H. Heinz, and A. M. Scheuhammer (2003), Ecotoxicology of mercury, in Handbook of Ecotoxicology, edited by D. J. Hoffman, B. A. Rattner, G. A. Burton and J. Cairns, pp. 409-463, CRC Press, Boca Raton, FL, USA.

Wiener, J. G., and D. J. Spry (1996), Toxicological significance of mercury in freshwater fish, in Environmental Contaminants in Wildlife: Interpreting Tissue Concentrations, edited by W. N. Beyer, G. H. Heinz and A. W. Redmon-Norwood, pp. 297-339, Lewis Publishers, Boca Raton, FL.

Wilson, F. H. H., C.P.; Mull, C.G.; Karl, S.M. (2015), Geologic map of Alaska, Report Rep. 3340, Reston, VA.

Supporting Information for Chapter 1

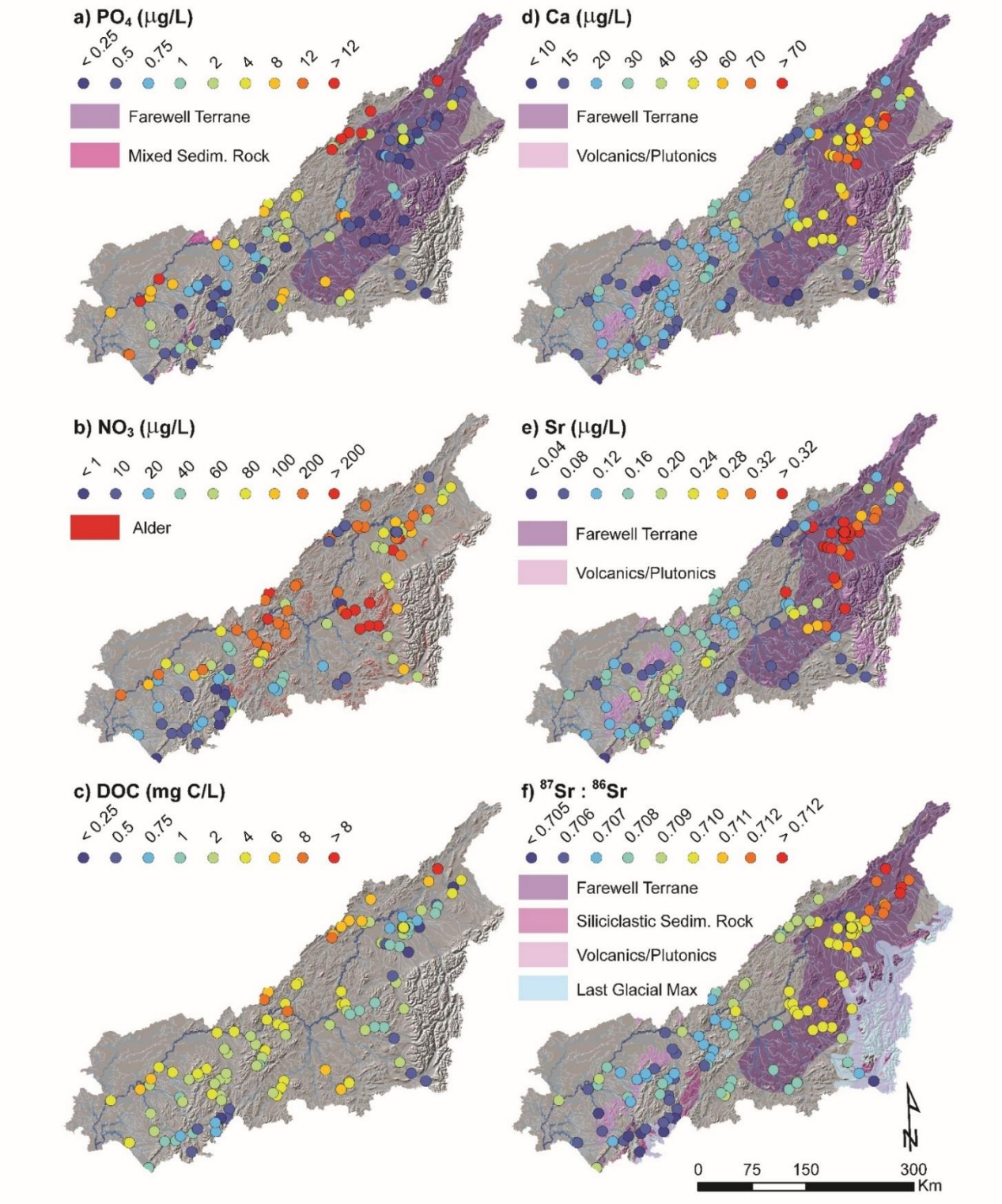

Figure S1.1. Watershed maps of streamwater constituent values at each sample point and spatial watershed covariates from spatial stream network models (SSNMs). SSNMs for PO_4 (a) and NO_3 (b) also included sample site DOC as a covariate. SSNMs for NO_3 and DOC (c) also included covariates for watershed latitude. NO_3, Ca (d), and Sr (e) included covariates for watershed elevation, and DOC and ^{87}Sr:^{86}Sr (f) included covariates for watershed relief, both depicted by hillshading.

Table S1.1. Watershed spatial covariates used in candidate spatial stream network models and geospatial data sources.

Covariate	Description	Data Source
Relief	Average watershed relief	USGS National Elevation Dataset, 2017
Slope	Average watershed slope	USGS National Elevation Dataset, 2017
Zmean	Average watershed elevation	USGS National Elevation Dataset, 2017
Precip	Mean annual precipitation	Scenarios Network for Alaska & Arctic Planning, 2017
Lat	Average watershed latitude	Calculated in Esri ArcMap
Long	Average watershed longitude	Calculated in Esri ArcMap
LWG	Late Wisconsin glaciated*	Manley & Kaufman, 2002
DecFor	Deciduous forest cover*	USGS National Land Cover Dataset, 2015
MixFor	Mixed deciduous-evergreen forest cover*	USGS National Land Cover Dataset, 2015
EverFor	Evergreen forest cover*	USGS National Land Cover Dataset, 2015
Dwarf	Dwarf shrub cover*	USGS National Land Cover Dataset, 2015
Shrub	Shrub-steppe cover*	USGS National Land Cover Dataset, 2015
Wet	Emergent and woody wetland cover*	USGS National Land Cover Dataset, 2015
Water	Open water cover*	USGS National Land Cover Dataset, 2015
Alder	Mesic alder shrubland*	USGS GAP/LANDFIRE, 2016
Bog	Boreal bog & fen cover*	USGS GAP/LANDFIRE, 2016
Marsh	Boreal freshwater meadow & marsh cover*	USGS GAP/LANDFIRE, 2016
Swamp	Boreal flooded & swamp forest cover*	USGS GAP/LANDFIRE, 2016
Mush	Combined open water, bog, swamp, & marsh cover*	USGS GAP/LANDFIRE, 2016
Peat	Peat soil cover*	USDA SSURGO Soil Map, 2016
Variable	Variable soil cover*	USDA SSURGO Soil Map, 2016
DPF	Discontinuous permafrost cover*	Jorgenson et al., 2008
SPF	Sporadic permafrost cover*	Jorgenson et al., 2008
IPF	Isolated permafrost cover*	Jorgenson et al., 2008
Geo1	Siliciclastic sedimentary rocks; mixed grain size; fossil plant organic material mentioned*	Hartman & Moosdorf, 2012
Geo2	Mixed sedimentary rocks; mixed and fine grain size; metamorphic influence mentioned*	Hartman & Moosdorf, 2012
Geo3	Siliciclastic sedimentary rocks; loess; glacial influence mentioned*	Hartman & Moosdorf, 2012

Covariate	Description	Data Source
Geo4	Siliciclastic sedimentary rocks; mixed grain size; subordinate volcanics mentioned*	Hartman & Moosdorf, 2012
Geo5	Siliciclastic and mixed sedimentary rocks; Pyroclastics mentioned; subordinate volcanics mentioned*	Hartman & Moosdorf, 2012
Geo6	Acid volcanic and acid plutonic rocks*	Hartman & Moosdorf, 2012
Geo7	Intermediate volcanic and plutonic rocks*	Hartman & Moosdorf, 2012
Geo8	Basic volcanic and plutonic rocks*	Hartman & Moosdorf, 2012
Geo9	Mixed sedimentary rocks; mixed grain size; Chert mentioned*	Hartman & Moosdorf, 2012
Geo10	Metamorphics*	Hartman & Moosdorf, 2012
Geo11	Carbonate sedimentary rocks; coarse grained; metamorphic influence mentioned*	Hartman & Moosdorf, 2012
Geo12	Ice and glaciers*	Hartman & Moosdorf, 2012

**Derived as watershed percent cover*

Table S1.2. Summary statistics, optimal spatial scale for best fit spatial stream network model (SSNM), SSNM covariate parameter estimates, root mean square prediction error (RMSPE), and leave-one-out-cross-validation R^2 statistics from SSNMs for each streamwater constituent.

Constituent	Units	Range	Mean	Std. Err.	Scale[1]	Covariate	β_i Estimate[2]	RMSPE	LOOCV R^2
PO_4	$\mu g\ L^{-1}$	0 - 30.7	2.92	0.534	DS - 3	Farewell Terrane	-0.39	4.14	0.456
						$\log_{10}$[DOC]	0.386		
						Mixed sedimentary rock	-0.182		
NO_3	$\mu g\ L^{-1}$	0.2 - 543	85.2	9.28	DS - 2	Alder	0.291	70.7	0.703
						$\log_{10}$[DOC]	-0.137		
						Latitude	0.048		
						Elevation	-0.005		
DOC	$mg\ L^{-1}$	0.18 - 16.0	2.12	0.185	DS - 3	Relief	-0.188	1.41	0.736
						Latitude	0.112		
Ca	$\mu g\ L^{-1}$	6.37 - 77.1	29.5	1.80	DS - 3	Farewell Terrane	0.074	6.09	0.898
						Acid volcanic/plutonic rocks	-0.044		
						Intermediate volcanic/plutonics	-0.036		
						Elevation	0.015		
Sr	$\mu g\ L^{-1}$	0.035 - 0.858	0.194	0.014	DS - 3	Farewell Terrane	0.101	0.058	0.835
						Intermediate volcanic/plutonics	-0.063		
						Acid volcanic/plutonic rocks	-0.062		
						Elevation	0.048		
$^{87}Sr:^{86}Sr$	-	0.7042 - 0.7131	0.708	0.0002	US - 2	Farewell Terrane	0.00077	0.0005	0.943
						Relief	0.00037		
						Glacial maximum	-0.00032		
						Intermediate volcanic/plutonics	-0.0003		
						Siliciclastic sedimentary rock	-0.00028		

1. Spatial scale of best model (see Fig. 2)

2. Covariate estimates are scaled to a mean of 0 and st. dev of 1 for effect size comparison

Table S1.3. Comparison of model performance across spatial scales for each streamwater constituent using root mean square prediction error (RMSPE), spatial Akaike's information criteria (AICc), delta AICc, and adjusted R^2.

Constituent	Units	Spatial Scale	RMSPE	AIC_c	ΔAIC_1	Adj. R^2_2
PO_4	μg L^{-1}	DS-3	4.19	245.51	0.00	0.30
		DS-4	4.18	246.22	0.70	0.29
		US-4	4.17	246.36	0.85	0.29
		US-7	4.17	246.81	1.30	0.28
		DS-5	4.19	246.92	1.41	0.29
		DS-6	4.19	246.94	1.43	0.29
		US-6	4.17	246.96	1.45	0.28
		DS-2	4.22	246.97	1.46	0.30
		DS-7	4.19	247.02	1.50	0.29
		DS-8	4.19	247.03	1.52	0.29
		US-3	4.30	250.38	4.86	0.27
		US-5	4.30	250.38	4.86	0.27
		US-1	4.54	256.64	11.13	0.25
		US-2	4.61	256.70	11.19	0.25
NO_3	μg L^{-1}	DS-2	2.56	176.63	0.00	0.11
		DS-5	2.51	177.01	0.38	0.11
		US-7	2.51	177.09	0.46	0.11
		DS-7	2.51	177.14	0.51	0.11
		DS-8	2.52	177.15	0.52	0.11
		DS-6	2.51	177.19	0.56	0.11
		US-6	2.51	177.35	0.73	0.11
		DS-3	2.52	177.37	0.75	0.11
		DS-4	2.54	177.96	1.33	0.10
		US-4	2.55	178.85	2.22	0.10
		US-3	2.51	179.12	2.49	0.09
		US-5	2.51	179.12	2.49	0.09
		US-2	2.62	183.12	6.49	0.06
		US-1	2.60	184.09	7.46	0.05
DOC	mg L^{-1}	DS-3	1.56	-8.95	0.00	0.31
		DS-4	1.57	-8.66	0.29	0.31
		DS-8	1.57	-7.85	1.09	0.32
		DS-7	1.57	-7.83	1.11	0.31
		DS-2	1.56	-7.74	1.21	0.31
		DS-6	1.57	-7.67	1.28	0.30
		DS-5	1.57	-7.53	1.42	0.30
		US-7	1.58	-5.84	3.11	0.29
		US-6	1.59	-5.20	3.75	0.30
		US-4	1.59	-5.03	3.91	0.30

Constituent	Units	Spatial Scale	RMSPE	AIC_c	ΔAIC_1	Adj. R^2_2
		US-3	1.67	12.00	20.95	0.19
		US-5	1.67	12.00	20.95	0.19
		US-2	1.67	14.66	23.61	0.14
		US-1	1.71	36.01	44.96	0.01
Ca	$\mu g\ L^{-1}$	DS-3	1.26	-208.87	0.00	0.27
		DS-2	1.24	-208.02	0.85	0.27
		DS-8	1.26	-207.41	1.46	0.25
		DS-7	1.26	-207.28	1.59	0.25
		DS-6	1.26	-207.24	1.64	0.25
		DS-4	1.27	-206.66	2.22	0.25
		DS-5	1.26	-206.46	2.41	0.24
		US-6	1.26	-201.84	7.03	0.22
		US-4	1.26	-201.41	7.47	0.22
		US-7	1.26	-200.68	8.20	0.20
		US-3	1.26	-200.09	8.78	0.20
		US-5	1.26	-200.09	8.78	0.20
		US-2	1.28	-188.84	20.03	0.12
		US-1	1.27	-174.46	34.42	0.01
Sr	$\mu g\ L^{-1}$	DS-3	1.34	-155.73	0.00	0.25
		DS-8	1.34	-155.11	0.61	0.25
		DS-7	1.34	-155.04	0.69	0.25
		DS-6	1.34	-154.99	0.73	0.25
		DS-4	1.34	-154.71	1.02	0.25
		DS-5	1.34	-154.34	1.39	0.24
		DS-2	1.31	-153.04	2.69	0.24
		US-3	1.33	-150.53	5.20	0.22
		US-5	1.33	-150.53	5.20	0.22
		US-6	1.35	-146.65	9.08	0.18
		US-4	1.34	-146.58	9.15	0.18
		US-7	1.35	-146.36	9.37	0.18
		US-2	1.36	-140.64	15.08	0.15
		US-1	1.35	-120.22	35.50	-0.01
$^{87}Sr:^{86}Sr$		US-4	0.00047	-1389.87	0.00	0.35
		DS-6	0.00047	-1389.36	0.51	0.35
		DS-7	0.00047	-1389.05	0.82	0.35
		DS-8	0.00047	-1389.01	0.86	0.35
		US-7	0.00046	-1388.93	0.94	0.35
		DS-5	0.00047	-1388.21	1.66	0.34
		US-6	0.00047	-1387.84	2.03	0.35
		DS-4	0.00047	-1386.41	3.46	0.33
		DS-3	0.00047	-1382.43	7.44	0.31

Constituent	Units	Spatial Scale	RMSPE	AIC_c	ΔAIC_1	Adj. R^2_2
		US-3	0.00053	-1376.68	13.19	0.27
		US-5	0.00053	-1376.68	13.19	0.27
		DS-2	0.00053	-1370.10	19.77	0.23
		US-2	0.00057	-1368.51	21.36	0.23
		US-1	0.00061	-1345.78	44.09	0.12

1. Delta AIC is calculated as difference between model AIC_c and the lowest AIC_c

2. Adjusted R^2 reflects fixed effects only

Supporting Information for Chapter 2

1. Description of spatial stream network models

We used spatial stream network (SSN) models to analyze tissue Hg for all sites sampled (n = 68). These models are described in detail elsewhere (Ver Hoef et al., 2006; Peterson & Ver Hoef, 2010; Ver Hoef & Peterson, 2010). SSN models explicitly account for complex relationships within a stream network, including flow direction, longitudinal connectivity, and flow magnitude. SSNs provide flexible covariance structures for stream data and yield improved model performance when spatial autocorrelation is present in sample data, allowing deviations from the mean to be explained, in part, by covariance with nearby sites (Peterson et al., 2006, 2007). Covariance is determined via both hydrologic and Euclidean distance. Spatial relationships among hydrologically connected sites are incorporated into covariance matrices via moving average spatial autocorrelation functions (Ver Hoef & Peterson, 2010).

We used a mixed-effects modeling framework in which the observed variance in Hg across the river network is explained by a set of covariates modeled as fixed effects (eg. wetland cover %), and these spatial covariance matrices as random effects.

The general form of the spatial linear mixed model is:

$$y=X\beta+z\_TU+z\_TD\ \ z\_E+\epsilon, \qquad (2)$$

Where y is the vector of a response variable (eg.Hg), X is a matrix of covariates, β is a vector of parameters for each covariate in X, and zTU, zTD, and zE are vectors of random variables with tail-up, tail-down, and Euclidean correlation structures, respectively; and ϵ is a vector of independent random errors.

Tail-up autocovariance functions for flow-connected relationships within the SSNs require a spatial weight to inform how the moving average function behaves at stream confluences (Ver

Hoef et al., 2006). Each segment has a 'segment proportional influence' (SPI) computed based on the relative influence of each stream segment at a confluence. The SPI of two segments sum to 1, with relative influences assigned based on watershed attributes for each segment. We derived SPI based on watershed area accumulated for all grid cells upstream of each stream segment using the Spatial Toolbox for the Analysis of River Systems (STARS) toolbox in ArcGIS (Peterson & Ver Hoef 2014). Flow accumulation and a synthetic channel network were derived from a 2-arc-second resolution (~60 m) digital elevation model (DEM) extracted from the USGS National Elevation Dataset. All spatial datasets were projected from latitude/longitude into an Albers Equal Area projection and referenced to the North American Datum of 1983, in horizontal and vertical units of meters.

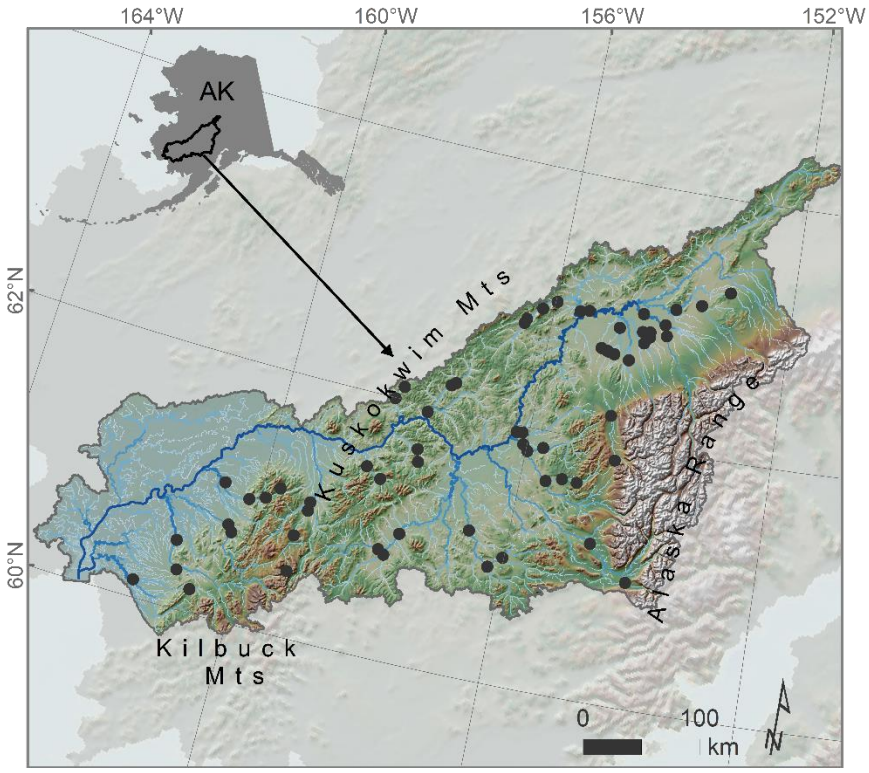

Figure S2.1. Map of sample sites in the Kuskokwim River watershed, Alaska.

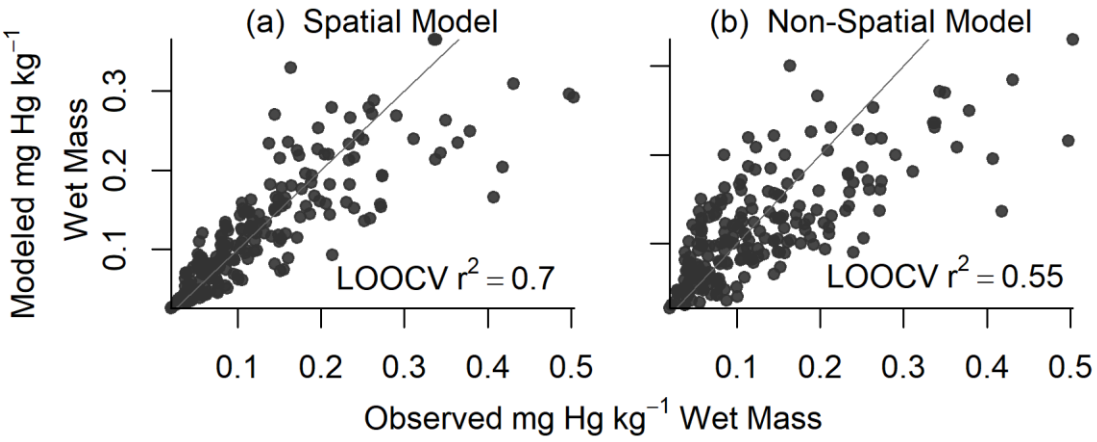

Figure S2.2. Modeled versus observed Hg and leave-one-out-cross-validation (LOOCV) statistics for a spatial model (a) and non-spatial model (b). Both models include fish mass, watershed slope, Farewell terrane watershed cover, and barren ice and rock watershed cover. The spatial model also includes a flow-connected or tail-up autocovariance function.

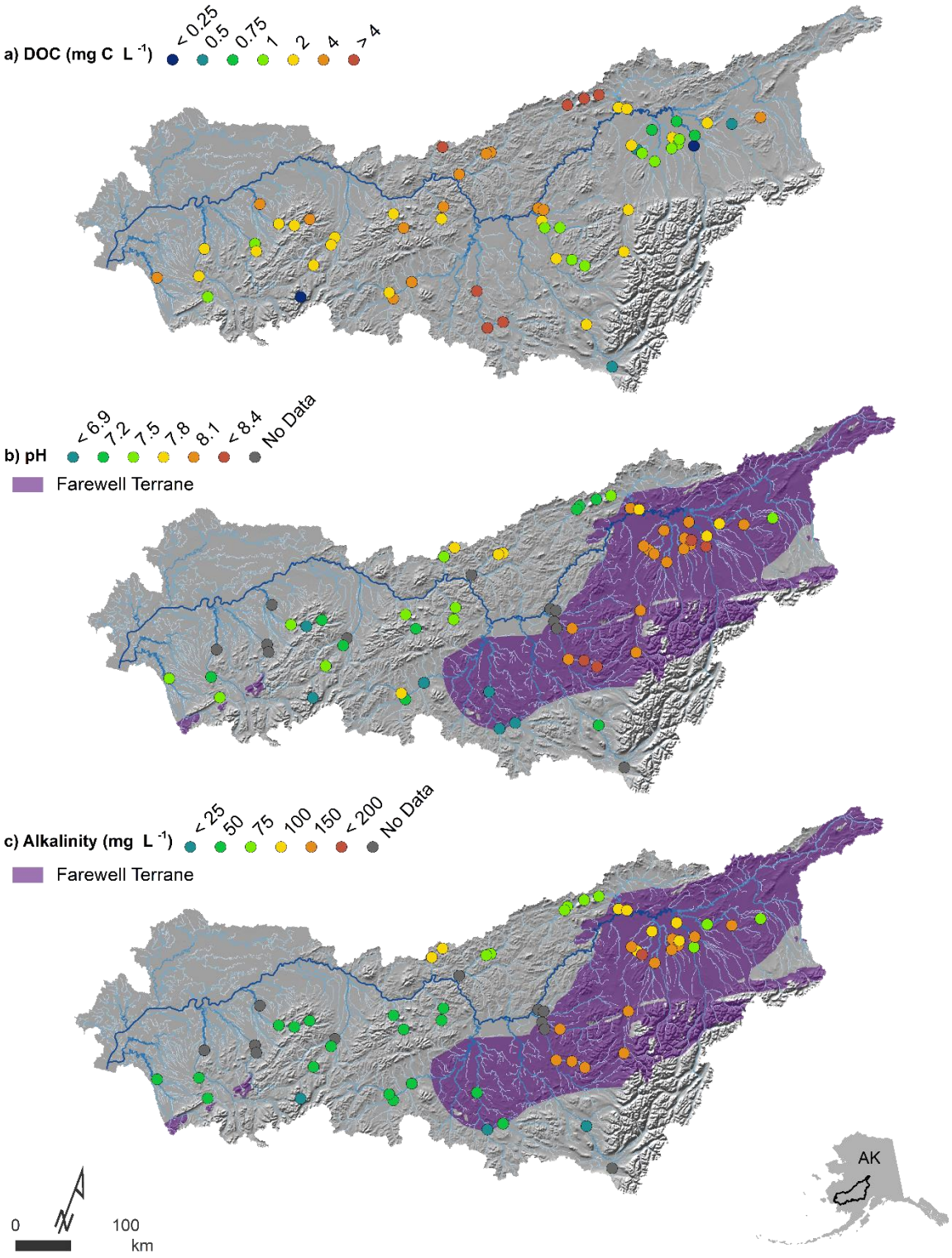

Figure S2.3. Maps of dissolved organic carbon concentrations (a), pH (b) and alkalinity (c) in the Kuskokwim overlaid with the Farewell Terrane geologic unit.

Table S2.1. Watershed spatial covariates and data sources.

Covariate	Description	Data Source
Relief	Average watershed relief	USGS National Elevation Dataset, 2017
Slope	Average watershed slope	USGS National Elevation Dataset, 2017
Zmean	Average watershed elevation	USGS National Elevation Dataset, 2017
Wet	Emergent and woody wetland cover*	USGS National Land Cover Dataset, 2015
Water	Open water cover*	USGS National Land Cover Dataset, 2015
Bog	Boreal bog & fen cover*	USGS GAP/LANDFIRE, 2016
Marsh	Boreal freshwater meadow & marsh cover*	USGS GAP/LANDFIRE, 2016
Swamp	Boreal flooded & swamp forest cover*	USGS GAP/LANDFIRE, 2016
Peat	Peat soil cover*	USDA SSURGO Soil Map, 2016
Variable	Variable soil cover*	USDA SSURGO Soil Map, 2016
DPF	Discontinuous permafrost cover*	Jorgenson et al., 2008
SPF	Sporadic permafrost cover*	Jorgenson et al., 2008
IPF	Isolated permafrost cover*	Jorgenson et al., 2008
HgMines	Historic Hg mines**	USGS Alaska Resource Data File, 2008
HgAll	Historic or recent Hg occurrences, mines, or claims**	USGS Alaska Resource Data File, 2008
AllMines	Historic or recent mines, all minerals**	USGS Alaska Resource Data File, 2008
Geo1	Siliciclastic sedimentary rocks; mixed grain size; fossil plant organic material mentioned*	Hartman & Moosdorf, 2012
Geo2	Mixed sedimentary rocks; mixed and fine grain size; metamorphic influence mentioned*	Hartman & Moosdorf, 2012
Geo3	Siliciclastic sedimentary rocks; loess; glacial influence mentioned*	Hartman & Moosdorf, 2012
Geo4	Siliciclastic sedimentary rocks; mixed grain size; subordinate volcanics mentioned*	Hartman & Moosdorf, 2012
Geo5	Siliciclastic and mixed sedimentary rocks; Pyroclastics mentioned; subordinate volcanics mentioned*	Hartman & Moosdorf, 2012
Geo6	Acid volcanic and acid plutonic rocks*	Hartman & Moosdorf, 2012
Geo7	Intermediate volcanic and plutonic rocks*	Hartman & Moosdorf, 2012
Geo8	Basic volcanic and plutonic rocks*	Hartman & Moosdorf, 2012
Geo9	Mixed sedimentary rocks; mixed grain size; Chert mentioned*	Hartman & Moosdorf, 2012
Geo10	Metamorphics*	Hartman & Moosdorf, 2012
Geo11	Carbonate sedimentary rocks; coarse grained; metamorphic influence mentioned*	Hartman & Moosdorf, 2012
Geo12	Ice and glaciers*	Hartman & Moosdorf, 2012

**Derived as watershed percent cover*

***Derived for each site as mean distance downstream from mining activity*

Table S2.2. Spatial stream network model comparison for fixed effects and model summary statistics.

Model Formula	RMSPE	AIC	Δ AIC[1]	Adj. R^2[2]
logHg ~ logFishMass.cent + h2oIce.Rock.cent + h2oFarewellTerrane.cent + h2oSlpMean.cent	0.137	-185.82	0.00	0.36
logHg ~ logFishMass.cent + h2oIce.Rock.cent + h2oFarewellTerrane.cent + h2oSlpMean.cent + logDOC.cent	0.137	-184.33	1.48	0.36
logHg ~ logFishMass.cent + h2oIce.Rock.cent + h2oKuskoGroup.cent + h2oVolcanics.cent + h2oFarewellTerrane.cent	0.136	-184.24	1.58	0.34
logHg ~ logFishMass.cent + h2oIce.Rock.cent + h2oKuskoGroup.cent + h2oVolcanics.cent + h2oRelief.cent + logDOC.cent + h2oFarewellTerrane.cent	0.137	-183.87	1.95	0.37
logHg ~ logFishMass.cent + h2oIce.Rock.cent + h2oKuskoGroup.cent + h2oVolcanics.cent + h2oRelief.cent + h2oFarewellTerrane.cent	0.136	-183.69	2.13	0.36
logHg ~ logFishMass.cent + h2oIce.Rock.cent + h2oKuskoGroup.cent + dist.mean.cent	0.137	-183.02	2.79	0.33
logHg ~ logFishMass.cent + h2oIce.Rock.cent + h2oKuskoGroup.cent + h2oVolcanics.cent + dist.mean.cent	0.136	-182.73	3.09	0.34
logHg ~ logFishMass.cent + h2oIce.Rock.cent + h2oKuskoGroup.cent + h2oFarewellTerrane.cent	0.137	-181.62	4.19	0.33
logHg ~ logFishMass.cent + h2oIce.Rock.cent + h2oFarewellTerrane.cent + logDOC.cent	0.137	-181.56	4.26	0.33
logHg ~ logFishMass.cent + h2oIce.Rock.cent + h2oKuskoGroup.cent + h2oVolcanics.cent + h2oRelief.cent + dist.mean.cent	0.136	-180.73	5.09	0.34
logHg ~ logFishMass.cent + h2oIce.Rock.cent + h2oKuskoGroup.cent	0.137	-180.27	5.55	0.31

1. Δ AIC is calculated as difference between each model and the best model

2. Includes fixed effects only, no spatial autocovariance functions

Table S2.3. Spatial stream network model random effects comparison and model summary statistics.

Model Formula	Spatial Structure	RMSPE	AIC	Δ AIC$_2$
Full model$_1$	Spherical.tailup + Nugget	0.137	-171.17	0.00
Full model$_1$	Mariah.tailup + Nugget	0.137	-170.12	1.05
Full model$_1$	Exponential.tailup + Exponential.taildown + Nugget	0.137	-168.72	2.45
Full model$_1$	LinearSill.tailup + Gaussian.Euclid + Nugget	0.137	-168.10	3.06
Full model$_1$	Exponential.tailup + Exponential.Euclid + Nugget	0.137	-167.82	3.35
Full model$_1$	Mariah.tailup + Gaussian.Euclid + Nugget	0.137	-167.01	4.15
Full model$_1$	LinearSill.tailup + LinearSill.taildown + Gaussian.Euclid + Nugget	0.136	-166.23	4.94
Full model$_1$	Exponential.taildown + Nugget	0.137	-166.01	5.16
Full model$_1$	Spherical.taildown + Nugget	0.137	-165.03	6.13
Full model$_1$	Exponential.tailup + Exponential.taildown + Exponential.Euclid + Nugget	0.137	-164.70	6.47
Full model$_1$	Exponential.taildown + Exponential.Euclid + Nugget	0.137	-162.01	9.16
Full model$_1$	LinearSill.taildown + Gaussian.Euclid + Nugget	0.138	-161.57	9.59
Full model$_1$	Exponential.Euclid + Nugget	0.138	-160.14	11.03
Full model$_1$	Gaussian.Euclid + Nugget	0.138	-158.07	13.10
Full model$_1$	Nugget	0.195	-68.39	102.77
logHg ~ logWt.cent + logDOC.cent	Nugget	0.241	13.91	185.08

1. Full model is defined as: logHg ~ logWt.cent + h2oGeo12.cent + h2oGeo2.cent + h2oSlpMean.cent
2. Δ AIC is calculated as difference between each model and the best model